COPPE
Instituto Alberto Luiz Coimbra de Pós-Graduação e Pesquisa de Engenharia
UFRJ

# CONTRIBUTIONS TO MASSIVE MIMO: POWER ALLOCATION, USER SELECTION, AND CELL-FREE COMMUNICATIONS

Rafael da Silva Chaves

Tese de Doutorado apresentada ao Programa de Pós-graduação em Engenharia Elétrica, COPPE, da Universidade Federal do Rio de Janeiro, como parte dos requisitos necessários à obtenção do título de Doutor em Engenharia Elétrica.

Orientadores: Wallace Alves Martins
Ediz Cetin
Markus Vinícius Santos Lima

Rio de Janeiro
Agosto de 2022

CONTRIBUTIONS TO MASSIVE MIMO: POWER ALLOCATION, USER SELECTION, AND CELL-FREE COMMUNICATIONS

Rafael da Silva Chaves

TESE SUBMETIDA AO CORPO DOCENTE DO INSTITUTO ALBERTO LUIZ COIMBRA DE PÓS-GRADUAÇÃO E PESQUISA DE ENGENHARIA (COPPE) DA UNIVERSIDADE FEDERAL DO RIO DE JANEIRO COMO PARTE DOS REQUISITOS NECESSÁRIOS PARA A OBTENÇÃO DO GRAU DE DOUTOR EM CIÊNCIAS EM ENGENHARIA ELÉTRICA.

Examinada por:

Prof. Wallace Alves Martins, D.Sc.

Prof. Markus Vinícius Santos Lima, D.Sc.

Prof. André Lima Férrer de Almeida, Ph.D.

Prof. Marcello Luiz Rodrigues de Campos, Ph.D.

Prof. Richard Demo Souza, D.Sc.

RIO DE JANEIRO, RJ – BRASIL
AGOSTO DE 2022

Chaves, Rafael da Silva

Contributions to Massive MIMO: Power Allocation, User Selection, and Cell-free Communications/Rafael da Silva Chaves. – Rio de Janeiro: UFRJ/COPPE, 2022.

XX, 116 p.: il.; 29, 7cm.

Orientadores: Wallace Alves Martins
Ediz Cetin
Markus Vinícius Santos Lima

Tese (doutorado) – UFRJ/COPPE/Programa de Engenharia Elétrica, 2022.

Referências Bibliográficas: p. 107 – 116.

1. Massive MIMO. 2. Line-of-sight. 3. UR-LoS. 4. User Selection. 5. Power Allocation. 6. Perron-Frobenius. 7. Cell-free. I. Martins, Wallace Alves *et al.* II. Universidade Federal do Rio de Janeiro, COPPE, Programa de Engenharia Elétrica. III. Título.

# Agradecimentos

Meu doutorado nunca teria sido possível sem a ajuda e o suporte de pessoas incríveis. Primeiramente, gostaria de agradecer à minha mãe Rose e ao me pai Ideny por todo o suporte e incentivo que eles me deram durante toda a minha vida. Eles me forneceram o ambiente perfeito para que eu pudesse prosperar na minha jornada. Cada palavra nessa tese carrega um pouco de vocês dois. Também gostaria de agradecer especialmente o meu irmão e melhor amigo por sempre ficar do meu lado em todos os momentos e por ter muita paciência comigo. O seu papel é crucial na minha vida e eu nunca teria chegado até aqui sem você.

Agradeço meus três orientadores que sempre acreditaram em mim, mesmo quando eu não conseguia acreditar em mim mesmo. Obrigado, Wallace por todas as oportunidades e apoio. Você está comigo desde o início da minha vida acadêmica em 2013. Obrigado, Ediz por ter sido muitas vezes mais do que um orientador e pelas reuniões mais agradáveis que já tive na minha vida. Você estava lá quando eu me mudei para Austrália, primeira vez que morei sozinho e longe da minha família. Você também esteve lá durante a COVID-19 quando o mundo estava mais doido do que o normal e minha família estava tão longe. Obrigado, Markus por ser uma pessoa e um orientador incrível. Você sempre me mostrou o valor das minhas contribuições e nunca me deixou desistir. Você sempre esteve presente e aberto para debater qualquer assunto comigo, variando desde a minha pesquisa até basquete, literalmente qualquer coisa.

Gostaria de fazer um agradecimento especial para Kate por ter estado presente nos meus momentos mais felizes e mais tristes. Austrália nunca teria sido possível sem você e suas aulas de inglês. Também gostaria de agradecer à Karina, uma amiga que entrou na minha vida de maneira inesperada e está aqui para ficar. Obrigado por me ouvir quando eu precisava ser ouvido e por me aconselhar quando eu precisava ser aconselhado. Obrigado, Rômulo por sempre ser um bom amigo, por sempre ser tão entusiasmado com a ciência e por sempre estar aqui por mim e pela minha família. Obrigado, Hugo por sempre estar disponível quando precisei durante a minha estadia na Austrália, apesar das diferenças de fuso horário. Na verdade, eu sou grato por você ser uma pessoa da noite. Obrigado, Marcelo Spelta e Marcelo Castro por serem bons amigos, apesar do gosto horrível para times de futebol e

futebol americano.

Obrigado, Stanis, Anne, Ollie, Giuly e Bree por fazerem me sentir em casa enquanto eu estava na Austrália. Vocês foram a minha família aí. Obrigado, Felipe e Bo Li pelo apoio acadêmico. Agradeço todos os meus amigos do SMT, Matheus, Lucas, Roberto, Wesley, Igor e Padilha. Obrigado por tudo.

Resumo da Tese apresentada à COPPE/UFRJ como parte dos requisitos necessários para a obtenção do grau de Doutor em Ciências (D.Sc.)

# CONTRIBUIÇÕES PARA MIMO MASSIVO: ALOCAÇÃO DE POTÊNCIA, SELEÇÃO DE USUÁRIOS E COMUNICAÇÕES CELL-FREE

Rafael da Silva Chaves

Agosto/2022

Orientadores: Wallace Alves Martins
Ediz Cetin
Markus Vinícius Santos Lima

Programa: Engenharia Elétrica

Essa tese apresenta novas contribuições para MIMO massivo (do inglês, *massive multiple-input multiple-output*), cobrindo alocação de potência, seleção de usuários e sistemas sem célula. Para alocação de potência, nós propomos um novo esquema de inicialização para o algoritmo max-min usado em sistemas MIMO massivo com visada direta. O esquema proposto garante convergência para o ponto ótimo. Além disso, propomos o teste dos estremos, um procedimento mais eficiente para inicializar o intervalo de busca. Para seleção de usuários, revisamos os algoritmos de seleção de usuários para sistemas MIMO massivo com visada direta, destacando o papel da propagação favorável e o projeto dos pré-codificadores lineares. Nós também propomos dois novos algoritmos. O primeiro, chamado ICIBS (do inglês, *inter-channel interference-based selection*), considera a interferência global do sistema, enquanto o segundo, chamado FRBS (do inglês, *fading-ratio-based selection*), considera a interferência global e o desvanecimento de grande escala. Os algoritmos apresentam vantagens em relação aos algoritmos da literatura, superando-os em alguns cenários como os aglomerados e superlotados. Para os sistemas MIMO massivo sem célula, avaliamos o desempenho em uplink dos sistemas MIMO massivo sem célula quando corrompidos por ruído de quantização e operando em canais com desvanecimento Rician correlacionado. Nós derivamos a eficiência espectral para qualquer pré-codificador linear, o estimador MMSE (do inglês, *minimum mean squared error*) de canal ótimo e um sub-ótimo combinador escalável.

Abstract of Thesis presented to COPPE/UFRJ as a partial fulfillment of the requirements for the degree of Doctor of Science (D.Sc.)

# CONTRIBUTIONS TO MASSIVE MIMO: POWER ALLOCATION, USER SELECTION, AND CELL-FREE COMMUNICATIONS

Rafael da Silva Chaves

August/2022

Advisors: Wallace Alves Martins
Ediz Cetin
Markus Vinícius Santos Lima

Department: Electrical Engineering

This thesis presents new contributions to the massive MIMO field, covering aspects related to power allocation, user selection, and cell-free systems. Regarding power allocation, we propose a new initialization scheme for the max-min fairness power allocation algorithm used in massive MIMO systems under line-of-sight (LoS) propagation. The proposed scheme guarantees convergence to the optimal point. Additionally, we propose the bound test procedure as an even more efficient way of initializing the search interval. As for the user selection, we review the user selection algorithms for massive MIMO systems under LoS propagation, highlighting the role of the favorable propagation condition in this scenario and the design of standard linear precoders. Moreover, we propose two new algorithms. The first one, called inter-channel interference-based selection (ICIBS), takes the global interference in the system into account, whereas the second one, namely fading-ratio-based selection (FRBS), considers both the global interference and the large-scale fading. These proposed algorithms present advantages over the algorithms in the literature, outperforming them in some scenarios, such as clustered and crowded scenarios. For the cell-free massive MIMO systems, we evaluate the uplink performance of cell-free massive MIMO systems corrupted by quantization noise under correlated Rician fading channels. We derive the uplink spectral efficiency for any linear combiner, the optimal minimum mean squared error channel estimator, and a suboptimal scalable combiner.

# List of Publications

## Conference Papers

[C1] R. S. Chaves, E. Cetin, M. V. S. Lima, and W. A. Martins, "User Selection Based on Inter-channel Interference for Massive MIMO under Line-of-sight Propagation," in *XXXIVth General Assembly and Scientific Symposium of the International Union of Radio Science*, Rome, August 2021.

## Journal Papers

[J1] R. S. Chaves, E. Cetin, M. V. S. Lima, and W. A. Martins, "On the Convergence of Max-Min Fairness Power Allocation in Massive MIMO Systems," *IEEE Communications Letters*, vol. 24, no. 12, pp. 2873–2877, December 2020.

[J2] R. S. Chaves, M. V. S. Lima, E. Cetin, and W. A. Martins, "User Selection for Massive MIMO under Line-of-sight Propagation," *IEEE Open Journal of the Communications Society*, vol. 3, pp. 867–887, 2022.

[J3] R. S. Chaves, E. Cetin, M. V. S. Lima, and W. A. Martins, "Fading-ratio-based Selection for Massive MIMO Systems under Line-of-sight Propagation (accepted for publication)," *Wireless Networks*, 2022.

[J4] R. S. Chaves, E. Cetin, M. V. S. Lima, and W. A. Martins, "On the Nonlinearities of Cell-Free Massive MIMO Systems Under Correlated Rician Fading Channels (in preparation)," 2022.

# Contents

**Agradecimentos** **iv**

**List of Publications** **viii**

**List of Figures** **xii**

**List of Tables** **xv**

**List of Acronyms** **xvii**

**1 Introduction** **1**

1.1 Massive MIMO . . . . . 1

1.1.1 Cellular Massive MIMO Systems . . . . . 1

1.1.2 Cell-free Massive MIMO Systems . . . . . 3

1.1.3 Massive MIMO in Practical Systems . . . . . 5

1.2 Problem Statements . . . . . 6

1.2.1 Power Allocation . . . . . 6

1.2.2 User Selection . . . . . 6

1.2.3 Cell-free Massive MIMO . . . . . 9

1.3 Contributions . . . . . 10

1.4 Publications . . . . . 12

1.5 Notation . . . . . 13

**I Cellular Massive MIMO Systems** **15**

**2 Massive MIMO: A Brief Overview** **16**

2.1 Introduction . . . . . 16

2.2 Massive MIMO Channel . . . . . 16

2.2.1 Favorable Propagation . . . . . 18

2.3 Downlink Transmission . . . . . 22

2.4 Spectral Efficiency . . . . . 23

2.5 Precoding Schemes . . . . . 27

2.5.1 Maximum Ratio Transmitter . . . 27
2.5.2 Zero-forcing . . . 28

**3 Power Allocation Algorithms** **31**
3.1 Introduction . . . 31
3.2 Preliminaries . . . 31
3.3 Equal Power Allocation . . . 32
3.4 Max-Min Fairness Power Allocation . . . 32
3.4.1 Maximum Ratio Transmitter . . . 32
3.4.2 Zero-forcing . . . 34
3.5 Perron-Frobenius Right Endpoints . . . 34
3.5.1 Perron-Frobenius Eigenvalue . . . 34
3.5.2 Bound Test . . . 36
3.6 Computational Complexity Analysis . . . 37
3.7 Simulation Results . . . 38
3.8 Concluding Remarks . . . 42

**4 User Selection Algorithms** **43**
4.1 Introduction . . . 43
4.2 The User Selection Problem . . . 43
4.3 Large-scale Fading Ratio Selection . . . 46
4.4 Semi-orthogonal Selection . . . 47
4.5 Correlation-based Selection . . . 49
4.6 Inter-channel Interference-based Selection . . . 49
4.6.1 ICIBS with MRT Precoder . . . 51
4.7 Fading-ratio-based Selection . . . 52
4.8 Computational Complexity . . . 53
4.8.1 Semi-orthogonal Selection . . . 54
4.8.2 Simplified Semi-orthogonal Selection . . . 56
4.8.3 Correlation-based Selection . . . 57
4.8.4 Inter-channel Interference-based Selection . . . 57
4.8.5 Simplified Inter-channel Interference-based Selection . . . 58
4.8.6 Fading-ratio Based Selection . . . 58
4.9 Concluding Remarks . . . 59

**5 Performance Evaluation of the ICIBS Algorithm** **60**
5.1 Overview . . . 60
5.2 System Parameters . . . 61
5.3 Perfect CSI . . . 61
5.4 Computational Complexity . . . 66

5.5 Imperfect CSI . . . 66
5.6 Ultra Clustered-crowded Scenario . . . 68
5.7 Practical Guidelines . . . 71
5.8 Concluding Remarks . . . 73

**6 Performance Evaluation of the FRBS Algorithm 74**
6.1 Simulation Parameters . . . 74
6.2 Performance of the FRBS . . . 75
6.2.1 FRBS *vs.* SSFA Algorithms . . . 78
6.2.2 FRBS *versus* LSFA Algorithms . . . 79
6.3 Concluding Remarks . . . 81

**II Cell-free Massive MIMO Systems 82**

**7 Nonlinearities of Cell-Free Massive MIMO 83**
7.1 Introduction . . . 83
7.2 Cell-free Massive MIMO . . . 84
7.3 The Bussgang Decomposition . . . 86
7.4 Uplink Channel Estimation . . . 89
7.4.1 Phase-aware MMSE Estimator . . . 90
7.5 Uplink Data Transmission . . . 92
7.6 Simulation Results . . . 98
7.6.1 Simulation Parameters . . . 98
7.6.2 Performance with Semi-distributed Implementation . . . 99
7.6.3 Effects of the Quantization . . . 101
7.7 Concluding Remarks . . . 101

**III Conclusion and Future Work 103**

**8 Conclusion 104**
8.1 Closing Thoughts . . . 104
8.2 Future Research Directions . . . 105

**Bibliography 107**

# List of Figures


1.1 Example of cellular centralized and distributed massive MIMO systems. 2
1.2 Example of cell-free massive MIMO system. . . . . 4

2.1 Line-of-sight channel between the $k$th user and the $M$-antenna ULA. 17
2.2 Magnitude of the correlation coefficient for $K = 2$ and $M \in \{50, 100\}$. 21
2.3 Massive MIMO system with an $M$-antenna BS serving $K$ single-antenna users. . . . . 22

3.1 Example of convergence to the optimal and wrong points using $\gamma_{\mathrm{r}}^{(1)}$. . 36
3.2 Probability of failure. (– $P = 1$ W and – – $P = 10$ W) . . . . . 39
3.3 $\mathsf{Pr}\{\gamma_{\mathrm{r}}^{(3)} < \gamma^{\star}\}$ for $M = 512$. . . . . 40
3.4 Number of iterations for $P = 1$ W. (– $\gamma_{\mathrm{r}}^{(1)}$, – – $\gamma_{\mathrm{r}}^{(2)}$, and ·· BT) . . . . 41

4.1 ICIBS and FRBS with $M = 50$, $K = 25$, $L = 5$, and $R = 500$ m. ($\bigtriangledown$ BS, ◯ selected user, and ◯ dropped user) . . . . . 54

5.1 Average throughput *versus* the number of users for $M \in \{50, 100\}$. (– MRT, – – ZF, and · · MMSE) . . . . . 62
5.2 Average throughput *versus* the number of selected users $L$ for $M \in \{50, 100\}$, considering different number of users $K$. The line style (solid, dashed or dotted line) determines the precoder, whereas the colors specify the user selection algorithm. The yellow solid line, e.g., represents the results achieved by the ICIBS scheme considering an MRT precoder. . . . . 64
5.3 *Cumulative distribution function* of the throughput for $L = \lceil K/2 \rceil$ and $M \in \{50, 100\}$, considering different number of users $K$. The line style (solid, dashed or dotted line) determines the precoder, whereas the colors specify the user selection algorithm. The yellow solid line, e.g., represents the results achieved by the ICIBS scheme considering an MRT precoder. . . . . 65
5.4 Giga flops count *versus* the number of selected users for $K = 100$ and $M \in \{50, 100\}$. . . . . 66

5.5 Average throughput *versus* the number of selected users $L$ with imperfect CSI knowledge for the ICIBS algorithm, considering $M = 50$, $K = 75$, different precoding algorithms, and different $\sigma_\varepsilon^2$. . . . . 67
5.6 Maximum achieved throughput and optimum number of selected users $L^\star$ *versus* the variance of the channel estimation error $\sigma_\varepsilon^2$ for $M \in \{50, 100\}$, considering different user selection and precoding algorithms. . . . . 69
5.7 Example of an ultra clustered-crowded scenario used in the simulations, where $\theta_0$ is the direction of the sector of the cell and $\Delta\theta$ is the aperture angle. . . . . 70
5.8 Average per-user throughput *versus* $\Delta\theta$ for $M = 50$ and $K = 75$. The line style (solid, dashed or dotted line) determines the precoder, whereas the colors specify the user selection algorithm. The yellow solid line, e.g., represents the results achieved by the ICIBS scheme considering an MRT precoder. . . . . 70
5.9 Average throughput *versus* the number of selected users $L$ for $M = 50$, $K = 75$, $\Delta\theta = 1.5°$, and $\theta_0 = 0°$. The line style (solid, dashed or dotted line) determines the precoder, whereas the colors specify the user selection algorithm. The yellow solid line, e.g., represents the results achieved by the ICIBS scheme considering an MRT precoder. . 71
5.10 *Cumulative distribution function* of the throughput for $M = 50$, $K = 75$, $L = 38$, $\Delta\theta = 1.5°$, and $\theta_0 = 0°$. The line style (solid, dashed or dotted line) determines the precoder, whereas the colors specify the user selection algorithm. The yellow solid line, e.g., represents the results achieved by the ICIBS scheme considering an MRT precoder. . 72

6.1 Average sum-throughput *versus* the number of selected users with EPA, considering different number of users. . . . . 75
6.2 Computational burden *versus* the number of selected users measured in flops count for SOS and FRBS. . . . . 77
6.3 Average min-throughput *versus* the number of selected users with MMFPA, considering different number of users. . . . . 78
6.4 Average sum-throughput *versus* the number of selected users with EPA for CBS, ICIBS, and FRBS with $M = 50$ and $K = 75$. . . . . 79
6.5 Average sum-throughput *versus* the number of selected users with EPA for LSFRS and FRBS with $M = 50$ and $K = 75$. . . . . 80

7.1 A CF massive MIMO network operating in uplink with $M$ APs equipped wit an $N$-antenna array distributed over a coverage area serving $K$ single-antenna UEs. . . . . 84

7.2 Block diagram of the CPU and APs for the CF massive MIMO network. 85
7.3 Spectral efficiency of the CF massive MIMO system over spatial correlated Rician fading channel with semi-distributed and distributed implementations. . . . . 100
7.4 Spectral efficiency of the CF massive MIMO system over spatial correlated Rician fading channel with semi-distributed and distributed implementations, and 5-bit AD converters. . . . . 101

# List of Tables


4.1 Main Characteristic of User Selection Algorithms . . . . . 45
4.2 Number of Operations and Complexity of the User Selection Algorithms 55
4.3 Number of Linear Searches per Iteration . . . . . 56
4.4 FRBS' Computational Complexity . . . . . 59

5.1 Simulation Parameters for the ICIBS . . . . . 61

6.1 Simulation Parameters for the FRBS . . . . . 75
6.2 Optimum Values Achieved by the Algorithms for $K = 10$ . . . . . 76
6.3 Optimum Values Achieved by the Algorithms for $K = 25$ . . . . . 76
6.4 Optimum Values Achieved by the SSFA Algorithms for $K = 75$ . . . 78
6.5 Optimum Values Achieved by the LSFA Algorithms for $K = 75$ . . . 80

7.1 Bussang Parameters for the Quantizer in (7.1) with Normalized Input 88
7.2 Simulation Parameters for the CF massive MIMO Network . . . . . 100

# List of Algorithms


1 MMFPA-based algorithm . . . . . 33
2 Bound test . . . . . 37
3 LSFRS algorithm . . . . . 46
4 SOS algorithm . . . . . 47
5 S-SOS algorithm . . . . . 49
6 CBS algorithm . . . . . 50
7 ICIBS algorithm . . . . . 51
8 S-ICIBS algorithm . . . . . 51
9 FRBS algorithm . . . . . 53

# List of Acronyms

**Symbols**

**3GPP** *3rd Generation Partnership Project.*

**95PT** *95%-probability throughput.*

**A**

**AD** *analog-to-digital.*

**AFP** *asymptotically favorable propagation.*

**AoA** *angle of arrival.*

**AP** *access point.*

**ASD** *angular standard deviation.*

**B**

**BS** *base station.*

**BT** *bound test.*

**C**

**CBS** *correlation-based selection.*

**CDF** *cumulative distribution function.*

**CF** *cell-free.*

**CoMP** *coordinated multipoint.*

**CPU** *central processing unit.*

**CSI** *channel state information.*

**D**

**DA** *digital-to-analog.*

**DAS** *distributed antenna systems.*

**DCC** *dynamic cooperation clustering.*

**DL** *downlink.*

**DML** *delete the minimum lambda.*

**DPC** *dirty paper coding.*

**DSP** *digital signal processor.*

**E**

**EE** *energy efficiency.*

**EPA** *equal power allocation.*

**ES** *exhaustive search.*

**ESEPA** *exhaustive search with equal power allocation.*

**ESMMFPA** *exhaustive search with max-min fairness power allocation.*

**F**

**flop** *floating point operation.*

**FP** *favorable propagation.*

**FR** *fading ratio.*

**FRBS** *fading-ratio-based selection.*

**I**

**ICI** *inter-channel interference.*

**ICIBS** *inter-channel interference-based selection.*

**IoT** *internet of things.*

**L**

**LoS** *line-of-sight.*

**LP-MMSE** *local partial minimum mean squared error.*

**LSFA** *large-scale fading aware.*

**LSFD** *large-scale fading decoding.*

**LSFR** *large-scale fading ratio.*

**LSFRS** *large-scale fading ratio selection.*

**M**

**M-SOS** *modified semi-orthogonal selection.*

**MIMO** *multiple-input multiple-output.*

**MISO** *multiple-input single-output.*

**MMFPA** *max-min fairness power allocation.*

**MMSE** *minimum mean squared error.*

**mmWave** *millimeter-wave.*

**MRC** *maximum ratio combiner.*

**MRT** *maximum ratio transmitter.*

**MU-MIMO** *multi-user multiple-input multiple-output.*

**N**

**n-opt** *nearly optimal.*

**NLoS** *non line-of-sight.*

**P**

**PFE** *Perron-Frobenius eigenvalue.*

**Q**

**QoS** *quality of service.*

**R**

**RS** *random selection.*

**S**

**S-ICIBS** *simplified inter-channel interference-based selection.*

**S-SOS** *simplified semi-orthogonal selection.*

**SE** *spectral efficiency.*

**SINR** *signal-to-interference-plus-noise-ratio.*

**SNR** *signal-to-noise ratio.*

**SOS** *semi-orthogonal selection.*

**SSFA** *small-scale fading aware.*

**T**

**TDD** *time-division duplex.*

**U**

**UCA** *uniform circular array.*

**UE** *user equipment.*

**UL** *uplink.*

**ULA** *uniform linear array.*

**UR-LoS** *uniformly random line-of-sight.*

**URA** *uniform rectangular array.*

**Z**

**ZF** *zero-forcing.*

# Chapter 1

# Introduction

## 1.1 Massive MIMO

### 1.1.1 Cellular Massive MIMO Systems

Massive *multiple-input multiple-output* (MIMO) emerged as a disruptive technology that promised to deliver very high *spectral efficiency* (SE) and reduced inter-cell interference by using spatial multiplexing and simple linear processing [1]. Massive MIMO systems can be implemented in both centralized (or collocated) [1] and distributed [2] manners — see Figure 1.1 for an illustration of these systems. The centralized version has been the main focus of massive MIMO related works since the initial proposal in [1]. Centralized massive MIMO systems employ a large number of antennas at the *base station* (BS), serving users within the same time-frequency radio resource. By using a large number of antennas, the small-scale fading effect can be eliminated through the so-called *channel hardening*, yielding a deterministic scalar channel [3]. Moreover, one of the unique and attractive advantages provided by the massive MIMO systems is the effective and computationally tractable power-control policy, which is essential to guarantee a good throughput performance for all users [4]. Furthermore, the mutually orthogonal channel vectors provided by the *favorable propagation* (FP) condition enable the use of simple linear processing to achieve very high throughput for massive MIMO systems [5]. These benefits make centralized massive MIMO very attractive for wireless communication systems.

One of the most critical aspects for the realization of massive MIMO systems is meeting the FP condition, which requires the channel vectors to be mutually orthogonal. However, this condition is rarely met in real propagation environments. Fortunately, the *asymptotically favorable propagation* (AFP) condition is sufficient to guarantee high throughput by using simple linear processing [5]. This condition is achieved by *non line-of-sight* (NLoS) environments with rich scattering, which can be modeled by an i.i.d. Rayleigh fading channel [6]. The i.i.d. Rayleigh channel

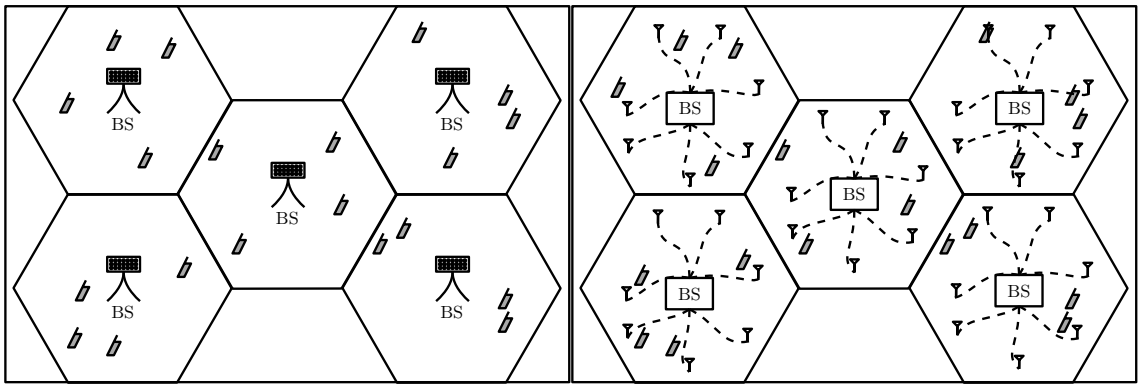


(a) Centralized massive MIMO (b) Distributed massive MIMO

Figure 1.1: Example of cellular centralized and distributed massive MIMO systems.

has the advantage of yielding tractable analytical expressions for the achievable rate of massive MIMO systems [7]. However, in practical applications, the propagation channel is composed of NLoS and *line-of-sight* (LoS) components. Studying the extreme cases, i.e., NLoS and LoS, is important to have performance bounds since, in practice, we will have a case lying in-between the LoS and NLoS cases. Therefore, although massive MIMO systems are frequently studied under the assumption of i.i.d. Rayleigh channel models, the LoS channels are also important [8–11]. In fact, the massive MIMO technology is a potential candidate for use in *millimeter-wave* (mmWave) bands, where LoS is the main form of propagation due to the high attenuation and low penetration of the electromagnetic waves at these frequencies [12–15].

In the LoS propagation environment, the array geometry and the *angle of arrival* (AoA) corresponding to each user determines the channel [16]. This is an example of real propagation environment in which the FP condition may be met, albeit in several cases this condition does not hold [17]. For instance, both the FP and AFP conditions are violated when users are close to each other, i.e., when they have similar AoAs [8, 9, 18–20]. The probability of having close users tends to increase as the number of users served by a given BS grows. This proximity of users has major impact on the SE of massive MIMO systems, degrading it severely when users have similar AoAs [8]. This scenario is recurrent in sports and cultural events, where the number of users in a given region is very high. Dealing with such crowded scenarios is also important for the *internet of things* (IoT) since a large number of devices may be connected to the wireless network [21]. Additionally, although high, the finite number of antennas at the BS limits the number of transmit beams that can be formed, thus constraining the number of users that can be served simultaneously. Therefore, performing user scheduling, which includes *user selection* in its core, is of paramount importance for the proper operation of massive MIMO systems.

### 1.1.2 Cell-free Massive MIMO Systems

Combined with massive MIMO, one way to further improve the SE is by deploying even smaller cells [22]. However, by increasing the density of the cells more and more, the inter-cell interference becomes a bottleneck for the performance of wireless communication systems, which is not different for centralized massive MIMO systems [23].

Distributed massive MIMO systems represent an alternative to the conventional collocated massive MIMO systems [2]. Unlike collocated massive MIMO systems that employ large number of antennas at the BS, distributed massive MIMO systems "break" the antenna array into single-antenna elements, called *access point*s (APs), and spread them across the cell. This distributed version of massive MIMO can provide uniformly good service for all users and a very high probability of coverage by exploiting macro-diversity and differences in the path-loss [24]. The general concept of distributed massive MIMO has different implementations in the literature and includes interesting ideas, such as the so-called network MIMO [25], the *coordinated multipoint* (CoMP) scheme [26], and the *distributed antenna systems* (DAS) [27]. The distributed massive MIMO concept has huge potential, at least theoretically, albeit it suffers from some practical limitations. Distributed massive MIMO systems require low-latency and high-rate fronthaul links since all the processing is performed by the BSs [24]. Moreover, if the BSs cooperate to cope with the inter-cell interference, the distributed systems also require network synchronization and a high-rate backhaul link [28].

In [29], the so-called *cell-free* (CF) massive MIMO was proposed as a possible implementation of the distributed massive MIMO concept. CF massive MIMO systems rely on the *time-division duplex* (TDD), like the centralized massive MIMO systems, and large number of geographically distributed APs serving a small number of users with the aid of a *central processing unit* (CPU) operating in the same time-frequency resource, as illustrated in Figure 1.2. The concept of cell boundary disappears in CF massive MIMO, and the APs simultaneously serve all users. Without the concept of cell boundary, we also do not have BSs anymore, eliminating the necessity of BS synchronization, one significant drawback of the network MIMO systems. Furthermore, CF massive MIMO systems use distributed signal processing, i.e., most of the processing is performed in the APs. During the uplink training phase, each AP estimates its own *channel state information* (CSI), and in the *downlink* (DL) payload transmission, they precode the signal to be transmitted. This distributed signal processing reduces the burden on the fronthaul links since the APs only need to transmit the large-scale fading information to the CPU in order to perform the power allocation. Additionally, CF massive MIMO systems can also

be a solution for applications with high connectivity demand, such as IoT [30, 31]. The main benefits of CF massive MIMO systems are listed below.

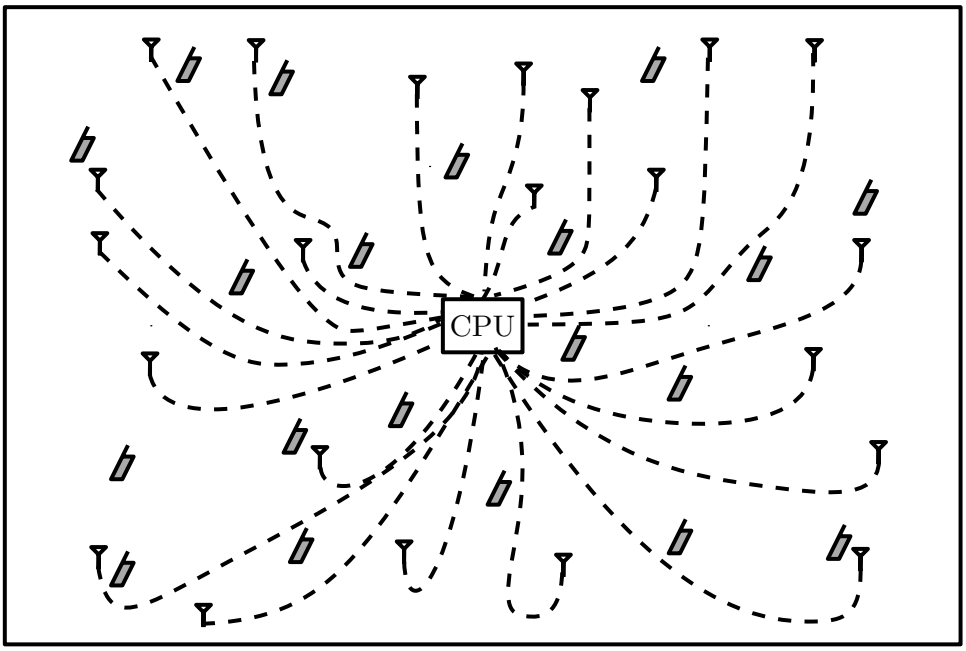


Figure 1.2: Example of cell-free massive MIMO system.

### Improved Energy Efficiency

The *energy efficiency* (EE) is a key performance metric in the design of future wireless communication systems [32]. Centralized massive MIMO systems can achieve high EE since the radiated power by each antenna is significantly reduced when a large number of antennas are employed in the array. In CF massive MIMO systems, the improved EE is one of the main benefits. At first glance, it is expected that the power consumption of fronthaul links connecting the APs to the CPU reduces the overall EE of the system when the number of APs increases significantly. However, this issue can be circumvented by employing AP selection and proper power allocation. Recent works show that with proper power allocation, the CF massive MIMO systems can double the EE of cellular massive MIMO ones [33]. Furthermore, by performing AP selection, the EE can be improved tenfold [34].

### Flexible and Cost-effective Deployment

Another advantage of CF massive MIMO systems is their flexible and cost-effective deployment. In centralized massive MIMO systems, the number of antennas at the BS is limited by the physical space available at the BS. For instance, at a carrier frequency of 3 GHz, the wavelength is 10 cm, and a 100-antenna uniform planar array has a dimension of 0.5 m $\times$ 0.5 m. Hence, a BS of a centralized massive

MIMO system equipped with this array cannot be employed in environments with limited space. On the other hand, this issue does not occur in CF massive MIMO systems since the AP is comprised of a much smaller antenna array, typically ranging from 1 to 4 antennas [35]. Therefore, in CF massive MIMO systems, it is possible to place the APs in space-constrained environments, availing the full potential of massive MIMO since the number of antennas is not constrained by the physical space of the BSs.

#### Uniform Quality of Service

In a CF massive MIMO system, it is expected that a considerable amount of APs surround each user. Additionally, it is also expected that the average distance between the closest APs and an arbitrary user is substantially reduced when compared with a centralized massive MIMOs system and a small-cell system. Based on this, an intuitive conclusion is that the CF massive MIMO system provides more uniform service than the collocated ones, which is indeed true. In [29], the authors show that by performing conjugated beamforming along with max-min power allocation based solely on the large scale fading, a CF massive MIMO system yields nearly a five-fold increase in *95%-probability throughput* (95PT) over small-cell systems when the shadow fading is uncorrelated and a tenfold increase for a correlated shadow fading.

### 1.1.3 Massive MIMO in Practical Systems

Massive MIMO is currently being used in the initial deployment stage of 5G networks in products and solutions developed by Ericsson and Nokia. In 2018, Ericsson and the Russian service provider MTS teamed up in order to provide a superior mobile broadband experience for the costumers during the 2018 FIFA World Cup. This setup was deployed in seven of the eleven tournament cities, including stadiums, fan zones, selected transportation hot spots, and some of the most famous Russian landmarks. Moreover, in 2019, Ericsson and service provider Claro presented the first 5G stadium in Brazil, during the Led Zeppelin in Concert show at Allianz Park.

The use of massive MIMO in 5G networks is already reality, but still under development even when we consider 5G-based networks. In 2019, *3rd Generation Partnership Project* (3GPP) released the first full set of 5G standards, covering standalone 5G, with a new radio system complemented by a next-generation core network [36]. For 5G phase 2, 3GPP aims to cover topics as diverse as multimedia priority service, vehicle-to-everything application layer services, 5G satellite access, local area network support in 5G, wireless and wireline convergence for 5G, terminal positioning and location, communications in vertical domains and network automation, and novel radio techniques [37]. Based on these facts, this Ph.D. work

contributes to the area, focusing on power allocation, user selection, and cell-free massive MIMO systems.

## 1.2 Problem Statements

### 1.2.1 Power Allocation

The power-control policy is essential to guarantee a good throughput performance for all users. A common power-control policy is the maximization of the sum-throughput within the cell [38, 39]. This approach does not consider each users' performance, only the "global" performance in the cell. A widely used power-control policy in massive MIMO systems is the *max-min fairness power allocation* (MMFPA) [9, 40–42], which guarantees egalitarian performance for each user in a given cell. The MMFPA aims to maximize the worst performance among all users in the cell by maximizing the minimum *signal-to-interference-plus-noise-ratio* (SINR). The MMFPA algorithm proposed in [9] uses a bisection search, solving a set of linear equations at each iteration. However, this implementation is susceptible to the choice of the initial search interval of the bisection method, which may fail to converge to the optimal point. The difficulty of analyzing this issue is further compounded by the fact that it is not always observable given its dependence on random variables such as the large-scale fading coefficients. The algorithm may converge to the optimal point even when the initial search interval is not chosen properly. Hence, it is not simple to find an initial search interval that provides the optimal point. In [9], the authors provide a heuristically-defined search interval, which can eventually be replaced by one obtained via an exhaustive search whenever the heuristic interval fails. While the heuristic search interval often leads to convergence to a wrong point (not the optimal point), as confirmed by the simulation results for a massive MIMO setup, the exhaustive search may take too long to find a proper initialization of the search interval. In Chapter 3, we present solution to this problem, proposing two new initialization approaches that guarantee the convergence of the algorithm proposed in [9].

### 1.2.2 User Selection

The SE of massive MIMO systems is directly related to the SINR associated with each user. Intuitively, users that cause strong interference among each other should not be transmitting simultaneously in order to maximize the overall SINR during a time slot. The general user selection formulation is coupled with power allocation, given its impact on the SE, thus entailing a joint optimization problem. However, as the resulting joint optimization problem is computationally hard to solve,

it is common to split it into a *user selection* followed by a *power allocation* problem [9, 43, 44]. Still, selecting users whose transmissions have the highest SINRs is computationally complex, requiring an *exhaustive search* (ES) across many possible combinations of users. For conventional *multi-user multiple-input multiple-output* (MU-MIMO) systems, the most popular user selection algorithms are the *greedy zero-forcing dirty-paper algorithm* [45], *greedy scheduler with equal power allocation* [46], and *semi-orthogonal selection* (SOS) [43]. While the former ones perform user selection by maximizing directly the DL SE of the system, the latter selects users in order to yield a subset comprised of the "most orthogonal" channel vectors. The greedy zero-forcing dirty-paper and greedy scheduler with equal power allocation algorithms are based on the *dirty paper coding* (DPC) [47], which achieves the capacity of DL MIMO systems with Gaussian channels [48]. However, the implementation of DPC is problematic in practical situations due to the high computational burden, particularly for a large number of antennas and users [43].

The SOS algorithm, on the other hand, does not suffer from the aforementioned problems and, therefore, has been widely employed for user selection in massive MIMO systems. In [49], the SOS algorithm is used along with an antenna selection algorithm to solve a joint antenna and user selection problem. In [50], the SOS algorithm is used for user scheduling in a scenario where the number of antennas is slightly larger than the number of users. Moreover, a new version of the SOS algorithm, called *massive MIMO pair-wise SOS* algorithm is proposed, in which the SOS is initialized with the full set of users instead of an empty set, which may lead to reduced complexity when the system has more antennas than users. In [51], the SOS algorithm is used to select users in a crowded environment, simulating an IoT application. Additionally, a new version of the SOS algorithm, called *modified semi-orthogonal selection* (M-SOS) is proposed in which the SOS operation is no longer limited by the number of antennas, but by a given number of users to be selected.

Unlike the SOS algorithm, there exist several user selection solutions aimed directly at the massive MIMO case, such as the *random selection* (RS) [52, 53], the *delete the minimum lambda* (DML) [54], and the *correlation-based selection* (CBS) [9, 44, 55] approaches. The RS approach is a naïve way to perform user selection without optimizing any performance criterion. The DML is a decremental user selection algorithm based on *zero-forcing* (ZF) precoding and, consequently, it can only be used in cases where the number of users is smaller than the number of antennas, not being suitable for applications involving crowded scenarios. The CBS algorithm, on the other hand, selects users based on the correlation between pairs of users' channels, iteratively removing those users that strongly interfere with one another. Hence, the CBS aims to maximize the SINR gain of a particular user and does not guarantee the best achievable overall SINR gain for the whole system.

Other classes of algorithms that can be used to perform user selection in massive MIMO are the *user grouping* algorithms [10, 56, 57] and recently proposed *machine learning-based selection* algorithms [58]. These algorithms separate users into clusters, serving a reduced number of users per cluster in the same time-frequency resource in order to decrease the interference between users within the same cluster. However, user grouping algorithms are more focused on the precoder design than on the selection of the users inside the clusters.

In summary, most of the aforementioned user selection algorithms depend on particular precoding and/or power allocation schemes, not being suitable to a wide range of applications involving massive MIMO systems. Therefore, in this thesis, we focus on the SOS and CBS algorithms as they require only CSI and are not constrained to a single precoding scheme. Moreover, the user selection algorithms can be categorized into two distinct classes: *large-scale fading aware* (LSFA) and *small-scale fading aware* (SSFA) algorithms. The LSFA algorithms are usually good solutions for massive MIMO systems under NLoS propagation since the small-scale fading does not affect the system performance under this type of propagation [59]. For the LoS case, due to the characteristics of the channel, the small-scale fading is not averaged out like in the NLoS propagation and it impacts the system performance, requiring the use of SSFA algorithms. Although the small-scale fading has a significant impact on the performance of massive MIMO systems under LoS propagation, the large-scale fading also plays a significant role in the SE of massive MIMO systems operating in this environment. Disregarding the large-scale fading, even in an LoS propagation environment, is equivalent to assuming that all users are equidistant from the base station and experience the same level of shadowing, which is not a reasonable approximation in practical applications. To the best of our knowledge, no such algorithms that can exploit both types of fading are reported in the literature.

In Chapter 4, we propose a new user selection approach based on *inter-channel interference* (ICI), namely *inter-channel interference-based selection* (ICIBS), that accounts for the ICI in a global manner, differently from other user selection algorithms. Morever, we propose another new user selection algorithm which relies on a metric that jointly considers the small- and large-scale fading effects, called *fading-ratio-based selection* (FRBS). The proposal is a generalization of the ICIBS, having improved maximum throughput and similar computational complexity. FRBS uses a ratio composed by the ICI and the square root of the large-scale fading. The idea behind this heuristic approach is to exploit the impact of the small- and large-scale fading effects for a given user. In Chapter 5, simulation results show that when compared to the competing algorithms, the proposed ICIBS approach provides an improvement of at least 10.9% in the maximum throughput and 7.7% in the 95PT

when half of the users were selected. Furthermore, in Chapter 6, simulation results show that the use of FRBS with ZF precoder results in 26.28% improvement in the maximum throughput when compared with SSFA algorithms, and 35.39% improvement when compared with LSFA.

### 1.2.3 Cell-free Massive MIMO

Although the benefits of CF massive MIMO are well articulated in the literature, there are still open research questions regarding the best appropriate network architecture to deploy these systems. CF massive MIMO systems can be deployed in three different ways: centralized, distributed, and semi-distributed [60]. In the centralized implementation, the APs simply work as relays, forwarding the received signals to the CPU that processes and detects the signal. This implementation allows the use of more powerful signal processing algorithms at the CPU that yields better SE, albeit results in increased fronthaul traffic since it requires exchange of CSI [61, 62]. In the distributed case, the APs are responsible for the major part of the signal processing, whereas the CPU is only responsible for the detection. In this implementation the fronthaul traffic is minimized, but the SE performance is degraded due to the distributed signal processing since the APs only have access to their signal information. The semi-distributed operation lies in between the other two where the signal processing is split among the APs and the CPU. This deployment guarantees a good trade-off between SE performance and fronthaul traffic. However, some of the assumptions made while studying the performance of the CF massive MIMO systems considering these network deployment architectures, such as all APs serving all *user equipment*s (UEs) [29, 63] and perfect hardware components [35, 64], are not realistic in practical systems.

The assumption that all APs serve all UEs is energy inefficient when realized in practical systems [34]. This inefficiency is due to the fact that APs may excessively waste energy by serving distant UEs. This assumption also makes the network unscalable, i.e., the complexity of the signal processing algorithms increases with the number of UEs, hindering their use in scenarios with large number of UEs [35]. The original algorithms proposed for CF massive MIMO systems fail in providing proper scalability, mainly regarding power allocation. This issue needs to be addressed when new algorithms are proposed for CF massive MIMO systems in order to make these systems viable for practical deployment [23, 35, 65]. Moreover, the main contributions in CF massive MIMO rely on ideal hardware [29, 35, 64], for example, infinite-resolution *analog-to-digital* (AD) and *digital-to-analog* (DA) converters. The ideal hardware assumption is unrealistic since the hardware cost dramatically increases with the number of APs, which may be a bottleneck for the practical

implementations of CF massive MIMO systems, calling for low-quality hardware. In practice, the hardware may induce signal distortion that affects the SE and the EE of the CF massive MIMO systems [66]. In [66], the authors studied the effect of general hardware impairment in the APs and UEs on the performance of CF massive MIMO systems. Additionally, practical hardware components in the CPU yield finite-capacity fronthaul links, which hinders the use of some signal processing algorithms that demand a high-rate communication between the CPU and APs. One of the critical components in the CPU are the AD converters that introduce nonlinearities due to the quantization process. The effect of this impairment has already been studied in some works [67–71].

In Chapter 7, we present a semi-distributed version of a CF massive MIMO network, where both the CPU and the APs suffer from the effects caused by the AD converters. We evaluate the performance of such network operating over a Rician fading channel. In order to evaluate the *uplink* (UL) performance of this network, we derive the *minimum mean squared error* (MMSE) channel estimator and its scalable version that limits the interference from the other users. Moreover, we derive the general expression of the UL SINR for any given linear combiner. This expression is useful because it allows us to analyze the performance of different combiners with different levels of distortions affecting the network. Additionally, we present the suboptimal *local partial minimum mean squared error* (LP-MMSE) combiner taking into account the effect of the AD converters. This combiner is a scalable version of the of the MMSE, which uses only the information from the UEs that are being served by the AP that is processing the signal. Furthermore, we derive the optimum *large-scale fading decoding* (LSFD) vector for this scenario as well as its nearly optimum scalable version.

## 1.3 Contributions

The specific contributions of this thesis are:

1. **Study of massive MIMO under LoS propagation:** This thesis provides a comprehensive study of massive MIMO systems under LoS propagation, covering some of the most fundamental aspects of massive MIMO systems, such as the FP and the SE. Additionally, the thesis shows the main differences between NLoS and LoS propagation models in terms of FP and extends previous results from the literature. Furthermore, an extensive set of simulation results considering several user selection algorithms, different linear precoders, various setups covering low and high interference levels, and also the effect of imperfect CSI are provided. To the best of our knowledge, there is no other

work providing such a detailed review and study of massive MIMO systems under LoS propagation model. This contribution is presented in Chapter 2.

2. **Power allocation:** We use the Perron-Frobenius theory [72] to explain why the bisection search algorithm may fail to converge to an optimal point, depending on the choice of the initial search interval. In addition, we use the Perron-Frobenius theory to derive an initial search interval for the algorithm in [9] that guarantees optimality by providing a power allocation vector for a massive MIMO system with *maximum ratio transmitter* (MRT) at each iteration of the bisection search. Moreover, we propose a simple procedure, herein called *bound test* (BT), which leads to reduced computational complexity. The BT procedure is a consequence of the Gershgorin circle theorem [72] that allows us to avoid the eigenvalue decomposition in some cases, decreasing the computational complexity. Furthermore, BT still reduces the computational load by providing a tight search interval when the eigenvalue decomposition is indeed required. Simulation results show that the proposed initial search interval leads to reduced computational complexity. This contribution is presented in Chapter 3.

3. **Literature review on user selection**: This thesis provides a comprehensive literature review of user selection algorithms for massive MIMO focusing on two important techniques, namely, the SOS and CBS algorithms. These algorithms work quite well in the massive MIMO scenario and require only CSI, thus they are not constrained to some specific precoding and power allocation schemes. These two techniques are covered in detail and a thorough analysis of their computational complexity is provided. This contribution is presented in Chapter 4.

4. **ICIBS algorithm:** This thesis proposes a new user selection algorithm based on ICI, called ICIBS, which has the same flexibility of SOS and CBS algorithms. However, unlike SOS and CBS, the ICIBS is designed to address those situations in which there are many users interfering with each other, which yields higher interference levels. In these cases, a significant advantage of ICIBS over the other algorithms can be observed. On the other hand, when dealing with lower interference levels, e.g., when the users were spread over the cell, the ICIBS performed as good as the other algorithms. Further, the computational complexity of ICIBS is much lower than that of SOS, and only slightly higher than that of CBS. This contribution is presented in Chapters 4 and 5.

5. **FRBS algorithm:** In this thesis, we also propose another user selection algorithm which relies on a metric that jointly considers the small- and large-scale fading effects, called FRBS. The proposal is a generalization of the ICIBS, having improved maximum throughput and similar computational complexity. FRBS uses a ratio composed by the ICI and the square root of the large-scale fading. The idea behind this heuristic approach is to exploit the impact of the small- and large-scale fading effects for a given user. Moreover, we present results for the SOS algorithm using the large-scale fading information, which to the best of our knowledge has not been done before. Results show that FRBS yields an SE close to the one obtained via the ES approach and outperforms the competing algorithms in terms of cost-benefit relation, i.e., FRBS achieves similar throughput with significantly lower computational complexity. Additionally, FRBS improves the maximum throughput of SSFA and LSFA user selection algorithms by at least 25.17% when combined with the ZF precoder. This contribution is presented in Chapters 4 and 6.

6. **Effects of quantization in CF massive MIMO:** We evaluate the UL performance of CF massive MIMO systems where the quantization effects are taken into consideration in both the CPU and the APs. This model closely represents a practical implementation of CF massive MIMO, which is the *radio stripe system* [23]. We use a semi-distributed implementation where, by reducing the fronthaul traffic, we aim to minimize the quantization effects on the performance of the system. An expression for the UL SE of a scalable semi-distributed CF massive MIMO system under correlated Rician fading is derived based on the channel statistics, taking into account the effect of the channel estimation errors due to pilot contamination and quantization distortion of practical hardware. Moreover, we derive the MMSE estimate for the Rician fading channel taking into account the quantization effects. Additionally, we derive the optimal LSFD vector for the semi-distributed implementation. Further, we present scalable version for both the MMSE channel estimate and the LSFD vector.

## 1.4 Publications

The contributions of Chapter 3 were published in the IEEE Communications Letters [J1]. The contributions of Chapter 2, part of Chapter 4 regarding the literature review and the ICIBS algorithm, and Chapter 5 were published in URSI GASS 2021 [C1] and in IEEE Open Journal of the Communications Society [J2]. Part of Chapter 4 regarding the FRBS algorithm and Chapter 6 were accepted for publica-

tion in the Wireless Networks [J3].

## 1.5 Notation

Throughout this work, vectors and matrices are represented in bold face with lowercase and uppercase letters, respectively. The symbols $\mathbb{C}$, $\mathbb{R}$, $\mathbb{R}_+$, $\mathbb{Z}$, and $\mathbb{N}$ denote the sets of complex, real, non-negative real, integer, and natural numbers, respectively. The set of $\mathbb{C}^{M\times K}$ denotes all $M \times K$ matrices comprised of complex-valued entries. The notation $|\mathcal{X}|$ stands for the cardinality of the $\mathcal{X}$. The symbol $\mathbf{I}_M$ denotes an $M \times M$ identity matrix and $\mathbf{0}_{M\times K}$ denotes an $M \times K$ zero matrix.

The vector $\mathbf{x} \in \mathbb{C}^{M\times 1}$ can be represented as

$$\mathbf{x} = \begin{bmatrix} x_1 & x_2 & \cdots & x_M \end{bmatrix}^{\mathrm{T}},$$

and the matrix $\mathbf{X} \in \mathbb{C}^{M\times K}$ can be represented as

$$\mathbf{X} = \begin{bmatrix} [\mathbf{X}]_{11} & [\mathbf{X}]_{12} & \cdots & [\mathbf{X}]_{1K} \\ [\mathbf{X}]_{21} & [\mathbf{X}]_{22} & \cdots & [\mathbf{X}]_{2K} \\ \vdots & \vdots & \ddots & \vdots \\ [\mathbf{X}]_{M1} & [\mathbf{X}]_{M2} & \cdots & [\mathbf{X}]_{MK} \end{bmatrix},$$

or

$$\mathbf{X} = \begin{bmatrix} \mathbf{x}_1 & \mathbf{x}_2 & \cdots & \mathbf{x}_K \end{bmatrix}.$$

The notation $\mathbf{X}^{\mathrm{T}}$, $\mathbf{X}^*$, $\mathbf{X}^{\mathrm{H}}$, and $\mathbf{X}^{-1}$ stand for transpose, conjugate, conjugate transpose, and inverse operations on $\mathbf{X}$, respectively. $\mathsf{Diag}\,(\mathbf{x})$ is a diagonal matrix with $\mathbf{x}$ on its main diagonal, and $\mathsf{span}\,\{\mathbf{x}_1, \cdots, \mathbf{x}_K\}$ is the set of all linear combinations of the vectors $\mathbf{x}_1, \cdots, \mathbf{x}_K$. The matrix $\mathbf{X}_{\mathcal{X}} \in \mathbb{C}^{|\mathcal{X}|\times|\mathcal{X}|}$ is a matrix whose rows and columns are selected from $\mathbf{X} \in \mathbb{C}^{M\times K}$ by the elements of $\mathcal{X}$. $\mathsf{abs}\,(\mathbf{X})$ is a matrix given by

$$\mathsf{abs}\,(\mathbf{X}) = \begin{bmatrix} |x_{11}| & |x_{12}| & \cdots & |x_{1K}| \\ |x_{21}| & |x_{22}| & \cdots & |x_{2K}| \\ \vdots & \vdots & \ddots & \vdots \\ |x_{M1}| & |x_{M2}| & \cdots & |x_{MK}| \end{bmatrix}.$$

The symbol $\otimes$ stands for the Kronecker product. The symbols $\mathcal{CN}(\mathbf{m}, \mathbf{C})$ and $\mathcal{U}(a, b)$ respectively denote a circularly symmetric Gaussian distribution with mean $\mathbf{m}$ and covariance matrix $\mathbf{C}$ and a uniform distribution between $a$ and $b$. The notations $\mathsf{E}\,\{x\}$ and $\mathsf{Var}\,\{x\}$ stand for the expected value and variance of $x$, respectively. The notations $\mathsf{Cov}\,\{\mathbf{x}\}$ and $\mathsf{Cov}\,\{\mathbf{x}, \mathbf{y}\}$ stand for the covariance matrix of $\mathbf{x}$ and the cross-covariance of $\mathbf{x}$ and $\mathbf{y}$, respectively. The notation $x \xrightarrow{p} y$ means that $x$

converges to $y$ in probability.

# Part I

# Cellular Massive MIMO Systems

# Chapter 2

# Massive MIMO: A Brief Overview

## 2.1 Introduction

Massive MIMO, also called large-scale antenna wireless communication system, was first proposed by Marzetta in [1]. As mentioned in Chapter 1, massive MIMO systems arose as a disruptive technology, with very promising results in terms of sum-rate capacity and spectral efficiency [2, 5, 73–75]. The main concept of massive MIMO is equipping the BS with a large number of antennas and serving multiple terminals using the same time-frequency resource [4], which is the main difference between massive MIMO systems and conventional MU-MIMO systems. By using very large arrays at the BS, massive MIMO systems can achieve nearly optimal capacity with simple linear processing techniques. Conventional MU-MIMO can only achieve the same capacity levels by using expensive nonlinear signal processing techniques. This chapter presents the basic concepts of massive MIMO systems under LoS propagation, highlighting the main differences among massive MIMO systems under NLoS propagation.

## 2.2 Massive MIMO Channel

The massive MIMO channel can be written as [1]

$$\mathbf{G} = \mathbf{H}\,\mathsf{Diag}\left(\boldsymbol{\beta}\right)^{1/2}, \tag{2.1}$$

where $\mathbf{H} \in \mathbb{C}^{M\times K}$ is the small-scale fading matrix and $\boldsymbol{\beta} \in \mathbb{R}_{+}^{K\times 1}$ is the large-scale fading vector. For massive MIMO systems, the most common models for the small-scale fading are the i.i.d. Rayleigh fading and the *uniformly random line-of-sight* (UR-LoS). These two types of channels model extreme propagation scenarios; for example, the UR-LoS models an LoS scenario whereas the i.i.d. Rayleigh models a NLoS scenario. The former is more suitable for short-range communications, and

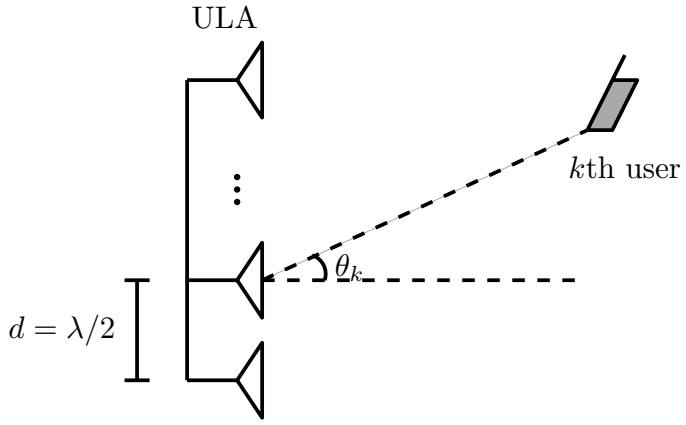


Figure 2.1: Line-of-sight channel between the $k$th user and the $M$-antenna ULA.

the latter is more suited for long-range communications. In practice, the actual propagation channel is likely to lie in-between these two extreme cases [4].

The UR-LoS channel vector with the $M$-antenna standard *uniform linear array* (ULA) illustrated in Fig. 2.1 is given by[1]

$$\mathbf{g}_k = \sqrt{\beta_k}\mathbf{h}_k, \ \forall\, k \in \mathcal{K}, \tag{2.2}$$

where $\beta_k \in \mathbb{R}_+$ is the large-scale coefficient for the $k$th user, $\mathbf{h}_k \in \mathbb{C}^{M\times 1}$ is the small-scale fading vector for the $k$th user denoted by [76]

$$\mathbf{h}_k = \mathrm{e}^{\mathrm{j}\phi_k}\left[1 \quad \mathrm{e}^{-\mathrm{j}\pi\sin(\theta_k)} \quad \cdots \quad \mathrm{e}^{-\mathrm{j}(M-1)\pi\sin(\theta_k)}\right]^{\mathrm{T}}, \tag{2.3}$$

$\phi_k \sim \mathcal{U}(-\pi,\ \pi)$ is the phase shift associated with the array and the $k$th user, $\theta_k \sim \mathcal{U}(-\pi,\ \pi)$ is the AoA for the $k$th user, and $\mathcal{K} = \{1, 2, \cdots, K\}$ is the set of all user indices.

Another popular array used in massive MIMO system is the *uniform rectangular array* (URA). This type of array, in addition to the azimuth angle, can also steer a beam in the elevation angle. Further, the use of URA enables the placement of the same number of antennas of ULA in a smaller area, allowing its use in space-limited scenarios. The small-scale fading vector for this array is given by [9]

$$\mathbf{h}_k = \mathrm{e}^{\mathrm{j}\phi_k}\mathbf{h}_k^{(1)} \otimes \mathbf{h}_k^{(2)} \in \mathbb{C}^{M_1 M_2 \times 1}, \tag{2.4}$$

[1] A standard ULA is an array in which the distance between adjacent antennas $d$ is equal to half of the signal wavelength $\lambda$ [76].

where

$$\mathbf{h}_k^{(1)} = \left[1 \ \mathrm{e}^{-\mathrm{j}\pi\sqrt{1-\nu_k^2}\cos(\psi_k)} \ \ldots \ \mathrm{e}^{-\mathrm{j}(M_1-1)\pi\sqrt{1-\nu_k^2}\cos(\psi_k)}\right]^{\mathrm{T}},$$
$$\mathbf{h}_k^{(2)} = \left[1 \ \mathrm{e}^{-\mathrm{j}\pi\sqrt{1-\nu_k^2}\sin(\psi_k)} \ \ldots \ \mathrm{e}^{-\mathrm{j}(M_2-1)\pi\sqrt{1-\nu_k^2}\sin(\psi_k)}\right]^{\mathrm{T}},$$

$M_1 \in \mathbb{N}$ and $M_2 \in \mathbb{N}$ are the number of antennas in $x$- and $y$-axes, $\psi_k \sim \mathcal{U}(-\pi, \ \pi)$ is the elevation angle for the $k$th user, and $\nu_k = \sin(\theta_k)$.

This thesis adopts the ULA as standard for the derivations due to its mathematical tractability. In practice, however, the use of ULAs may be limited for some frequency ranges due to the physical space required to deploy a ULA with so many antennas. On the other hand, the ULA yields better SE than other arrays such as the URA and the *uniform circular array* (UCA) in practical scenarios, with and without LoS [17, 77–79]. Moreover, the ULA simplifies the *inter-channel interference* model, which plays a fundamental role in user selection algorithms.

***Remark 2.1***. One of the main differences between the i.i.d. Rayleigh channel and the UR-LoS channel is the $\ell_2$-norm of their small-scale fading vectors. For the UR-LoS channel, $\|\mathbf{h}_k\|_2^2 = M$, for any value of $M$. However, for the i.i.d. Rayleigh channel, $\|\mathbf{h}_k\|_2^2 \xrightarrow{p} M$, as $M \longrightarrow \infty$, which is the so-called *channel hardening* property [3].

### 2.2.1 Favorable Propagation

Intuitively, to maximize the performance of a wireless communication system from an information-theoretic perspective, the massive MIMO channel vectors should be as different as possible, according to some appropriate metric. This appropriate metric is the so-called *favorable propagation* offered by the channel [4, 8, 80], defined as

$$\mathbf{h}_k^{\mathrm{H}}\mathbf{h}_{k'} = 0, \quad \forall\, k, k' \in \mathcal{K}, \text{ with } k \neq k', \tag{2.5}$$

meaning that FP requires the massive MIMO channel vectors corresponding to different users to be pair-wise orthogonal. Since there are many cases that violate the FP condition, as it will be discussed later, it is interesting to measure how close two channel vectors are from being orthogonal. To do so, we define

$$r_{kk'} = \frac{|\mathbf{h}_k^{\mathrm{H}}\mathbf{h}_{k'}|}{\|\mathbf{h}_k\|_2 \, \|\mathbf{h}_{k'}\|_2}, \tag{2.6}$$

i.e., $r_{kk'}$ is the magnitude of the channel correlation coefficient. For the UR-LoS channel, $r_{kk'}$ is given in *Theorem* 2.1.

**Theorem 2.1**

*The magnitude of the channel correlation coefficient of a UR-LoS massive MIMO channel is given by [8]*

$$r_{kk'} = \frac{1}{M}\left|\frac{\sin\left(M\frac{\pi}{2}(\sin\theta_{k'} - \sin\theta_k)\right)}{\sin\left(\frac{\pi}{2}(\sin\theta_{k'} - \sin\theta_k)\right)}\right|. \tag{2.7}$$

From Theorem 2.1, the UR-LoS channel offers FP when (2.7) is equal to zero for all $k, k' \in \mathcal{K}$, with $k \neq k'$. Thus, the numerator of (2.7) must be equal to zero and the denominator of (2.7) must be nonzero. The condition for which FP holds in an LoS channel is given in the following corollary of *Theorem* 2.1.

**Corollary *2.1***

*The UR-LoS channel offers favorable propagation iff for all $k' \in \mathcal{K} \setminus \{k\}$, $\exists\ n_{k'} \in \{\pm 1, \pm 2, \cdots, \pm(M-1)\}$ such that*

$$\theta_{k'} = \arcsin\left(\sin\theta_k + \frac{2n_{k'}}{M}\right), \tag{2.8}$$

*and all of the following three conditions are satisfied:*

1. $\theta_{k'} \neq \theta_k,\ \forall k, k' \in \mathcal{K},$ *with* $k \neq k'$;
2. $\theta_{k'} \neq \pi - \theta_k,\ \forall k, k' \in \mathcal{K},$ *with* $k \neq k'$;
3. *If* $\theta_k = \pm\pi/2$ *for some* $k \in \mathcal{K}$, *then* $\theta_{k'} \neq \mp\pi/2\ \forall k' \in \mathcal{K} \setminus \{k\}$.

*Proof.* An LoS environment offers FP when (2.7) is equal to zero for all $k, k' \in \mathcal{K}$, with $k \neq k'$. First, we show the condition that guarantees orthogonality between two users. Then, we expand this result to guarantee orthogonality for all users. The $k$th user and the $k'$th user are orthogonal when (2.7) is equal to zero, iff

$$\sin\left(M\frac{\pi}{2}(\sin\theta_{k'} - \sin\theta_k)\right) = 0, \tag{2.9}$$

and

$$\sin\left(\frac{\pi}{2}(\sin\theta_{k'} - \sin\theta_k)\right) \neq 0. \tag{2.10}$$

Equation (2.9) is zero if there exists an integer $n_{k'}$ such that

$$\sin\theta_{k'} - \sin\theta_k = \frac{2n_{k'}}{M}, \tag{2.11}$$

where $n_{k'} \in \{0, \pm 1, \cdots, \pm M\}$, as the left-hand side of the previous equation lies in the interval $[-2, 2]$. Solving this equation for $\theta_{k'}$, yields

$$\theta_{k'} = \arcsin\left(\sin\theta_k + \frac{2n_{k'}}{M}\right), \tag{2.12}$$

for some $n_{k'} \in \{0, \pm 1, \cdots, \pm M\}$. Moreover, to guarantee (2.10), we must satisfy

$$\sin\theta_{k'} - \sin\theta_k \notin \{-2, 0, 2\}, \tag{2.13}$$

which results in $\theta_{k'} \neq \theta_k$ and $\theta_{k'} \neq \pi - \theta_k$ for the case $\sin\theta_{k'} - \sin\theta_k \neq 0$, and if $\theta_k = \pm\pi/2$, then $\theta_{k'} \neq \mp\pi/2$ for the cases $\sin\theta_{k'} - \sin\theta_k \neq \pm 2$, respectively. To satisfy (2.11), (2.13) and (2.14) simultaneously. Therefore,

$$r_{kk'} = 0 \Longleftrightarrow \theta_{k'} = \arcsin\left(\sin\theta_k + \frac{2n_{k'}}{M}\right), \tag{2.14}$$

for some $n_{k'} \in \{\pm 1, \cdots, \pm(M-1)\}$.

Given that (2.12) does not depend on a specific pair of users, to have $r_{kk'} = 0$ for all $k, k' \in \mathcal{K}$, with $k \neq k'$, the users need to satisfy (2.14) for all $k, k' \in \mathcal{K}$, with $k \neq k'$. □

*Corollary **2.1*** is a more general version of the result provided in [8], in that we state the exact user positions that lead to favorable propagation.

Fig. 2.2 depicts the magnitude of the correlation coefficient with varying positions for two users, $K = 2$, for BS with $M = 50$ and 100 antennas. As can be observed, the massive MIMO channel offers favorable propagation or a moderately favorable propagation for different values of $\theta_1$ and $\theta_2$. However, due to the geometry of the array the users have high correlation when they have the same AoA, or when $\theta_1 = \pm\pi/2$ with $\theta_2 = \mp\pi/2$, or when $\theta_2 = -\theta_1 \pm \pi$. In these regions, the users have high mutual interference, degrading the SE performance of the massive MIMO system.

***Remark 2.2***. In order to validate *Corollary **2.1***, consider two users, $k_1$ and $k_2$, whose channels are orthogonal to the $k$th user, then

$$\theta_{k_1} = \arcsin\left(\sin\theta_k + \frac{2n_{k_1}}{M}\right), \tag{2.15}$$

$$\theta_{k_2} = \arcsin\left(\sin\theta_k + \frac{2n_{k_2}}{M}\right), \tag{2.16}$$

for some $n_{k_1}, n_{k_2} \in \{\pm 1, \cdots, \pm(M-1)\}$. The magnitude of the correlation coefficient

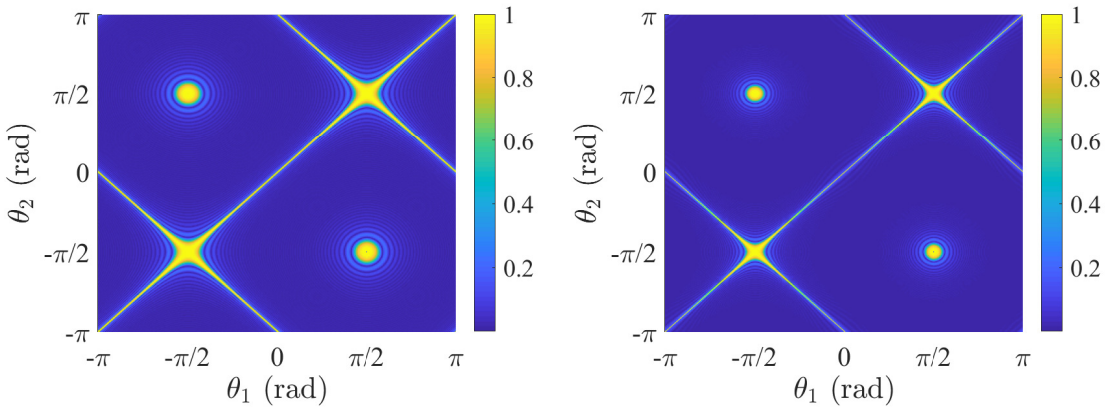


(a) $M = 50$ (b) $M = 100$

Figure 2.2: Magnitude of the correlation coefficient for $K = 2$ and $M \in \{50, 100\}$.

between these two users can be written as

$$r_{k_1 k_2} = \frac{1}{M} \left| \frac{\sin\left(M \frac{\pi}{2}(\sin\theta_{k_2} - \sin\theta_{k_1})\right)}{\sin\left(\frac{\pi}{2}(\sin\theta_{k_2} - \sin\theta_{k_1})\right)} \right|, \tag{2.17}$$

as long as the denominator is nonzero, which boils down to the condition $\sin\theta_{k_2} - \sin\theta_{k_1} \notin \{-2, 0, 2\}$. That means $\theta_{k_2} \neq \theta_{k_1}$, $\theta_{k_2} \neq \pi - \theta_{k_1}$, and if $\theta_{k_1} = \pm\pi/2$, then $\theta_{k_2} \neq \mp\pi/2$. Note that, based on (2.15) and (2.16), the sine function in the numerator of the correlation coefficient in (2.17) can be rewritten as $\sin(\pi(n_{k_2} - n_{k_1}))$, which is always zero. This result shows that if two different users are orthogonal to a third one, then they will themselves be orthogonal to one another if they satisfy *Corollary* ***2.1***. It is worth highlighting that although the set of possible values for $n_{k'}$ is comprised of $2(M-1)$ integers, as stated in *Corollary* ***2.1***, only $M-1$ of these values generate a valid solution. By a valid solution, we mean choices of $n_{k'}$ that, simultaneously, yield $\sin\theta_k + 2n_{k'}/M$ lying in $[-1, 1]$ and $\theta_{k'}$ satisfying the conditions stated in *Corollary* ***2.1***.

***Remark 2.3***. Another important difference between the i.i.d. Rayleigh and UR-LoS channels lies in the asymptotically favorable propagation property. The i.i.d. Rayleigh channel does not offer favorable propagation, only asymptotically favorable propagation, which is defined as [81]

$$\frac{1}{M}\mathbf{h}_k^{\mathrm{H}}\mathbf{h}_{k'} \xrightarrow{p} 0, \quad \forall\, k, k' \in \mathcal{K}, \text{ with } k \neq k', \tag{2.18}$$

and $K \ll M \longrightarrow \infty$. The asymptotically favorable propagation is one of the key factors to enable massive MIMO systems with linear precoding [81]. In general, UR-LoS channels can provide more favorable propagation condition than the i.i.d.

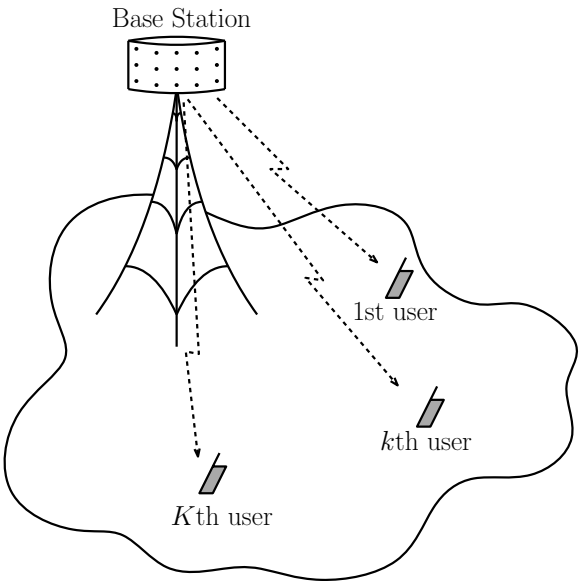


Figure 2.3: Massive MIMO system with an $M$-antenna BS serving $K$ single-antenna users.

Rayleigh channel. However, the UR-LoS channel model can also provide non favorable channels with a non negligible probability, especially when users are very close to each other in the cell. In these cases, employing a user selection algorithm is of paramount importance for the SE of the massive MIMO system.

***Remark 2.4***. For the URAs, there is an extra degree of freedom in addition to the azimuth angle, which is the elevation angle. This means that URAs can distinguish users (through their channel vectors exhibiting low correlation coefficient $r_{kk'}$) in both azimuth and elevation, whereas ULAs have only the azimuth, thus cannot distinguish users that have the same azimuth but different elevations. For a ULA and a URA with the same number of antennas, the ULA presents higher resolution in the azimuth coordinate and no resolution in the elevation coordinate. In comparison with the ULA, one can think that the URA trades resolution in the azimuth for resolution in the elevation coordinate/angle.

## 2.3 Downlink Transmission

Consider a single-cell massive MIMO system equipped with an $M$-antenna base station that serves $K$ single-antenna users as illustrated in Fig. 2.3. For a DL transmission operating in TDD mode, the received signal by the users can be expressed as

$$\mathbf{y} = \sqrt{\rho}\,\mathbf{G}^{\mathrm{T}}\mathbf{x} + \mathbf{n}, \tag{2.19}$$

where vector $\mathbf{y} \in \mathbb{C}^{K\times 1}$ contains the signals received by the $K$ users, $\rho \in \mathbb{R}_+$ is the DL *signal-to-noise ratio* (SNR), $\mathbf{G} \in \mathbb{C}^{M\times K}$ is the massive MIMO channel matrix, $\mathbf{x} \in \mathbb{C}^{M\times 1}$ is the precoded signal transmitted by the BS, and $\mathbf{n} \sim \mathcal{CN}(\mathbf{0}_{K\times 1},\ \mathbf{I}_K)$ is the additive noise.

The transmitted signal is digitally precoded (i.e., the number of radio-frequency chains is equal to the number of antennas) before the transmission in order to mitigate the effects of the channel. In massive MIMO, linear precoding is asymptotically optimal in terms of achievable spectral efficiency. The linear-precoded signal can be written as

$$\mathbf{x} = \mathbf{W}\mathsf{Diag}(\boldsymbol{\eta})^{1/2}\mathbf{s}, \tag{2.20}$$

where $\mathbf{W} \in \mathbb{C}^{M\times K}$ is the precoding matrix, whose columns $\mathbf{w}_k$ are normalized (i.e., $\|\mathbf{w}_k\|_2 = 1$), $\boldsymbol{\eta} \in \mathbb{R}_+^{K\times 1}$ is the power allocation vector, and $\mathbf{s} \sim \mathcal{CN}(\mathbf{0}_{K\times 1},\ \mathbf{I}_K)$ is the vector of transmitted symbols. Due to power limitations, the precoded signal is constrained by

$$\mathsf{E}\left\{\mathbf{x}^{\mathrm{H}}\mathbf{x}\right\} \leq 1, \tag{2.21}$$

yielding the following constraint for the power allocation coefficients

$$\sum_{k\in\mathcal{K}} \eta_k \leq 1, \tag{2.22}$$

where $\eta_k \in \mathbb{R}_+$ is the power allocation coefficient for the $k$th user.

## 2.4 Spectral Efficiency

Having CSI in the BS is critical for the proper operation of massive MIMO systems. The BS estimates the channel through an uplink pilot transmission by receiving $K$ signals related to orthogonal pilot signals of length (in samples) $\tau_{\mathrm{p}} \in \mathbb{N}$ sent by the users. Mathematically, the $k$th user transmits a pilot signal $\boldsymbol{\varphi}_k \in \mathbb{C}^{\tau_{\mathrm{p}}\times 1}$, which is the $k$th column of a matrix $\boldsymbol{\Phi} \in \mathbb{C}^{\tau_{\mathrm{p}}\times K}$ that satisfies $\boldsymbol{\Phi}^{\mathrm{H}}\boldsymbol{\Phi} = \mathbf{I}_K$. Then, the signal transmitted by the $k$th user is given by

$$\mathbf{x}_{\mathrm{p},k} = \sqrt{\tau_{\mathrm{p}}}\boldsymbol{\varphi}_k^{\mathrm{H}}, \tag{2.23}$$

where $\tau_c \geq \tau_p \geq K$, with $\tau_c \in \mathbb{N}$ being the coherence time in samples. Therefore, the signal received by the BS is given by

$$\begin{aligned}\mathbf{Y}_p &= \sqrt{\rho_p}\,\mathbf{G}\mathbf{X}_p + \mathbf{N}_p \\ &= \sqrt{\rho_p \tau_p}\,\mathbf{H}\mathsf{Diag}\left(\boldsymbol{\beta}\right)^{1/2}\boldsymbol{\Phi}^H + \mathbf{N}_p,\end{aligned} \tag{2.24}$$

where $\mathbf{X}_p = \sqrt{\tau_p}\boldsymbol{\Phi}^H$, $\rho_p \in \mathbb{R}_+$ is the pilot transmission SNR, and the entries of $\mathbf{N}_p \in \mathbb{C}^{M\times\tau_p}$ are i.i.d. circularly symmetric Gaussian distributed with zero mean and unitary variance. In order to estimate the channel of the $k$th user, the BS processes the received signal $\mathbf{Y}_p$ as follows:

$$\begin{aligned}\mathbf{y}'_{p,k} &= \mathbf{Y}_p\boldsymbol{\varphi}_k \\ &= \sqrt{\rho_p\tau_p}\,\mathbf{H}\mathsf{Diag}\left(\boldsymbol{\beta}\right)^{1/2}\boldsymbol{\Phi}^H\boldsymbol{\varphi}_k + \mathbf{N}_p\boldsymbol{\varphi}_k \\ &= \sqrt{\rho_p\tau_p\beta_k}\,\mathbf{h}_k + \mathbf{n}'_{p,k},\end{aligned} \tag{2.25}$$

where $\mathbf{n}'_{p,k} \sim \mathcal{CN}(\mathbf{0}_{M\times 1}, \mathbf{I}_M)$ since $\|\boldsymbol{\varphi}_k\|_2 = 1$. Finally, assuming the knowledge of the large-scale fading, the channel estimate for the $k$th user is obtained from $\mathbf{y}'_{p,k}$ and is given by

$$\begin{aligned}\hat{\mathbf{h}}_k &= \mathbf{h}_k + \frac{\mathbf{n}'_{p,k}}{\sqrt{\rho_p\tau_p\beta_k}} \\ &= \mathbf{h}_k + \boldsymbol{\varepsilon}_k,\ \forall k \in \mathcal{K},\end{aligned} \tag{2.26}$$

where $\boldsymbol{\varepsilon}_k \sim \mathcal{CN}(\mathbf{0}_{M\times 1},\ \sigma_\varepsilon^2\mathbf{I}_M)$ is the channel estimation error and $\sigma_\varepsilon^2 = 1/\rho_p\tau_p\beta_k$ represents the "quality" of the channel estimation. Moreover, this estimate is normalized to guarantee that $\left\|\hat{\mathbf{h}}_k\right\|_2 = \sqrt{M}$.

Under an LoS propagation scenario, the AoA is constant for few coherence time intervals. Thus, one can assume that the effective channel is known by the users. The SE for a massive MIMO UR-LoS channel is given in the following theorem.

**Theorem 2.2**

*The spectral efficiency of a massive MIMO system under LoS propagation with linear precoding and channel estimate as* (2.26) *is lower bounded by*

$$R_{\text{sum}} \geq \frac{1}{2}\left(1 - \frac{\tau_p}{\tau_c}\right)\sum_{k\in\mathcal{K}}\log_2\left(1+\gamma_k\right), \tag{2.27}$$

*where $\gamma_k \in \mathbb{R}_+$ is the DL SINR for the $k$th user given by*

$$\gamma_k = \frac{\rho\beta_k\eta_k|\hat{\mathbf{h}}_k^T\mathbf{w}_k|^2}{1+\rho\beta_k\sum\limits_{k'\in\mathcal{K}\setminus\{k\}}\eta_{k'}|\hat{\mathbf{h}}_k^T\hat{\mathbf{w}}_{k'}|^2 + \rho\beta_k\sigma_\varepsilon^2\sum\limits_{k'\in\mathcal{K}}\eta_{k'}},\ \forall k \in \mathcal{K}. \tag{2.28}$$

*Additionally, the equality holds when* $\sigma_\varepsilon^2 = 0$.

*Proof.* The signal received by the $k$th user $y_k$ in (2.19) can be expanded in

$$y_k = \sqrt{\rho\beta_k\eta_k}\hat{\mathbf{h}}_k^{\mathrm{T}}\mathbf{w}_k s_k + \sum_{k'\in\mathcal{K}\setminus\{k\}} \sqrt{\rho\beta_k\eta_{k'}}\hat{\mathbf{h}}_k^{\mathrm{T}}\mathbf{w}_{k'}s_{k'} - \sum_{k'\in\mathcal{K}} \sqrt{\rho\beta_k\eta_{k'}}\boldsymbol{\varepsilon}_k^{\mathrm{T}}\mathbf{w}_{k'}s_{k'} + n_k. \tag{2.29}$$

The first term in the RHS of (2.29) corresponds to the signal of interest, the second one to the interference caused from the other users, the third one to the interference caused by the uncertainty in the channel estimation, and the last one represents the additive noise.

Equation (2.29) is a point-to-point channel with deterministic channel $\hat{\mathbf{h}}_k^{\mathrm{T}}\mathbf{w}_k$ and additive non-Gaussian noise. Therefore, assuming that the $k$th user knows the equivalent channel $\mathbf{h}_k^{\mathrm{T}}\mathbf{w}_k$ for decoding the received signal, the DL SE is given by [4, 82]

$$R_{\mathrm{sum}} \geq \frac{1}{2}\left(1 - \frac{\tau_{\mathrm{p}}}{\tau_{\mathrm{c}}}\right)\sum_{k\in\mathcal{K}} \log_2\left(1+\gamma_k\right), \tag{2.30}$$

where $\tau_{\mathrm{p}} \in \mathbb{N}$ is the pilot time in samples, $\tau_{\mathrm{c}} \in \mathbb{N}$ is the coherence time in samples, and $\gamma_k \in \mathbb{R}_+$ is the DL SINR related to the $k$th user. In this case, due to the independence of the random variables, the SINR for the $k$th user is given by

$$\gamma_k = \frac{p_{\mathrm{s}}}{p_{\mathrm{n}} + p_{\mathrm{i}} + p_{\mathrm{u}}}, \tag{2.31}$$

where

$$p_{\mathrm{s}} = \mathsf{Var}\left\{\sqrt{\rho\beta_k\eta_k}\hat{\mathbf{h}}_k^{\mathrm{T}}\mathbf{w}_k s_k\right\}, \tag{2.32}$$

$$p_{\mathrm{n}} = \mathsf{Var}\left\{n_k\right\} = 1, \tag{2.33}$$

$$p_{\mathrm{i}} = \mathsf{Var}\left\{\sum_{k'\in\mathcal{K}\setminus\{k\}} \sqrt{\rho\beta_k\eta_{k'}}\hat{\mathbf{h}}_k^{\mathrm{T}}\mathbf{w}_{k'}s_{k'}\right\}, \tag{2.34}$$

$$p_{\mathrm{u}} = \mathsf{Var}\left\{\sum_{k'\in\mathcal{K}} \sqrt{\rho\beta_k\eta_{k'}}\boldsymbol{\varepsilon}_k^{\mathrm{T}}\mathbf{w}_{k'}s_{k'}\right\}. \tag{2.35}$$

Then, yielding (2.28).

When $\sigma_\varepsilon^2 = 0$, i.e., the BS has perfect CSI knowledge, (2.29) is reduced to

$$y_k = \sqrt{\rho\beta_k\eta_k}\hat{\mathbf{h}}_k^{\mathrm{T}}\mathbf{w}_k s_k + \sum_{k'\in\mathcal{K}\setminus\{k\}} \sqrt{\rho\beta_k\eta_{k'}}\hat{\mathbf{h}}_k^{\mathrm{T}}\mathbf{w}_{k'}s_{k'} + n_k, \tag{2.36}$$

which corresponds to a point-to-point channel with deterministic channel $\hat{\mathbf{h}}_k^{\mathrm{T}}\mathbf{w}_k$ and

additive Gaussian noise. Therefore, assuming that the $k$th user knows the equivalent channel $\mathbf{h}_k^{\mathrm{T}}\mathbf{w}_k$ for decoding the received signal, the DL SE is given by [4, 82]

$$R_{\mathrm{sum}} = \frac{1}{2}\left(1 - \frac{\tau_{\mathrm{p}}}{\tau_{\mathrm{c}}}\right)\sum_{k\in\mathcal{K}} \log_2\left(1+\gamma_k\right), \tag{2.37}$$

where $\gamma_k$ is given by (2.28) with $\sigma_\varepsilon^2 = 0$. □

Another figure of merit commonly used to evaluate the performance of DL massive MIMO systems is the min-SE, which is given by

$$R_{\mathrm{min}} = 0.5\left(1 - \frac{\tau_{\mathrm{p}}}{\tau_{\mathrm{c}}}\right)\log_2\left(1 + \min_{k\in\mathcal{K}} \gamma_k\right). \tag{2.38}$$

Equation (2.27) evaluates the performance of the network as whole. On the other hand, equation (2.38) evaluates the performance of the user with the worst SE. The min-SE is really useful for the design of practical systems since each user has a *quality of service* (QoS) to be attained in practical networks, such as a minimum throughput to be attained. Furthermore, the min-SE is the cost function used in the MMFPA-based algorithms.

***Remark 2.5***. The LoS propagation is expected to occur within the context of short-range communications, while inter-cell interference is expected to be i.i.d. Rayleigh distributed [9, 15]. Thus, in a multi-cell model, the interference from different cells, i.e., pilot contamination, can be incorporated in the channel estimation error since the multi-cell interference is i.i.d. Rayleigh distributed. However, the single-cell scenario is frequently adopted since it can easily isolate the effect of the LoS channel [9, 10, 83].

***Remark 2.6***. Although in this section we used uplink pilot transmission to estimate $MK$ complex-valued coefficients, it is possible to use different estimation approaches since we are dealing with LoS propagation. Under LoS propagation, it is possible to estimate only the real-valued AoAs and the complex gain for each user. This approach is usually less computationally expensive and demands less pilot signals, which leads to a better usage of the communication resources in general. However, it is important to highlight that such approach would provide a different model to (2.26), (2.27), and (2.28).

## 2.5 Precoding Schemes

Precoding is a crucial step for the DL operation of massive MIMO systems that is employed to mitigate multi-user interference. Linear precoding schemes are particularly useful for massive MIMO systems, achieving the same performance of the dirty paper code in the asymptotic case [5]. By definition, the precoding vectors have $\|\mathbf{w}_k\|_2^2 = 1$, and hence, every linear precoding vector can be written as

$$\mathbf{w}_k = \frac{\mathbf{v}_k}{\|\mathbf{v}_k\|_2}. \tag{2.39}$$

### 2.5.1 Maximum Ratio Transmitter

The maximum ratio transmitter aims to amplify the signal of interest for each user, disregarding the impact of this amplification on other users. In the *multiple-input single-output* (MISO) case, the MRT is the precoding scheme that yields the highest capacity for this type of system by maximizing the SNR of the desired user. For the massive MIMO case, the MRT precoding technique can deliver high throughput in the asymptotic case [1]. The MRT precoding vector is given by [4]

$$\mathbf{w}_k^{\mathrm{MRT}} = \frac{\hat{\mathbf{h}}_k^*}{\sqrt{M}}, \ \forall \ k \in \mathcal{K}. \tag{2.40}$$

The DL SE of a massive MIMO UR-LoS channel with MRT can be easily derived from (2.27), by replacing $\mathbf{w}_k$ with $\mathbf{w}_k^{\mathrm{MRT}}$. Therefore, the SE is bounded by

$$R_{\mathrm{sum}}^{\mathrm{MRT}} \geq \frac{1}{2}\left(1 - \frac{\tau_{\mathrm{p}}}{\tau_{\mathrm{c}}}\right) \sum_{k \in \mathcal{K}} \log_2\left(1 + \gamma_k^{\mathrm{MRT}}\right), \tag{2.41}$$

where $\gamma_k^{\mathrm{MRT}} \in \mathbb{R}_+$ is denoted by

$$\gamma_k^{\mathrm{MRT}} = \frac{\rho M \beta_k \eta_k}{1 + \rho \beta_k M \sum\limits_{k' \in \mathcal{K} \setminus \{k\}} \eta_{k'} r_{kk'}^2 + \rho \beta_k \sigma_\varepsilon^2 \sum\limits_{k' \in \mathcal{K}} \eta_{k'}}. \tag{2.42}$$

It is worth highlighting the dependence of the small-scale fading in (2.41). The magnitude of the channel correlation can be used as a measure of favorable propagation for the massive MIMO channel. In this case, a non-favorable channel can have a significant impact on the system performance. For the i.i.d. Rayleigh channel, the favorable propagation condition is basically impacted by the number of antennas $M$. However, for the UR-LoS channel, even with a very large number of antennas, the system is still susceptible to have a non-favorable channel as explained in Subsection 2.2.1.

### 2.5.2 Zero-forcing

In the zero-forcing precoder, the precoding vectors $\mathbf{w}_k$ are selected in order to satisfy the zero-interference condition $\mathbf{h}_k^{\mathrm{T}}\mathbf{w}_{k'} = 0 \ \forall k' \in \mathcal{K} \setminus \{k\}$. The zero-interference condition can be achieved by using the Moore-Penrose inverse of the channel matrix as the precoding matrix. In the case of full CSI knowledge, the ZF precoding can perfectly eliminate the interference among the users. The ZF precoding vector is given by [4]

$$\mathbf{w}_k^{\mathrm{ZF}} = \frac{\hat{\mathbf{H}}^*\mathbf{r}_k}{\left\|\hat{\mathbf{H}}^*\mathbf{r}_k\right\|_2}, \ \forall \ k \in \mathcal{K}, \tag{2.43}$$

where $\mathbf{r}_k$ is the $k$th column of $\mathbf{R} = (\hat{\mathbf{H}}^{\mathrm{T}}\hat{\mathbf{H}}^*)^{-1}$. Note that the Moore-Penrose inverse computation is only possible if $M \geq K$ and $\hat{\mathbf{H}}^{\mathrm{T}}$ is a full-row rank matrix.

**Corollary *2.2***

*The DL SE of a massive MIMO UR-LoS channel with ZF precoding is lower bounded by*

$$R_{\mathrm{sum}}^{\mathrm{ZF}-1} \geq \frac{1}{2}\left(1 - \frac{\tau_{\mathrm{p}}}{\tau_{\mathrm{c}}}\right)\sum_{k\in\mathcal{K}}\log_2\left(1+\gamma_k^{\mathrm{ZF}-1}\right), \tag{2.44}$$

*where* $\gamma_k^{\mathrm{ZF}-1} \in \mathbb{R}_+$ *is denoted by*

$$\gamma_k^{\mathrm{ZF}-1} = \frac{\rho\beta_k\eta_k}{[(\hat{\mathbf{H}}^{\mathrm{T}}\hat{\mathbf{H}}^*)^{-1}]_{kk}\left(1+\rho\beta_k\sigma_\varepsilon^2\sum\limits_{k'\in\mathcal{K}}\eta_{k'}\right)}. \tag{2.45}$$

*Proof.* Using (2.43) in (2.28), we have

$$\gamma_k^{\text{ZF-1}} = \frac{\rho\beta_k\eta_k\left|\dfrac{\hat{\mathbf{h}}_k^{\mathrm{T}}\hat{\mathbf{H}}^*\mathbf{r}_k}{\left\|\hat{\mathbf{H}}^*\mathbf{r}_k\right\|_2}\right|^2}{1+\rho\beta_k\sum\limits_{k'\in\mathcal{K}\setminus\{k\}}\eta_{k'}\left|\dfrac{\hat{\mathbf{h}}_k^{\mathrm{T}}\hat{\mathbf{H}}^*\mathbf{r}_{k'}}{\left\|\hat{\mathbf{H}}^*\mathbf{r}_{k'}\right\|_2}\right|^2+\rho\beta_k\sigma_\varepsilon^2\sum\limits_{k'\in\mathcal{K}}\eta_{k'}}. \tag{2.46}$$

The vector $\mathbf{r}_k$ can be written as

$$\mathbf{r}_k = (\hat{\mathbf{H}}^{\mathrm{T}}\hat{\mathbf{H}}^*)^{-1}\mathbf{e}_k, \tag{2.47}$$

where $\mathbf{e}_k$ is the $k$th column of $\mathbf{I}_K$. Using (2.47) in (2.46), $\gamma_k^{\text{ZF-1}}$ can be rewritten as

$$\begin{aligned}\gamma_k^{\text{ZF-1}} &= \rho\beta_k\eta_k \frac{|\mathbf{e}_k^{\mathrm{T}}\mathbf{e}_k|^2}{\left\|\hat{\mathbf{H}}^*\mathbf{r}_k\right\|_2^2}\left(1+\rho\beta_k\sum_{k'\in\mathcal{K}\setminus\{k\}}\eta_{k'}\frac{|\mathbf{e}_k^{\mathrm{T}}\mathbf{e}_{k'}|^2}{\left\|\hat{\mathbf{H}}^*\mathbf{r}_{k'}\right\|_2^2}+\rho\beta_k\sigma_\varepsilon^2\sum_{k'\in\mathcal{K}}\eta_{k'}\right)^{-1} \\ &= \frac{\rho\beta_k\eta_k}{\left\|\hat{\mathbf{H}}^*\mathbf{r}_k\right\|_2^2\left(1+\rho\beta_k\sigma_\varepsilon^2\sum_{k'\in\mathcal{K}}\eta_{k'}\right)} \\ &= \frac{\rho\beta_k\eta_k}{[(\hat{\mathbf{H}}^{\mathrm{T}}\hat{\mathbf{H}}^*)^{-1}]_{kk}\left(1+\rho\beta_k\sigma_\varepsilon^2\sum_{k'\in\mathcal{K}}\eta_{k'}\right)}. \end{aligned} \tag{2.48}$$

□

Like in (2.41), (2.44) also depends on the small-scale fading, albeit this dependence is less evident in comparison with the MRT case. If $\hat{\mathbf{H}}^{\mathrm{T}}$ is a full-row rank matrix, then all users are geographically separated, i.e., have different AoAs. However, even in this case, if they have similar AoAs, then $\hat{\mathbf{H}}^{\mathrm{T}}$ becomes ill-conditioned leading to performance degradation.

***Remark 2.7***. Instead of normalizing the precoding vector $\mathbf{w}$, one can normalize the precoded vector $\mathbf{x}$ as explained below. Let the ZF-precoded signal $\mathbf{x}$ be

$$\mathbf{x} = \sqrt{c}\,\hat{\mathbf{H}}^*(\hat{\mathbf{H}}^{\mathrm{T}}\hat{\mathbf{H}}^*)^{-1}\mathsf{Diag}\left(\boldsymbol{\eta}\right)^{1/2}\mathbf{s}, \tag{2.49}$$

where $c \in \mathbb{R}_+$ is the normalization constant. The power of $\mathbf{x}$ is given by

$$\mathsf{E}\left\{\mathbf{x}^{\mathrm{H}}\mathbf{x}\right\} = c\,\mathsf{E}\left\{\mathbf{s}^{\mathrm{H}}\mathsf{Diag}\left(\boldsymbol{\eta}\right)^{1/2}(\hat{\mathbf{H}}^{\mathrm{H}}\hat{\mathbf{H}})^{-1}\mathsf{Diag}\left(\boldsymbol{\eta}\right)^{1/2}\mathbf{s}\right\}. \tag{2.50}$$

Using the equality in (2.21) and (2.50), one gets [9]

$$c = \frac{1}{\sum_{k\in\mathcal{K}}[(\hat{\mathbf{H}}^{\mathrm{H}}\hat{\mathbf{H}})^{-1}]_{kk}\eta_k}. \tag{2.51}$$

Therefore, the new SE expression is bounded by

$$R_{\text{sum}}^{\text{ZF-2}} \geq \frac{1}{2}\left(1-\frac{\tau_{\mathrm{p}}}{\tau_{\mathrm{c}}}\right)\sum_{k\in\mathcal{K}}\log_2\left(1+\gamma_k^{\text{ZF-2}}\right), \tag{2.52}$$

where $\gamma_k^{\text{ZF-2}} \in \mathbb{R}_+$ is denoted by

$$\gamma_k^{\text{ZF-2}} = \frac{\rho\beta_k\eta_k}{\left(1+\rho\beta_k\sigma_\varepsilon^2\sum\limits_{k'\in\mathcal{K}}\eta_{k'}\right)\sum\limits_{k'\in\mathcal{K}}[(\hat{\mathbf{H}}^{\text{H}}\hat{\mathbf{H}})^{-1}]_{k'k'}\eta_{k'}}. \tag{2.53}$$

# Chapter 3

# Power Allocation Algorithms

## 3.1 Introduction

In the previous chapter, the basic principles of the massive MIMO systems under LoS propagation were discussed, including propagation characteristics and precoding design. However, the ultimate performance of massive MIMO networks can only be achieved through power allocation. The power allocation is necessary due to power constraint as stated in (2.22) and, possibly, to guarantee some QoS, such as uniform performance among the users in the cell. Massive MIMO systems can achieve uniformly good performance for each user in the cell by implementing simple power control policy. This chapter presents the most popular power allocation algorithms along with a new technique proposed to overcome initialization issues faced by the proposal in [9].

## 3.2 Preliminaries

For massive MIMO systems, the optimum power allocation coefficients that maximizes (2.27) are found trough computationally expensive optimization problem, given by

$$\begin{aligned} &\underset{\boldsymbol{\eta}}{\text{maximize}} \;\; R_{\text{sum}}(\boldsymbol{\eta}) \\ &\text{subject to} \;\; \|\boldsymbol{\eta}\|_1 \leq 1, \;\; \boldsymbol{\eta} \succeq \mathbf{0}. \end{aligned} \tag{P-1}$$

Due to the high computational cost for solving P-1, power allocation techniques for massive MIMO systems usually are based on heuristic approaches, such as the *equal power allocation* (EPA), which guarantees equal power to all users, and the MMFPA, which guarantees the same throughput to all users.

## 3.3 Equal Power Allocation

The simplest power allocation algorithm for massive MIMO systems is the EPA, which allocates the same amount of power to all users. However, this algorithm does not guarantee any kind of fairness among the performance of the users and, in fact, it can be considered as if no power allocation were implemented [4]. For the EPA, the power allocation coefficients are given by

$$\eta_k^{\text{EPA}} = 1/K, \ \forall k \in \mathcal{K}. \tag{3.1}$$

Although this power control policy is not useful to practical networks, it is still useful in theoretical analyses and in the simulation of some aspects of massive MIMO systems. For instance, by substituting $\eta_k^{\text{EPA}}$ in (2.42), (2.45), or (2.46), theoretical analyses are extremely simplified.

## 3.4 Max-Min Fairness Power Allocation

The most commonly used power control policy in massive MIMO is the max-min fairness power allocation, which aims to maximize the worst SINR among all users in the cell. The original MMFPA problem can be mathematically written as the following optimization problem [4]:

$$\begin{aligned} \underset{\gamma,\, \boldsymbol{\eta}}{\text{maximize}} \ & \gamma \\ \text{subject to} \ & 0 \leq \gamma \leq \gamma_k, \quad \forall k \in \mathcal{K}, \\ & \|\boldsymbol{\eta}\|_1 \leq 1, \ \boldsymbol{\eta} \succeq \mathbf{0}, \end{aligned} \tag{P-2}$$

where $\gamma$ is the max-min SINR and $\mathbf{x} \succeq \mathbf{0}$ means that all entries of $\mathbf{x}$ are greater or equal to zero. One characteristic of the MMFPA problem is yielding the same SINR for each user, i.e., $\gamma_k = \gamma$, $\forall k \in \mathcal{K}$ [4].

### 3.4.1 Maximum Ratio Transmitter

In order to derive the MMFPA coefficients for the MRT precoding, firstly, consider (2.42) with perfect CSI knowledge, i.e., $\sigma_\varepsilon^2 = 0$. For the $k$th user, the power allocation vector can be written as

$$\begin{bmatrix} \frac{1}{\gamma} & -r_{12}^2 & \cdots & -r_{kK}^2 \end{bmatrix} \boldsymbol{\eta} = \frac{1}{\rho \beta_k M}. \tag{3.2}$$

Since all users have the same SINR due to the property of the MMFPA problem, the SINR constraints in (P-2) can be rewritten as a matrix equation given by [9]

$$(\mathbf{I}_K/\gamma - \mathbf{R})\,\boldsymbol{\eta} = \mathbf{b}/\rho, \tag{3.3}$$

where $\mathbf{I}_K$ stands for the identity matrix, whereas the $K \times K$ nonnegative matrix $\mathbf{R}$ and the vector $\mathbf{b} \succ \mathbf{0}$ are defined as

$$\mathbf{R} = \begin{bmatrix} 0 & r_{12}^2 & \cdots & r_{1K}^2 \\ r_{21}^2 & 0 & \cdots & r_{2K}^2 \\ \vdots & \vdots & \ddots & \vdots \\ r_{K1}^2 & r_{K2}^2 & \cdots & 0 \end{bmatrix} \text{ and } \mathbf{b} = \begin{bmatrix} (\beta_1 M)^{-1} \\ (\beta_2 M)^{-1} \\ \vdots \\ (\beta_K M)^{-1} \end{bmatrix}.$$

In order to tackle the problem in (P-2), we can use Algorithm 1, proposed in [9], which uses a bisection search, solving (3.3) at each iteration. Other approaches to solve (P-2) can be found in [4].

**Algorithm 1** MMFPA-based algorithm

**Input:** $\mathbf{R}$, $\mathbf{b}$, $\rho$, $\gamma_\text{l}$, $\gamma_\text{r}$, and $\varepsilon$

```
while γ_r − γ_l > ε do
    γ = (γ_r + γ_l)/2
    Solve (3.3) using γ
    if ‖η‖_1 ≤ 1 then
        γ_l = γ
    else
        γ_r = γ
    end if
end while
```

**Return:** $\gamma_\text{o} = \gamma$ and $\boldsymbol{\eta}_\text{o} = \boldsymbol{\eta}$

A critical aspect of this algorithm is the initial search interval $[\gamma_\text{l}, \gamma_\text{r}]$, which is related to complexity and convergence matters. The initial search interval must be chosen so that $\gamma^\star \in [\gamma_\text{l},\ \gamma_\text{r}]$, where $\gamma^\star$ is the optimal max-min SINR obtained from the solution of the MMFPA problem in (P-2). A common choice for the left endpoint is $\gamma_\text{l} = 0$, since the SINR is positive, and $\gamma_\text{r} = M\rho \max_{k\in\mathcal{K}} \beta_k$, which is an upper bound for $\gamma_k$ in (2.42). However, such choice of initial search interval may lead to a *wrong point*, which is any output point $\gamma_\text{o}$ of Algorithm 1 such that $|\gamma_\text{o} - \gamma^\star| > \varepsilon$. Sometimes, such wrong point $\gamma_\text{o}$ corresponds to $\boldsymbol{\eta}_\text{o} \in \mathbb{R}_+^{K\times 1}$; in these cases, we call $\gamma_\text{o}$ a *suboptimal point*. However, in most cases, a wrong point $\gamma_\text{o}$ is associated with a meaningless $\boldsymbol{\eta}_\text{o}$ comprised of negative entries. In this last case, although such problem can be easily verified, it is not straightforward to solve it. In [9], as an alternative to $\gamma_\text{r} = M\rho \max_{k\in\mathcal{K}} \beta_k$, the authors propose an exhaustive search to determine a suitable right endpoint $\gamma_\text{r}$ to initialize the search interval. Such

procedure is indeed effective to eliminate these meaningless solutions, but it may take too long to find a proper $\gamma_{\mathrm{r}}$ for the initial search interval and suboptimal points can still be attained. In Section 3.5, we use the Perron-Frobenius theory not only to explain this behavior but also to provide search intervals that guarantee convergence to the solution of the problem in (P-2), i.e., guaranteeing that $|\gamma_{\mathrm{o}} - \gamma^{\star}| \leq \varepsilon$.

### 3.4.2 Zero-forcing

For the ZF precoder, the power allocation coefficients of the MMFPA algorithm are given by

$$\eta_k = \frac{\gamma[(\mathbf{H}^{\mathrm{T}}\mathbf{H}^{*})^{-1}]_{kk}}{\rho\beta_k}, \ \forall k \in \mathcal{K}. \tag{3.4}$$

Note that $[(\mathbf{H}^{\mathrm{T}}\mathbf{H}^{*})^{-1}]_{kk}$ is equal for all $k \in \mathcal{K}$ due to the characteristics of the UR-LoS channel, and so as $\gamma$ due to the property of the MMFPA algorithm. Thus, equation (3.4) can be rewritten as

$$\eta_k = \frac{\xi}{\beta_k}, \ \forall k \in \mathcal{K}, \tag{3.5}$$

where $\xi \in \mathbb{R}_{+}$ is a constant that is chosen in order to satisfy (2.22), yielding

$$\xi \leq \left( \sum_{k' \in \mathcal{K}} \frac{1}{\beta_{k'}} \right)^{-1}. \tag{3.6}$$

Since the MMFPA policy requires (2.22) to be satisfied with equality [4], then the MMFPA coefficients and the max-min SINR are given by

$$\eta_k^{\text{ZF-MMFPA}} = \left( \sum_{k' \in \mathcal{K}} \frac{\beta_k}{\beta_{k'}} \right)^{-1}, \ \forall k \in \mathcal{K}, \tag{3.7}$$

$$\gamma^{\text{ZF-MMFPA}} = \frac{\rho}{[(\mathbf{H}^{\mathrm{T}}\mathbf{H}^{*})^{-1}]_{kk} \left( \sum_{k' \in \mathcal{K}} \beta_{k'}^{-1} \right)}. \tag{3.8}$$

Differently from the MRT precoder, the MMFPA for ZF precoder has an analytical solution for the power allocation coefficients.

## 3.5 Perron-Frobenius Right Endpoints

### 3.5.1 Perron-Frobenius Eigenvalue

For every $1/\gamma \in \mathbb{R}_{+} \setminus \mathcal{L}$, where $\mathcal{L}$ denotes the set containing all eigenvalues of $\mathbf{R}$, matrix $(\mathbf{I}/\gamma - \mathbf{R})$ has full rank, implying that (3.3) has a single solution $\boldsymbol{\eta} \in \mathbb{R}^{K \times 1}$. However, the power allocation vector $\boldsymbol{\eta}$ must have nonnegative entries and this con-

dition cannot be guaranteed for every $1/\gamma \in \mathbb{R}_+ \setminus \mathcal{L}$. Nonnegative solutions of linear system of equations like (3.3) are closely related to the *Perron-Frobenius eigenvalue* (PFE) $\lambda_{\max}$, which is the maximum eigenvalue of a nonnegative irreducible matrix,[1] in our case, the maximum eigenvalue of $\mathbf{R}$.[2] In order to derive a new right endpoint for Algorithm 1, we first have to state the following theorem [72]:

**Theorem 3.1**
*A necessary and sufficient condition for a solution* $\boldsymbol{\eta} \succeq \mathbf{0}$ *and* $\boldsymbol{\eta} \neq \mathbf{0}$ *to the linear system of equations*

$$(s\mathbf{I} - \mathbf{R})\,\boldsymbol{\eta} = \mathbf{b} \tag{3.9}$$

*to exist for any* $\mathbf{b} \succeq \mathbf{0}$ *and* $\mathbf{b} \neq \mathbf{0}$ *is that* $s > \lambda_{\max}$. *In this case, there is only one solution* $\boldsymbol{\eta}$, *which is strictly positive and given by*

$$\boldsymbol{\eta} = (s\mathbf{I} - \mathbf{R})^{-1}\,\mathbf{b}.$$

*Proof.* A detailed proof is available in [72]. □

Due to Theorem 3.1, we know that $1/\gamma > \lambda_{\max}$ to have a positive solution of (3.3), yielding $\gamma < 1/\lambda_{\max}$. Therefore, in order to guarantee that Algorithm 1 always converges to the optimal point $\gamma^\star$, $1/\lambda_{\max}$ must be used as the right endpoint of the search interval.

While using $\gamma_{\mathrm{r}} = M\rho \max_{k\in\mathcal{K}} \beta_k$ as the right endpoint does not guarantee convergence to the optimal point, there might be times when Algorithm 1 does converge to the optimal point. For instance, consider the case in which $\gamma_{\mathrm{l}} = 0$ and the two possible right endpoints

$$\gamma_{\mathrm{r}}^{(1)} = M\rho \max_{k\in\mathcal{K}} \beta_k, \tag{3.10}$$

$$\gamma_{\mathrm{r}}^{(2)} = \frac{1}{\lambda_{\max}}. \tag{3.11}$$

For $\gamma_{\mathrm{r}}^{(1)} < \gamma_{\mathrm{r}}^{(2)}$, Algorithm 1 converges to the optimal point with possibly fewer iterations when employing $\gamma_{\mathrm{r}}^{(1)}$ as the right endpoint. However, for $\gamma_{\mathrm{r}}^{(1)} > \gamma_{\mathrm{r}}^{(2)}$, Algorithm 1, employing $\gamma_{\mathrm{r}}^{(1)}$, may fail to attain the MMFPA solution. In order to explain this issue, we use the toy examples depicted in Figure 3.1 to illustrate the iterative process of the algorithm for $l$ iterations. In this figure, the thick line represents the guaranteed convergence region $[0, \gamma_{\mathrm{r}}^{(2)}]$, whereas the blue line represents the search interval $[\gamma_{\mathrm{l}}^{(1)}(l), \gamma_{\mathrm{r}}^{(1)}(l)]$, and the red line represents the region out of the

[1] A nonnegative matrix $\mathbf{R}$ is said to be irreducible if for every pair $(m, k)$, there exist a positive integer $n$ such that $[\mathbf{R}^n]_{mk} > 0$.

[2] The maximum eigenvalue of a matrix is usually called the spectral radius of the matrix, but for nonnegative matrices, it is also called the Perron-Frobenius eigenvalue.

search interval. Figure 3.1a and Figure 3.1b describe a case of convergence to the optimal and wrong points, respectively. Consider that, at the first iteration, for both examples, we have $\|\boldsymbol{\eta}(1)\|_1 > 1$, yielding $[0, \gamma_{\mathrm{r}}^{(1)}(1)]$ as the new search interval. At the second iteration, we have $\|\boldsymbol{\eta}(2)\|_1 > 1$ for Figure 3.1a and $\|\boldsymbol{\eta}(2)\|_1 \leq 1$ for Figure 3.1b, yielding $[0, \gamma_{\mathrm{r}}^{(1)}(2)]$ and $[\gamma_{\mathrm{r}}^{(1)}(2), \gamma_{\mathrm{r}}^{(1)}(1)]$ as the new search intervals for each case, respectively. At the third iteration, in Figure 3.1a, $\|\boldsymbol{\eta}(3)\|_1 > 1$ and $\gamma_{\mathrm{r}}^{(1)}(3) \in [0, \gamma_{\mathrm{r}}^{(2)}]$; therefore, from now on, $\boldsymbol{\eta}(l)$ will always be nonnegative, guaranteeing the convergence to the optimal point. However, in Figure 3.1b, $\gamma_{\mathrm{r}}^{(1)}(3) \notin [0, \gamma_{\mathrm{r}}^{(2)}]$ and consequently, $\gamma^\star \notin [\gamma_{\mathrm{r}}^{(1)}(2), \gamma_{\mathrm{r}}^{(1)}(1)]$. It is worth mentioning that at the first two iterations of the example depicted in Figure 3.1a, $\boldsymbol{\eta}$ had nonpositive entries, but luckily the bisection search was still able to converge to the optimal point. We used the word "luckily" here for it could also have converged to a wrong point, as illustrated in Figure 3.1b.

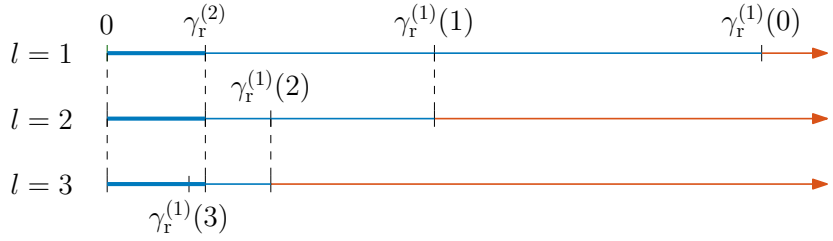


(a) Correct convergence

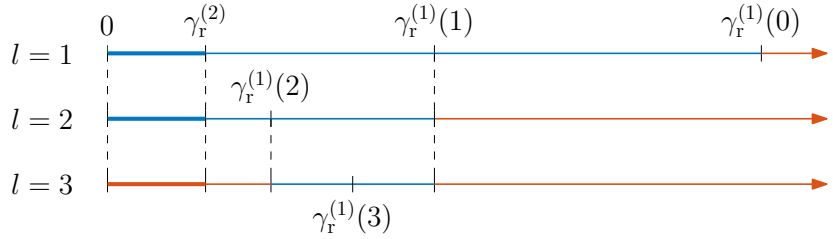


(b) Wrong convergence

Figure 3.1: Example of convergence to the optimal and wrong points using $\gamma_{\mathrm{r}}^{(1)}$.

### 3.5.2 Bound Test

An alternative to $\gamma_{\mathrm{r}}^{(2)}$ can be found by using the Gershgorin circle theorem, which for the case of a nonnegative matrix can be written as [72, Corollary 1]

$$\lambda_{\max} \leq \max_{k \in \mathcal{K}} \sum_{k' \in \mathcal{K} \setminus \{k\}} r_{kk'}^2, \tag{3.12}$$

yielding a new right endpoint given by

$$\gamma_{\mathrm{r}}^{(3)} = \frac{1}{\max\limits_{k \in \mathcal{K}} \sum\limits_{k' \in \mathcal{K} \setminus \{k\}} r_{kk'}^2}. \tag{3.13}$$

Observe that $\gamma_{\mathrm{r}}^{(3)} \leq \gamma_{\mathrm{r}}^{(2)}$ and, therefore, we might have a case where

$$\gamma_{\mathrm{r}}^{(3)} < \gamma^{\star} < \gamma_{\mathrm{r}}^{(2)}. \tag{3.14}$$

In this case, $\gamma_{\mathrm{r}}^{(3)}$ should be used as the left endpoint, whereas $\gamma_{\mathrm{r}}^{(2)}$ should be used as the right endpoint. On the other hand, the resulting interval is usually very tight, meaning that the bisection search converges in a few iterations. Furthermore, (3.14) can be used in a beneficial way by incorporating a test to check whether $\gamma_{\mathrm{r}}^{(3)}$ is the left or the right endpoint. This BT can be performed by solving (3.3) with $\gamma_{\mathrm{r}}^{(3)}$ and checking the resulting $\boldsymbol{\eta}$ for:

$$\begin{cases} \gamma_{\mathrm{r}}^{(3)} < \gamma^{\star}, & \text{if } \|\boldsymbol{\eta}\|_1 \leq 1 \\ \gamma_{\mathrm{r}}^{(3)} > \gamma^{\star}, & \text{if } \|\boldsymbol{\eta}\|_1 > 1 \end{cases}. \tag{3.15}$$

Therefore, Algorithm 1 can use either the initial search interval $[0, \gamma_{\mathrm{r}}^{(3)}]$ or $[\gamma_{\mathrm{r}}^{(3)}, \gamma_{\mathrm{r}}^{(2)}]$, depending on (3.15). The proposed BT procedure is described in Algorithm 2.

**Algorithm 2** Bound test

**Input:** $\mathbf{R}$, $\mathbf{b}$, and $\rho$
1: Solve (3.3) using $\gamma_{\mathrm{r}}^{(3)}$
2: **if** $\|\boldsymbol{\eta}\|_1 \leq 1$ **then**
3: $\quad \gamma_{\mathrm{l}} = \gamma_{\mathrm{r}}^{(3)}$
4: $\quad \gamma_{\mathrm{r}} = \gamma_{\mathrm{r}}^{(2)}$
5: **else**
6: $\quad \gamma_{\mathrm{l}} = 0$
7: $\quad \gamma_{\mathrm{r}} = \gamma_{\mathrm{r}}^{(3)}$
8: **end if**
**Return:** $\gamma_{\mathrm{l}}$ and $\gamma_{\mathrm{r}}$

## 3.6 Computational Complexity Analysis

Algorithm 1 is based on the bisection search, and the core of this search involves solving a $K \times K$ linear system of equations, which can be solved with complexity $\mathcal{O}(K^3)$.[3] The number of iterations Algorithm 1 takes to converge is

$$L(\gamma_{\mathrm{r}}, \gamma_{\mathrm{l}}, \varepsilon) = \left\lceil \log_2 \left( \frac{\gamma_{\mathrm{r}} - \gamma_{\mathrm{l}}}{\varepsilon} \right) \right\rceil, \tag{3.16}$$

[3] A theoretical measure of the execution of an algorithm, usually the time or memory needed, given the problem size $n$, which is usually the number of items [84]. Informally, saying some equation $f(n) = \mathcal{O}(g(n))$ means it is less than some constant multiple of $g(n)$.

where $\varepsilon \in \mathbb{R}_+$ is a given accuracy and $\lceil \cdot \rceil$ is the ceil function. Hence, the general complexity of Algorithm 1 for a given interval $[\gamma_\mathrm{l}, \gamma_\mathrm{r}]$ is $\mathcal{O}(LK^3)$, where $L$, given in (3.16), is related to the length of the search interval.

One of the main differences between the method in [9] and our approach is the search interval used to initialize Algorithm 1. For [9] and PFE, (3.16) can be used to calculate the number of iterations taken by Algorithm 1, whereas with the BT method, the number of iterations is given by

$$L(\gamma_\mathrm{r}^{(2)}, \gamma_\mathrm{r}^{(3)}, \varepsilon) = \begin{cases} \left\lceil \log_2 \left( \frac{\gamma_\mathrm{r}^{(2)} - \gamma_\mathrm{r}^{(3)}}{\varepsilon} \right) \right\rceil, & \text{if } \gamma_\mathrm{r}^{(3)} < \gamma^\star \\ \left\lceil \log_2 \left( \frac{\gamma_\mathrm{r}^{(3)}}{\varepsilon} \right) \right\rceil, & \text{if } \gamma_\mathrm{r}^{(3)} > \gamma^\star \end{cases}, \tag{3.17}$$

which can be smaller than (3.16) depending on the $\gamma_\mathrm{r}^{(2)}$ and $\gamma_\mathrm{r}^{(3)}$ values.

It is not possible to draw any conclusions about the length of the search intervals provided by each scheme since all the right endpoints studied are random variables. In [9], $\gamma_\mathrm{r}^{(1)}$ is related to the large-scale fading, which is related to the user position. Moreover, $\gamma_\mathrm{r}^{(2)}$ and BT are related to the eigenvalue decomposition of a random matrix and the sum of the entries in the row of a random matrix, respectively. Therefore, it is not possible to carry out classical complexity analysis. However, based on the simulations in Section 3.7, on average, [9] provides a loose search interval that may not converge to the optimal point, while PFE and BT provide tight search intervals and guaranteed convergence to the optimal point.

Another important aspect is the complexity associated with finding the right endpoints. The approach in [9] requires a linear search in a $K$-dimensional vector with complexity $\mathcal{O}(K)$, whereas the PFE requires eigenvalue decomposition with complexity $\mathcal{O}(K^3)$, and the BT requires eigenvalue decomposition in the worst case and linear search in the best case.

## 3.7 Simulation Results

The performance of Algorithm 1 is assessed via numerical simulations in terms of the probability of failure and number of iterations, considering $\varepsilon = 10^{-6}$. An $R$-m radius hexagonal single-cell massive MIMO system with $M \in \{64, 128, 256, 512\}$, $K \in \{8, 16, 32, 64\}$, and $R \in \{100, 500, 1000, 2000\}$ m are used in the simulations. The users are randomly distributed within the hexagonal cell centered at the BS. A UR-LoS channel with a ULA models the small-scale fading [4], whereas the large-scale coefficient is defined using the COST231 propagation model [85] for the path loss and a log-normal distribution for the shadow fading with zero mean and 8 dB standard deviation. The radiated power at the BS is $P \in \{1,\ 10\}$ W, the BS and user antenna gain is 0 dBi, and the noise figure for the users is 9 dB. The performance

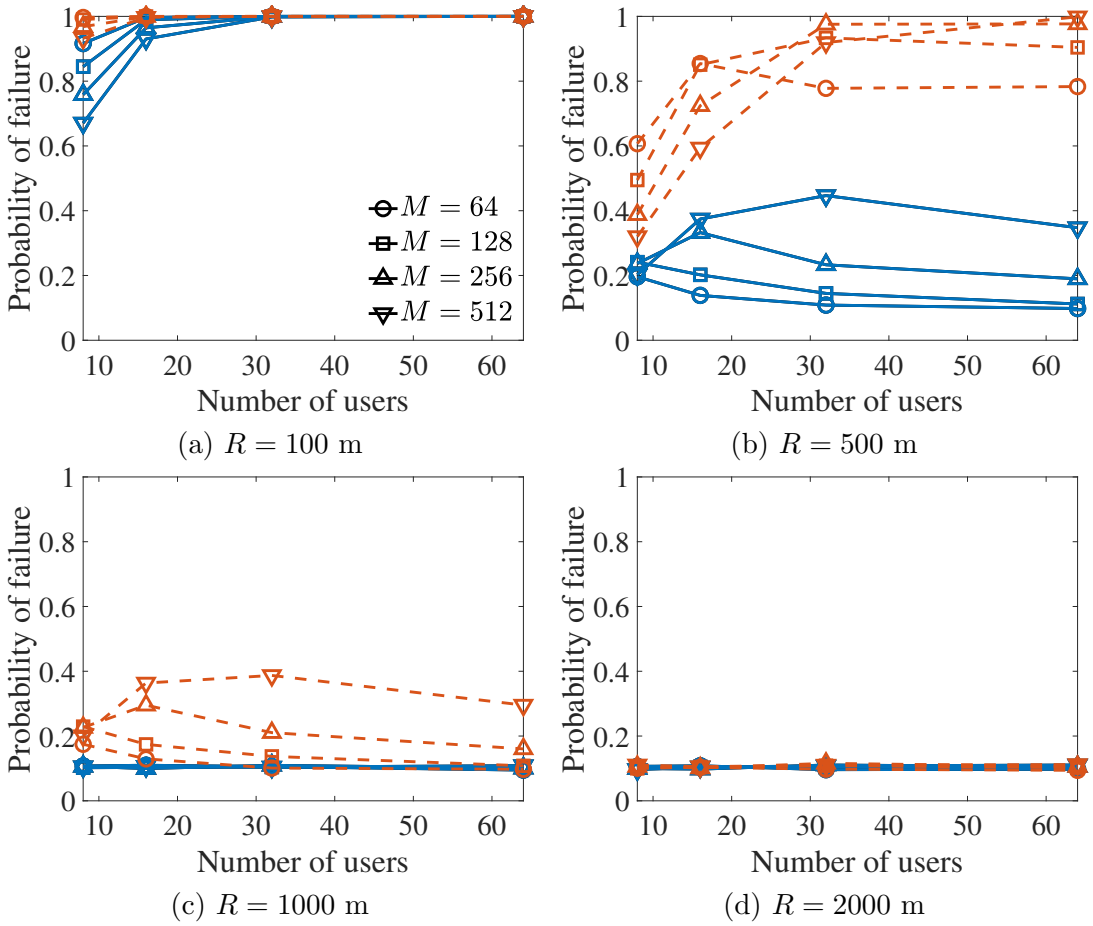


(a) $R = 100$ m (b) $R = 500$ m

(c) $R = 1000$ m (d) $R = 2000$ m

Figure 3.2: Probability of failure. (– $P = 1$ W and – – $P = 10$ W)

of the algorithms is evaluated using 1000 realizations of the channel.

Figure 3.2 depicts the probability of failure of Algorithm 1 when $\gamma_{\mathrm{r}}^{(1)}$ is used as right endpoint. A failure occurs when Algorithm 1 converges to a wrong point, as defined in Section 3.4. As can be observed in Figure 3.2a, the algorithm has a high probability of failure for small $R$, but it drops significantly when $R$ increases. However, even for $R = 2000$ m, the algorithm still has 11% of probability of failure, as illustrated in Figure 3.2d. Moreover, the number of antennas and BS power are also related to the failures of Algorithm 1, wherein an increase in $M$ or $P$ yields an increase in the probability of failure. This behavior implies that $\gamma_{\mathrm{r}}^{(1)}$ is not a suitable choice for massive MIMO scenarios. Furthermore, it is worth highlighting that in Figure 3.2d and 3.2c (only for $P = 1$), all points $\gamma_{\mathrm{o}}$ yield power allocation vectors $\boldsymbol{\eta}_{\mathrm{o}}$ with nonnegative entries, so they can be considered acceptable suboptimal points, differently from the other cases, where the wrong points frequently yield power allocation vectors with negative entries.

Figure 3.3 illustrates the $\mathsf{Pr}\{\gamma_{\mathrm{r}}^{(3)} < \gamma^{\star}\}$ for $M = 512$. From Section 3.5, we know that the initial search interval provided by the BT depends on whether $\gamma_{\mathrm{r}}^{(3)} < \gamma^{\star}$ or $\gamma_{\mathrm{r}}^{(3)} > \gamma^{\star}$. Hence, the $\mathsf{Pr}\{\gamma_{\mathrm{r}}^{(3)} < \gamma^{\star}\}$ is important to quantify, in probability,

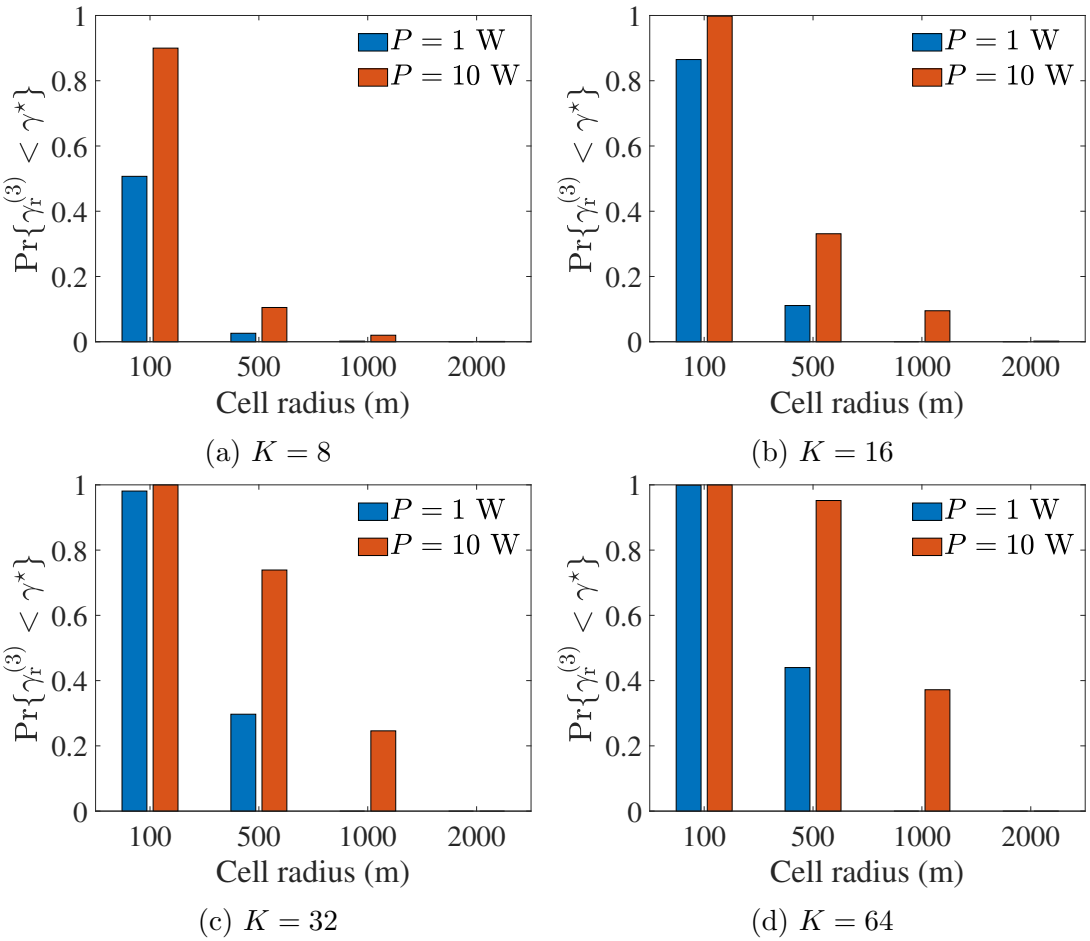


(a) $K = 8$ (b) $K = 16$

(c) $K = 32$ (d) $K = 64$

Figure 3.3: $\mathsf{Pr}\{\gamma_{\mathrm{r}}^{(3)} < \gamma^{\star}\}$ for $M = 512$.

when $\gamma_{\mathrm{r}}^{(3)}$ is a left or right endpoint, where high values of $\mathsf{Pr}\{\gamma_{\mathrm{r}}^{(3)} < \gamma^{\star}\}$ means that we have high probability of using a tight search interval, whereas low values of $\mathsf{Pr}\{\gamma_{\mathrm{r}}^{(3)} < \gamma^{\star}\}$ means that we have high probability of avoiding the eigenvalue decomposition. As can be observed in this figure, $\mathsf{Pr}\{\gamma_{\mathrm{r}}^{(3)} < \gamma^{\star}\}$ significantly drops as the cell-size increases, reaching 0% for $R = 2000$ m, whereas it increases with $P$ and $K$. Although not depicted here, the same conclusions for $\mathsf{Pr}\{\gamma_{\mathrm{r}}^{(3)} < \gamma^{\star}\}$, regarding $R$ and $P$, can be drawn for $M \in \{64, 128, 256\}$. However, when it comes to $K$, the pattern changes, decreasing with $K$ for $R = 1000$ m.

Figure 3.4 shows the average number of iterations the bisection search needs to converge when using $\gamma_{\mathrm{r}}^{(1)}$ and $\gamma_{\mathrm{r}}^{(2)}$ as the right endpoint, as well as the BT for $P = 1$ W. As can be observed in Figure 3.4, Algorithm 1 takes fewer iterations by using the BT than by using $\gamma_{\mathrm{r}}^{(1)}$ and $\gamma_{\mathrm{r}}^{(2)}$ as right endpoints. Additionally, the number of iterations is invariant with $R$ when $\gamma_{\mathrm{r}}^{(2)}$ is used. This happens because $\mathbf{R}$ is affected only by how close the users are and not by the cell size. The same is not true for the BT, which yields a small increase in the number of iterations when $R$ increases. This behavior is due to the fact that $\mathsf{Pr}\{\gamma_{\mathrm{r}}^{(3)} < \gamma^{\star}\}$ is high for a small cell, but it decreases when $R$ increases, as depicted in Figure 3.3. Therefore,

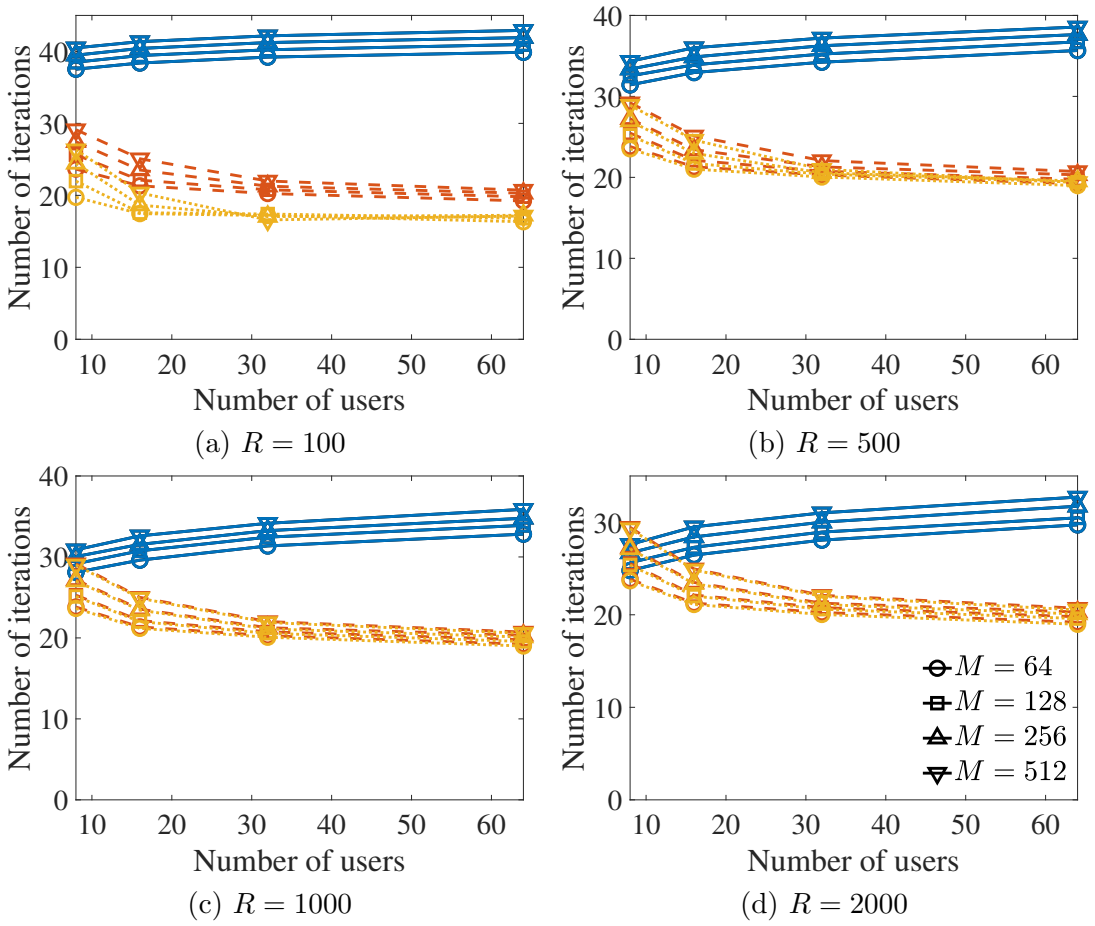


Figure 3.4: Number of iterations for $P = 1$ W. ($-$ $\gamma_{\mathrm{r}}^{(1)}$, $- -$ $\gamma_{\mathrm{r}}^{(2)}$, and $\cdot\cdot$ BT)

for $R = 100$ m, the BT provides a tighter interval than $\gamma_{\mathrm{r}}^{(2)}$, and for large $R$, they provide initial search intervals that yield the same number of iterations. Note that the number of iterations with $\gamma_{\mathrm{r}}^{(1)}$ decreases with $R$. This happens because the large-scale fading decreases when $R$ increases and, therefore, $\gamma_{\mathrm{r}}^{(1)}$ yields a tighter initial search interval when $R$ increases.

Another important conclusion that can be drawn from Figure 3.4 is the behavior of the number of iterations with $K$. Both proposed $\gamma_{\mathrm{r}}^{(2)}$ and the BT yield a reduced number of iterations when $K$ increases. This occurs because $\lambda_{\max}$ tends to increase as $K$ increases. Indeed, with large $K$, the probability of having users close to each other in the cell is higher, increasing the condition number of matrix $\mathbf{R}$, resulting in high values of $\lambda_{\max}$ and shorter initial search intervals. On the other hand, the number of iterations when $\gamma_{\mathrm{r}}^{(1)}$ is used increases with $K$. This behavior happens because with a larger $K$, the probability of having users close to the BS increases, yielding a higher large-scale fading, consequently increasing the search interval. Furthermore, based on the decreased number of iterations, we can empirically conclude that the initial search intervals provided by $\gamma_{\mathrm{r}}^{(2)}$ and the BT are tighter than the one provided by $\gamma_{\mathrm{r}}^{(1)}$. The only case in which $\gamma_{\mathrm{r}}^{(1)}$ provides a tighter search interval is when $M = 512$,

$K = 8$, and $R = 2000$ m.

## 3.8 Concluding Remarks

In this chapter, we used the Perron-Frobenius theory to show how an implementation of the max-min fairness power allocation algorithm is affected by the initialization of the search interval. Moreover, we also used the Perron-Frobenius theory to derive a new search interval for this algorithm, which guarantees the convergence to the max-min fairness solution. Additionally, we used the Gershgorin circle theorem to create a bound test that guarantees convergence and reduces the computational load. Simulation results showed that this algorithm, when using the search interval known in the literature, frequently converges to wrong points. Furthermore, the proposed search interval and the bound test guarantee convergence with fewer iterations.

# Chapter 4

# User Selection Algorithms

## 4.1 Introduction

As discussed in Chapter 2, the small-scale fading plays an important role in the SE of massive MIMO systems under LoS propagation, degrading the performance in non-favorable propagation conditions. Additionally, the number of users can also be a critical aspect when the ZF precoder is used and $K > M$. One way to cope with these issues is by performing user selection. The user selection problem has not received much attention in the massive MIMO research for several reasons. Firstly, massive MIMO systems rely on the favorable propagation and channel hardening properties, which consider that the number of antennas at the BS is much larger than the number of users ($M \gg K$). Secondly, i.i.d. Rayleigh channel model is usually assumed, which is not severely affected by the position of the users [8]. However, these assumptions may not fully hold in practical scenarios; for example, there may be situations where the number of users is very close to the number of BS antennas or even larger. The MRT precoding algorithm used in massive MIMO does not have a restriction on the number of users, but the ZF precoding requires the number of users to be smaller or equal to the number of BS antennas. One critical issue here is how to select the best set of users in order to yield the highest spectral efficiency to the network and the remaining users.

## 4.2 The User Selection Problem

Consider a case where $K$ is large enough to degrade the massive MIMO system performance, yielding a non-favorable propagation environment or simply a situation where $K > M$. In this scenario, the BS should choose $L$ out of $K$ users to transmit and receive data in a given time slot in order to guarantee that the number of antennas is greater or equal to the number of selected users so that favorable

propagation is achieved. Mathematically, let $\mathcal{S} \subset \mathcal{K}$ be the set of selected users in a given time slot. The user selection problem consists of the optimization problem to find $\boldsymbol{\eta} \in \mathbb{R}_{+}^{|\mathcal{S}|\times 1}$ and $\mathcal{S}$, with $|\mathcal{S}|= L$, that maximize the SE,[1] i.e.,

$$\begin{aligned} \underset{\boldsymbol{\eta},\mathcal{S}}{\text{maximize}} \;\; & \frac{1}{2}\left(1-\frac{\tau_{\mathrm{p}}}{\tau_{\mathrm{c}}}\right)\sum_{k\in\mathcal{S}}\log_2\left(1+\gamma_k(\boldsymbol{\eta},\mathcal{S})\right) \\ \text{subject to } & \boldsymbol{\eta}\succeq\mathbf{0},\;\|\boldsymbol{\eta}\|_1\leq 1, \\ & |\mathcal{S}|=L,\mathcal{S}\subset\mathcal{K}. \end{aligned} \tag{P-3}$$

The user selection problem in (P-3) is not only non-convex, but also involves combinatorial optimization. One alternative approach is to define a simpler surrogate problem that separates the user selection and the power allocation into two different problems, where the user selection is performed before power allocation [9, 43]. However, the solution for the user selection problem can only be found through an ES for a given $\boldsymbol{\eta}$, which is impractical due to the high-dimensional search space in massive MIMO systems. For EPA, the optimal user set can be found through an ES with $\eta_k = 1/L$, $\forall k \in \mathcal{S}$. On the other hand, for MMFPA, the solution is slightly different since for this scheme, the power allocation cannot be dissociated from the user selection due to the dependence on the large-scale fading. Thus, the MMFPA is computed for each set of users.

To overcome the limitations of the ES solutions, the user selection problem is tackled by using suboptimal greedy solutions [9, 43, 44]. The main advantage of these solutions is that they do not depend on specific precoding and power allocation algorithms, but simply rely on the CSI. The user selection algorithms can be categorized into two distinct classes: LSFA and SSFA algorithms. The LSFA algorithms are usually good solutions for massive MIMO systems under NLoS propagation since the small-scale fading does not affect the system performance under this type of propagation [59]. The most popular algorithms that belong to this class are the *large-scale fading ratio selection* (LSFRS) [4] and SOS [43]. For the LoS case, the small-scale fading has a great impact on the system performance [8, 9]. Due to the characteristics of the channel, the small-scale fading is not averaged out like in the NLoS propagation and it impacts the system performance, requiring the use of SSFA algorithms. The most popular approaches that belong to this class are the SOS [43], CBS [9], and ICIBS.

Although the small-scale fading has a significant impact on the performance of massive MIMO systems under LoS propagation, the large-scale fading also plays a significant role in the SE of massive MIMO systems operating in this environ-

[1] An alternative criterion is used in [9], but the maximization of the SE is the most widely used [43, 45, 46, 49–54].

ment. Disregarding the large-scale fading, even in an LoS propagation environment, is equivalent to assuming that all users are equidistant from the base station and experience the same level of shadowing, which is not a reasonable approximation in practical applications. Indeed, taking the large-scale fading into account is interesting because users that experience less path loss/shadowing can be served with lower transmission power, thus reducing the interference level to the remaining users. Furthermore, user selection algorithms that use both fading information can leverage the popular power allocation algorithm, namely, MMFPA [40–42]. MMFPA aims to maximize the SINR improvement for the user with the worst channel conditions. If this user is affected by severe path loss/shadowing, the network throughput is compromised. As mentioned in the Introduction, to the best of our knowledge, no such algorithms that can cope with both types of fading are reported in the literature. However, the SOS is an algorithm that can be adapted to deal with this issue, albeit its high computational complexity can be a hindrance in some applications. The recently proposed *machine learning-based selection* [58] can also deal with this issue if it is properly trained. Besides those two algorithms, another algorithm that can jointly considers the small- and large-scale fading effects to perform the selection is the FRBS algorithm, which is a generalization of the ICIBS. Table 4.1 summarizes the main characteristics of the user selection algorithms.

Table 4.1: Main Characteristic of User Selection Algorithms

| | **SSFA** | **LSFA** | **Complexity** |
|---|---|---|---|
| **LSFRS** | No | Yes | Very Low |
| **SOS** | Yes | Yes | Very High |
| **CBS** | Yes | No | Low |
| **ICIBS** | Yes | No | Low |
| **FRBS** | Yes | Yes | Low |

***Remark 4.1***. Despite not providing performance improvements to massive MIMO systems under i.i.d. Rayleigh fading channels, user selection algorithms can bring advantages under Rician fading channels. In [86], the authors show that in the asymptotic case ($M \longrightarrow \infty$) the SE of a massive MIMO system under Rician fading is maximized when the channel is dominated by LoS propagation, and the LoS channel components corresponding to different users are orthogonal to one another. The orthogonality among these LoS components can be guaranteed by some user selection algorithms. Furthermore, the user selection may help the statistical beamforming approach proposed in [86] in dealing with some of the limitations due to the finite number of antennas and the scheduling process. Also, the user selection algorithms could be adapted to take advantage of the statistical CSI when dealing with Rician channels like in [86]. That is, under the statistical CSI hypothesis, the BS

**Algorithm 3** LSFRS algorithm

**Input:** $L$ and $\boldsymbol{\beta}$
**Return:** $\mathcal{S}_0 = \mathcal{K}$
1: **for** $l = 1$ to $K - L$ **do**
2: $\quad k^\star = \underset{k \in \mathcal{S}_{l-1}}{\operatorname{argmin}} \boldsymbol{\beta}_{\mathcal{S}_{l-1}}$
3: $\quad \mathcal{S}_l = \mathcal{S}_{l-1} \setminus \{k^\star\}$
4: **end for**
5: **return** $\mathcal{S} = \mathcal{S}_L$

knows not only the LoS component but also other parameters of the Rician $\kappa$-factor model [63]; therefore, when dealing with these channel models, it would be interesting to add this additional piece of information into the user selection algorithms. In the Rician fading scenario, using only the LoS components is not enough to perform a good user selection since the Rician $\kappa$-factor is also relevant to maximize the SE of massive MIMO systems under Rician fading channels.

## 4.3 Large-scale Fading Ratio Selection

For massive MIMO systems under NLoS propagation, the large-scale fading is more relevant for the SE performance since the small-scale fading is averaged out due to the channel hardening property [81]. For this scenario, LSFA algorithms like the LSFRS can be used. The *large-scale fading ratio* (LSFR) is defined as [4]

$$\text{LSFR}_{ck} = \frac{\beta_{ck}^{c}}{\sum_{c' \in \mathcal{C}} \beta_{ck}^{c'}}, \tag{4.1}$$

where $\beta_{ck}^{c'} \in \mathbb{R}_+$ is the large-scale fading of the $k$th user in $c$ cell with the BS in the $c'$th cell and $\mathcal{C} \subset \mathbb{N}$ is the set with the cell indices. The metric in (4.1) is handy since the $k$th user does not need to know any information from any other user.

The LSFRS heuristic strategy was proposed for dropping users in a multi-cell scenario, but it can also be used in a single-cell scenario by keeping the users with the highest large-scale fading coefficients.[2] Although this strategy does not guarantee any kind of fairness among the users, it is the most intuitive way for selecting users if the goal is to maximize the network throughput. Similar approaches have been used for cell-free massive MIMO systems [65, 68]. The LSFRS algorithm is summarized in Algorithm 3.

[2]This approach does not use the LSFR in (4.1). However, the same algorithm name was kept due to the similarity with the algorithm in the literature.

**Algorithm 4** SOS algorithm

**Input:** $L$ and $\mathbf{H}$
**Return:** $\mathcal{T}_0 = \mathcal{K}$ and $\mathcal{S}_0 = \emptyset$
1: **for** $l = 1$ to $L$ **do**
2: **if** $l = 1$ **then**
3: $\mathbf{h}_k^{\perp} = \mathbf{h}_k,\ \forall\ k \in \mathcal{T}_{l-1}$
4: **else**
5: $\mathbf{P}_{l-1} = \mathbf{I}_M - \mathbf{Q}_{l-1}\mathbf{Q}_{l-1}^{\mathrm{H}}$
6: $\mathbf{h}_k^{\perp} = \mathbf{P}_{l-1}\mathbf{h}_k,\ \forall\, k \in \mathcal{T}_{l-1}$
7: **end if**
8: $k^{\star} = \underset{k \in \mathcal{T}_{l-1}}{\operatorname{argmax}} \left\|\mathbf{h}_k^{\perp}\right\|_2$
9: $\mathbf{q}_l = \mathbf{h}_{k^{\star}}^{\perp} / \left\|\mathbf{h}_k^{\perp}\right\|_2$
10: $\mathcal{T}_l = \mathcal{T}_{l-1} \setminus \{k^{\star}\}$
11: $\mathcal{S}_l = \mathcal{S}_{l-1} \cup \{k^{\star}\}$
12: $\mathbf{Q}_l = \begin{bmatrix}\mathbf{q}_1 & \mathbf{q}_2 & \cdots & \mathbf{q}_l\end{bmatrix}$
13: **end for**
14: **return** $\mathcal{S} = \mathcal{S}_L$

## 4.4 Semi-orthogonal Selection

The semi-orthogonal selection is a user selection algorithm that is asymptotically optimum when $K \longrightarrow \infty$ in a MIMO system under i.i.d. Rayleigh fading channel [43]. This algorithm aims to select the set of users that yields the most orthogonal effective small-scale fading channel matrix. This selection is made in an iterative manner by choosing the user with the most orthogonal small-scale fading channel with respect to the previously selected users. At the $l$th iteration, the algorithm first calculates the orthogonal complement of $\mathbf{h}_k$ to the subspace $\mathsf{span}\,\{\mathbf{q}_1, \cdots, \mathbf{q}_{l-1}\}$ for all the $K - l + 1$ remaining users in $\mathcal{T}_{l-1}$. The orthogonal component $\mathbf{h}_k^{\perp}$ is given by

$$\mathbf{h}_k^{\perp} = \mathbf{P}_{l-1}\mathbf{h}_k,\ \forall\, k \in \mathcal{T}_{l-1}, \tag{4.2}$$

where $\mathbf{P}_{l-1} \in \mathbb{C}^{M \times M}$ is the orthogonal projection matrix denoted by

$$\mathbf{P}_{l-1} = \mathbf{I}_M - \mathbf{Q}_{l-1}\mathbf{Q}_{l-1}^{\mathrm{H}}, \tag{4.3}$$

and $\mathbf{Q}_{l-1} \in \mathbb{C}^{M \times l}$ is denoted by

$$\mathbf{Q}_{l-1} = \begin{bmatrix}\mathbf{q}_1 & \mathbf{q}_2 & \cdots & \mathbf{q}_{l-1}\end{bmatrix}. \tag{4.4}$$

The users are then selected based on the orthogonal complement with the largest

$\ell_2$-norm as follows:

$$k^\star = \underset{k \in \mathcal{T}_{l-1}}{\operatorname{argmax}} \left\| \mathbf{h}_k^\perp \right\|_2 . \tag{4.5}$$

Finally, vector $\mathbf{q}_l$, sets $\mathcal{T}_l$, and $\mathcal{S}_l$ are updated as

$$\mathbf{q}_l = \frac{\mathbf{h}_{k^\star}^\perp}{\left\| \mathbf{h}_k^\perp \right\|_2}, \tag{4.6}$$

$$\mathcal{T}_l = \mathcal{T}_{l-1} \setminus \{k^\star\}, \tag{4.7}$$

$$\mathcal{S}_l = \mathcal{S}_{l-1} \cup \{k^\star\}. \tag{4.8}$$

This process is repeated until $l = L$. The SOS algorithm is summarized in Algorithm 4. Note that the first selected user is randomly chosen since for the UR-LoS fading channel, $\|\mathbf{h}_k\|_2 = \sqrt{M},\ \forall k \in \mathcal{K}$. It is worth highlighting that the original SOS algorithm proposed in [43] was created to deal with small-scale fading only. However, by using the matrix $\mathbf{G}$ instead of $\mathbf{H}$ as an input of the algorithm, SOS can perfectly deal with both small- and large-scale fading effects. That is why the SOS algorithm belongs to both classes of user selection algorithms.

***Remark 4.2***. The classical version of the SOS has a last step that forces the semi-orthogonality of the non-selected users at a given iteration. In the classical algorithm, $\mathcal{T}_l$ is updated as follows:

$$\mathcal{T}_l = \left\{ k \in \mathcal{T}_{l-1}, k \neq k^\star \,\middle|\, \frac{|\mathbf{h}_k^{\mathrm{H}} \mathbf{q}_l|}{\|\mathbf{h}_k\|_2 \|\mathbf{q}_l\|_2} < \delta \right\}, \tag{4.9}$$

where $\delta \in \mathbb{R}_+$ is the level of semi-orthogonality. This step speeds up the selection by eliminating the users with poor levels of orthogonality. This last step is useful for MIMO systems since the user selection is only performed in cases where $K > M$ and terminated when $L = M$. However, this is not necessarily the case for massive MIMO systems and by using this criteria, the algorithm may select less users than the initially desired $L$.

The Algorithm 4 can be optimized if a recursive approach is used to compute the orthogonal projection matrix [87]. Equation (4.3) can be re-written as

$$\begin{aligned}
\mathbf{P}_l &= \mathbf{I}_M - \mathbf{Q}_l \mathbf{Q}_l^{\mathrm{H}} \\
&= \mathbf{I}_M - \begin{bmatrix} \mathbf{Q}_{l-1} & \mathbf{q}_l \end{bmatrix} \begin{bmatrix} \mathbf{Q}_{l-1}^{\mathrm{H}} \\ \mathbf{q}_l^{\mathrm{H}} \end{bmatrix} \\
&= \mathbf{I}_M - \mathbf{Q}_{l-1} \mathbf{Q}_{l-1}^{\mathrm{H}} - \mathbf{q}_l \mathbf{q}_l^{\mathrm{H}} \\
&= \mathbf{P}_{l-1} - \mathbf{q}_l \mathbf{q}_l^{\mathrm{H}}.
\end{aligned} \tag{4.10}$$

**Algorithm 5** S-SOS algorithm

**Input:** $L$ and $\mathbf{H}$
**Return:** $\mathbf{P}_0 = \mathbf{I}_M$, $\mathcal{T}_0 = \mathcal{K}$, and $\mathcal{S}_0 = \emptyset$
1: **for** $l = 1$ to $L$ **do**
2: $\quad \mathbf{h}_k^{\perp} = \mathbf{P}_{l-1}\mathbf{h}_k, \ \forall\, k \in \mathcal{T}_{l-1}$
3: $\quad k^{\star} = \underset{k \in \mathcal{T}_{l-1}}{\operatorname{argmax}} \left\| \mathbf{h}_k^{\perp} \right\|_2$
4: $\quad \mathbf{q}_l = \mathbf{h}_{k^{\star}}^{\perp} / \left\| \mathbf{h}_k^{\perp} \right\|_2$
5: $\quad \mathbf{P}_l = \mathbf{P}_{l-1} - \mathbf{q}_l \mathbf{q}_l^{\mathrm{H}}$
6: $\quad \mathcal{T}_l = \mathcal{T}_{l-1} \setminus \{k^{\star}\}$
7: $\quad \mathcal{S}_l = \mathcal{S}_{l-1} \cup \{k^{\star}\}$
8: **end for**
9: **return** $\mathcal{S} = \mathcal{S}_L$

By using (4.10), we have the new SOS algorithm, named *simplified semi-orthogonal selection* (S-SOS), summarized in Algorithm 5.

## 4.5 Correlation-based Selection

The correlation-based selection algorithm is an alternative to the SOS algorithm. The CBS algorithm is a greedy method that searches for a pair of users $(k, k')$ with the highest $r_{kk'}$ and removes the one with the highest magnitude of the correlation coefficient with the remaining users. From the SINR perspective, the CBS aims to maximize the SINR of one specific user, disregarding the SINR of the remaining users. It must be noted, however, that in some cases removing a user might inadvertently result in increased SINR of the remaining users. For example, the user with the highest correlation coefficient may have a high correlation with only one user and a small correlation with the others, and another user may have a moderate correlation with all other users. In this case, dropping the second user may lead to better improvement in SE than dropping the first one. The CBS algorithm is summarized in Algorithm 6. Differently from the SOS algorithm, the CBS algorithm cannot take the large-scale fading into account. The use of $\mathbf{g}_k$ instead of $\mathbf{h}_k$ will not yield different results since the magnitude of the correlation coefficient defined in (2.6) normalize the vectors, which would remove the effect of the large-scale fading effect. That is why the CBS belongs to the class of SSFA algorithms.

## 4.6 Inter-channel Interference-based Selection

The proposed inter-channel interference-based selection algorithm can be seen as a generalization of the CBS algorithm. Unlike CBS, which takes into account local

**Algorithm 6** CBS algorithm

**Input:** $L$ and $\mathbf{G}$
**Return:** $\mathcal{S}_0 = \mathcal{K}$

1: **for** $l = 1$ to $K - L$ **do**
2: $\quad r_{kk'} = \frac{|\mathbf{h}_k^{\mathrm{H}} \mathbf{h}_{k'}|}{\|\mathbf{h}_k\|_2 \|\mathbf{h}_{k'}\|_2} \; \forall \, (k, k') \in \mathcal{S}_{l-1} \times \mathcal{S}_{l-1} \,|\, k \neq k'$
3: $\quad (i, j) = \underset{(k,k') \in \mathcal{S}_{l-1} \times \mathcal{S}_{l-1} | k \neq k'}{\operatorname{argmax}} r_{kk'}$
4: $\quad$ **if** $\max_{k' \in \mathcal{S}_{l-1} \setminus \{i,j\}} r_{ik'} > \max_{k' \in \mathcal{S}_{l-1} \setminus \{i,j\}} r_{jk'}$ **then**
5: $\quad\quad k^\star = i$
6: $\quad$ **else if** $\max_{k' \in \mathcal{S}_{l-1} \setminus \{i,j\}} r_{ik'} < \max_{k' \in \mathcal{S}_{l-1} \setminus \{i,j\}} r_{jk'}$ **then**
7: $\quad\quad k^\star = j$
8: $\quad$ **end if**
9: $\quad \mathcal{S}_l = \mathcal{S}_{l-1} \setminus \{k^\star\}$
10: **end for**
11: **return** $\mathcal{S} = \mathcal{S}_{K-L}$

(pair-wise) interference information, ICIBS considers the global interference.[3] That is, at each iteration it finds the user whose removal will lead to the highest overall SINR gain for the remaining/selected users. Thus, starting with set $\mathcal{S}_0 = \mathcal{K}$, it iteratively generates $\mathcal{S}_l \subset \mathcal{S}_{l-1}$, $l \in \mathbb{N}$, by removing the user that maximizes the ICI defined as

$$\psi_k^{(l)} = \frac{1}{|\mathcal{S}_{l-1}| - 1} \sum_{k' \in \mathcal{S}_{l-1} \setminus \{k\}} r_{kk'}, \; \forall \, k \in \mathcal{S}_{l-1}. \tag{4.11}$$

The algorithm stops at iteration $K - L$ since $|\mathcal{S}_{K-L}| = L$. It is worth highlighting the intuitive connection between the ICI and the SE. For example, by dropping the user with the highest ICI, we indirectly reduce the interference on the remaining users, increasing the SINR and consequently increasing the SE. Additionally, when the MRT precoder is used, the ICI has a more straightforward connection with the SE since the SE when MRT is used is upper and lower bounded by functions of the ICI. The ICIBS method is summarized in Algorithm 7.

ICIBS can be improved by computing step 2 in an efficient manner through the following recursion

$$\psi_k^{(l)} = \frac{(|\mathcal{S}_{l-2}| - 1)\psi_k^{(l-1)} - r_{kk^\star}}{|\mathcal{S}_{l-1}| - 1} \; \forall \, k \in \mathcal{S}_{l-1}, \tag{4.12}$$

where $k^*$ is the user index that is removed from iteration $l - 1$ to $l$. Hence, the summation in step 2 is computed just once at the first iteration, to obtain $\psi_k^{(1)}$. The new version of the ICIBS, aptly named *simplified inter-channel interference-based*

[3] The term interference is being used loosely since the transmission powers are not taken into account. In fact, it is a *potential interference*. Further, we perform power allocation after user selection as in [9, 43, 49–51, 53, 54, 88].

**Algorithm 7** ICIBS algorithm

**Input:** $L$ and $\mathbf{H}$
**Return:** $\mathcal{S}_0 = \mathcal{K}$

1: **for** $l = 1$ to $K - L$ **do**
2: $\quad \psi_k^{(l)} = \frac{1}{|\mathcal{S}_{l-1}|-1} \sum_{k' \in \mathcal{S}_{l-1} \setminus \{k\}} r_{kk'}, \ \forall\, k \in \mathcal{S}_{l-1}$
3: $\quad k^\star = \underset{k \in \mathcal{S}_{l-1}}{\operatorname{argmax}}\, \psi_k^{(l)}$
4: $\quad \mathcal{S}_l = \mathcal{S}_{l-1} \setminus \{k^\star\}$
5: **end for**
6: **return** $\mathcal{S} = \mathcal{S}_{K-L}$

**Algorithm 8** S-ICIBS algorithm

**Input:** $L$ and $\mathbf{G}$
**Return:** $\mathcal{S}_0 = \mathcal{K}$

1: **for** $l = 1$ to $K - L$ **do**
2: $\quad$ **if** $l = 1$ **then**
3: $\quad\quad \psi_k^{(1)} = \frac{1}{|\mathcal{S}_0|-1} \sum_{k' \in \mathcal{S}_0 \setminus \{k\}} r_{kk'}, \ \forall\ k \in \mathcal{S}_0$
4: $\quad$ **else**
5: $\quad\quad \psi_k^{(l)} = \frac{(|\mathcal{S}_{l-2}|-1)\psi_k^{(l-1)} - r_{kk^*}}{|\mathcal{S}_{l-1}|-1}$
6: $\quad$ **end if**
7: $\quad k^\star = \underset{k \in \mathcal{S}_{l-1}}{\operatorname{argmax}}\, \psi_k^{(l)}$
8: $\quad \mathcal{S}_l = \mathcal{S}_{l-1} \setminus \{k^\star\}$
9: **end for**
10: **return** $\mathcal{S} = \mathcal{S}_{K-L}$

*selection* (S-ICIBS), is summarized in Algorithm 8.

### 4.6.1 ICIBS with MRT Precoder

The proposed ICIBS algorithm is independent of precoders used, however, for the MRT, we can show that the SE is upper and lower bounded by functions of the ICI. The following theorem addresses the DL SE, assuming that all users' channels have the same large-scale fading.

**Theorem 4.1**
*For a massive MIMO system with an $M$-antenna base station serving $L$ users with the same large-scale coefficient $\beta$, the DL SE is bounded as follows:*

$$\alpha \sum_{k \in \mathcal{S}} \log_2 \left(1 + \breve{\gamma}_k\right) \leq R_{sum} \leq \alpha \sum_{k \in \mathcal{S}} \log_2 \left(1 + \tilde{\gamma}_k\right), \tag{4.13}$$

*where*

$$\breve{\gamma}_k = \frac{\rho \beta M}{|\mathcal{S}| + \rho \beta M (|\mathcal{S}| - 1)^2 \max\limits_{k \in \mathcal{S}} \psi_k^2}, \tag{4.14}$$

*and*

$$\tilde{\gamma}_k = \frac{\rho\beta M}{|\mathcal{S}| + \rho\beta M(|\mathcal{S}|-1)\psi_k^2}. \tag{4.15}$$

*Proof.* The expressions for the ICI in (4.11) and DL SINR in (2.42) can be rewritten, respectively, as

$$\psi_k = \frac{1}{|\mathcal{S}|-1} \left\|\mathbf{r}_k\right\|_1, \tag{4.16}$$

and

$$\gamma_k = \frac{\rho\beta M}{|\mathcal{S}| + \rho\beta M \left\|\mathbf{r}_k\right\|_2^2}, \ \forall k \in \mathcal{S}, \tag{4.17}$$

where $\mathbf{r}_k \in \mathbb{R}_+^{(|\mathcal{S}|-1)\times 1}$ collects all correlations $r_{kk'}$, but $r_{kk}$.

Since $\frac{1}{|\mathcal{S}|-1}\left\|\mathbf{r}_k\right\|_1^2 \leq \left\|\mathbf{r}_k\right\|_2^2 \leq \left\|\mathbf{r}_k\right\|_1^2$ holds [89], then it follows from (4.16) that

$$(|\mathcal{S}|-1)\psi_k^2 \leq \left\|\mathbf{r}_k\right\|_2^2 \leq (|\mathcal{S}|-1)^2\psi_k^2 \leq (|\mathcal{S}|-1)^2 \max_{k\in\mathcal{S}} \psi_k^2. \tag{4.18}$$

Given (4.14) and (4.15), one therefore has $\check{\gamma}_k \leq \gamma_k \leq \tilde{\gamma}_k$, from which the bounds for the DL SE in (4.13) follow. □

The inequalities in (4.13) show a direct relation between the ICI and the DL SE with MRT precoder. Therefore, by minimizing the maximum ICI, it is possible to improve the SE of the massive MIMO system, which is the main idea of the ICIBS approach.

## 4.7 Fading-ratio-based Selection

Although the ICIBS approach yields improvement in SE compared to the case where all the users are kept, it does not take the large-scale fading into account, which is a valuable information for selecting users. In (2.28), one can observe that the large-scale fading has also an impact on the SINR, which sometimes can be more relevant for the SINR improvement than the ICI. For instance, consider two users to be served in a massive MIMO system. If user 1 has a slightly higher ICI than user 2, but much higher large-scale fading, then it would be better for the SE of the network to drop user 2 and keep user 1 than the opposite. To deal with this issue, we propose the FRBS as a generalization of the ICIBS. The FRBS, summarized in Algorithm 9, drops the users that maximize the *fading ratio* (FR) defined as

$$\delta_k = \frac{\psi_k}{\sqrt{\beta_k}} \ \forall\, k \in \mathcal{S}. \tag{4.19}$$

This metric takes into account both small- and large-scale fading effects. This new algorithm yields performance improvements when compared to ICIBS in some cases, as it will be discussed in Section 6. It is worth highlighting two important points

**Algorithm 9** FRBS algorithm

**Input:** $L$ and $\mathbf{H}$
**Return:** $\mathcal{S}_0 = \mathcal{K}$

1: **for** $l = 1$ to $K - L$ **do**
2: $\quad \psi_k^{(l)} = \frac{1}{|\mathcal{S}_{l-1}|-1} \sum_{k' \in \mathcal{S}_{l-1} \setminus \{k\}} r_{kk'}, \ \forall\, k \in \mathcal{S}_{l-1}$
3: $\quad \delta_k^{(l)} = \frac{\psi_k^{(l)}}{\sqrt{\beta_k}}, \ \forall\, k \in \mathcal{S}_{l-1}$
4: $\quad k^\star = \underset{k \in \mathcal{S}_{l-1}}{\operatorname{argmax}}\, \delta_k^{(l)}$
5: $\quad \mathcal{S}_l = \mathcal{S}_{l-1} \setminus \{k^\star\}$
6: **end for**
7: **return** $\mathcal{S} = \mathcal{S}_{K-L}$

regarding the heuristic criteria in (4.19) used to select users. Firstly, the large-scale fading considered in this work is composed by the path loss and the shadow fading, which is the most usual formulation in the massive MIMO literature [63, 90]. Usually in the massive MIMO literature, other impairments such as hardware distortions are incorporated in the small-scale fading vector, necessitating channel estimation and leading to scenarios with imperfect CSI knowledge [52, 91]. In Chapter 5, simulation results have shown that the relative performance of user selection algorithms are not affected by the imperfect CSI scenarios. Secondly, the user selection algorithms are not responsible for controlling the network traffic to ensure all users are served. This task is the responsibility of the user scheduling/assignment algorithms [10, 57]. The user selection is a part of the scheduling that selects the best users to be served in a given time slot.

Fig. 4.1 illustrates the user selection performed by ICIBS and FRBS. As can be observed from the figure, when ICIBS is used the selected users were spread across the cell since the ICIBS does not take the large-scale fading into consideration, only considering the users that minimize the ICI. In the case of FRBS, as can be observed in Fig. 4.1b, some of the selected users were "clustered" in a region close to the BS since, in this case, the large-scale fading was more relevant to the minimization of the global interference. The FRBS, therefore, tends to select users that have a better link to the BS, leaving to the user-scheduling algorithm the task of guaranteeing fairness in the coverage.

## 4.8 Computational Complexity

This section discusses and summarizes the computational complexities of the user selection approaches previously detailed in this chapter. Table 4.2 details the number of additions, multiplications, divisions, and square root operations that are required by each algorithm. Table 4.3 captures the number of linear searches per iteration

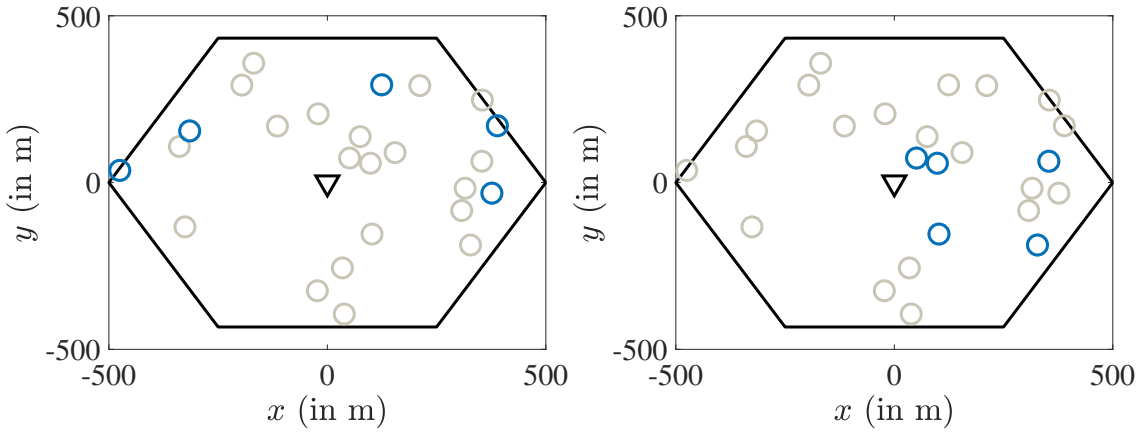


(a) ICIBS (b) FRBS

Figure 4.1: ICIBS and FRBS with $M = 50$, $K = 25$, $L = 5$, and $R = 500$ m. ($\bigtriangledown$ BS, ◯ selected user, and ◯ dropped user)

required by the various user selection algorithms. In the following, we discuss the computational complexities of the SOS, S-SOS, CBS, ICIBS, S-ICIBS, and FRBS, respectively.

### 4.8.1 Semi-orthogonal Selection

The complexity of SOS presented in Algorithm 4 is measured in terms of the number of operations used to select the best set of users. The most expensive operations are in (4.2), (4.3), (4.5), and (4.6). At the $l$th iteration, Algorithm 4 requires $2(M^3+M^2-M)(K-l+1)$ additions and $4M^3(K-l+1)$ multiplications to compute (4.2). Moreover, it requires $4M^2(l-1)$ additions and $4M^2(l-1)$ multiplications to compute (4.3). Additionally, Algorithm 4 requires $2M$ divisions, $(K-l+1)$ $\ell_2$-norm calculations, and one linear search in a $(K-l+1)$- dimensional space to compute (4.5) and (4.6). However, in order to compute $\|\mathbf{x}\|_2$, where $\mathbf{x} \in \mathbb{C}^{M\times 1}$, $2M-1$ additions, $2M$ multiplications, and 1 square root operation are needed. Therefore, the number of additions $A_l^{\text{SOS}}$, multiplications $M_l^{\text{SOS}}$, divisions $D_l^{\text{SOS}}$, and square root $S_l^{\text{SOS}}$ computations required by Algorithm 4 per iteration are given by

$$\begin{aligned}
A_l^{\text{SOS}} =& 2(M^3+M^2-M)(K-l+1)+ \\
&+(2M-1)(K-l+1)4M^2(l-1), \\
M_l^{\text{SOS}} =& 4M^3(K-l+1)+4M^2(l-1) \\
&+2M(K-l+1), \\
D_l^{\text{SOS}} =& 2M, \\
S_l^{\text{SOS}} =& K-l+1,
\end{aligned}$$

Table 4.2: Number of Operations and Complexity of the User Selection Algorithms

| | **Addition** | **Multiplication** | **Division** | **Square Root** |
|---|---|---|---|---|
| **SOS** | $(M^3+M^2-M)(L-1)(2K-L)$ $+(2M-1)(KL-L(L-1)/2)$ $+2M^2L(L-1)$ | $2M^2(L-1)(2MK-ML+L)$ $+M(2KL-L(L-1))$ | $2ML$ | $KL-L(L-1)/2$ |
| **S-SOS** | $(M^3+M^2-M)(L-1)(2K-L)$ $+(2M-1)(KL-L(L-1)/2)$ $+4M^2(L-1)$ | $2M^2(L-1)(2MK-ML+2)$ $+M(2KL-L(L-1))$ | $2ML$ | $KL-L(L-1)/2$ |
| **CBS** | $4K^2M+K(K-1)/2$ | $4K^2M+K^2-K$ | $2MK$ | $K(K-1)/2$ |
| **ICIBS** | $4K^2M+K(K-1)(2K+5)/6$ $-L(L+1)(L-1)/3$ | $4K^2M+K^2-K$ | $2MK+K(K+1)/2$ $-L(L+1)/2$ | $K(K-1)/2$ |
| **S-ICIBS** | $4K^2M+K^2-L(L+1)/2$ | $4K^2M+K(3K-1)/2$ $-L(L+1)/2$ | $2MK+K(K+1)/2$ $-L(L+1)/2$ | $K(K-1)/2$ |

Table 4.3: Number of Linear Searches per Iteration

| | **Linear Search** |
|---|---|
| **SOS** | 1 search in $(K-l+1)$ elements |
| **Fast-SOS** | 1 search in $(K-l+1)$ elements |
| **CBS** | 1 search in $((K-l+1)(K-L)/2)$ elements and 2 searches in $(K-l-1)$ elements |
| **ICIBS** | 1 search in $(K-l+1)$ elements |
| **Fast-ICIBS** | 1 search in $(K-l+1)$ elements |

respectively. By summing these quantities across $L$ iterations the total number of a given operation can be obtained as summarized in Table 4.2. It is worth highlighting that the additions and multiplications are only computed from the second iteration onward.

One characteristic of the SOS algorithm is its incremental approach for selecting users, i.e., it starts with an empty set of selected users. This behavior can be seen in Table 4.2 with the number of operations necessary to compute the algorithm increasing with $L$. This incremental characteristic leads to low computational complexity when the number of selected users is very small.

### 4.8.2 Simplified Semi-orthogonal Selection

For the S-SOS the most expensive operations are equations (4.2), (4.5), (4.6), and (4.10). The only difference between S-SOS and SOS is in (4.3) that is replaced with (4.10), which leads to the following required number of additions $A_l^{\text{S-SOS}}$, multiplications $M_l^{\text{S-SOS}}$, divisions $D_l^{\text{S-SOS}}$, and square root $S_l^{\text{S-SOS}}$ computations per iteration are given by

$$\begin{aligned} A_l^{\text{S-SOS}} =& 2(M^3+M^2-M)(K-l+1)+4M^2 \\ &+(2M-1)(K-l+1), \\ M_l^{\text{S-SOS}} =& 4M^3(K-l+1)+4M^2+2M(K-l+1), \\ D_l^{\text{S-SOS}} =& 2M, \\ S_l^{\text{S-SOS}} =& K-l+1, \end{aligned}$$

respectively. One can observe that the second term of $A_l^{\text{S-SOS}}$ and $M_l^{\text{S-SOS}}$ is not linear with index $l$, differently from $A_l^{\text{SOS}}$ and $M_l^{\text{SOS}}$. This difference yields a reduced computational burden for S-SOS. The total number of operations required for S-SOS is summarized in Table 4.2.

### 4.8.3 Correlation-based Selection

The complexity of the CBS algorithm is mostly concentrated in the computation of the magnitude of the correlation coefficient $r_{kk'}$. In order to help in the calculation of $r_{kk'}$, we define the matrix $\boldsymbol{\Upsilon} \in \mathbb{R}_{+}^{K \times K}$ as

$$\boldsymbol{\Upsilon} = \begin{bmatrix} 0 & r_{12} & \cdots & r_{1K} \\ r_{21} & 0 & \cdots & r_{2K} \\ \vdots & \vdots & \ddots & \vdots \\ r_{K1} & r_{K2} & \cdots & 0 \end{bmatrix}. \tag{4.20}$$

Note that matrix $\boldsymbol{\Upsilon}$ is not exactly a correlation matrix because it is a hollow matrix and does not have the $r_{kk}$ information. Another definition for $\boldsymbol{\Upsilon}$ is given by

$$\boldsymbol{\Upsilon} = \mathsf{abs}\left(\mathbf{I}_K - \bar{\mathbf{H}}^{\mathrm{H}}\bar{\mathbf{H}}\right), \tag{4.21}$$

where $\bar{\mathbf{H}} \in \mathbb{C}^{M \times K}$ is the normalized small-scale fading channel matrix of the users. In order to build $\boldsymbol{\Upsilon}$ it is necessary to carry out $4K^2M$ additions, $4K^2M$ multiplications, and $K(K-1)/2$ absolute value operations, which requires one addition, two multiplications, and one square root operation. Note that it is only necessary to do $K(K-1)/2$ absolute value operations because $\boldsymbol{\Upsilon}$ is a symmetric hollow matrix. Another important step is the $\ell_2$-norm calculations and divisions to build the matrix $\bar{\mathbf{H}}$. However, since $\|\mathbf{h}_k\|_2 = \sqrt{M}\ \forall k \in \mathcal{K}$, it is just necessary to undertake $2KM$ divisions. The total number of operations required by CBS is summarized in Table 4.2.

After calculating $\boldsymbol{\Upsilon}$, three linear searches are carried out to find the user to be dropped at that iteration. Therefore, at the $l$th iteration, the CBS first searches in $(K-l+1)(K-l)/2$ elements in order to find the pair $(k, k')$ with the highest $r_{kk'}$. Then, it performs two searches in $(K-l-1)$-dimensional space to find which user has the second highest magnitude of the correlation coefficient. These three searches have computational complexities of $\mathcal{O}((K-l+1)(K-l)/2)$, $\mathcal{O}(K-l-1)$, and $\mathcal{O}(K-l-1)$, respectively.

There are no arithmetic calculations inside the loop of CBS, which is a big advantage compared to SOS and S-SOS. However, it requires 3 searches that depend on $K$, which can be a real bottleneck depending on the size of the massive MIMO system.

### 4.8.4 Inter-channel Interference-based Selection

The computational burden of ICIBS is very similar to that of CBS, with one of the main differences being the additional step required by ICIBS to compute the ICI.

Equation (4.11) can be rewritten as matrix equation given by

$$\boldsymbol{\psi}^{(l)} = \frac{1}{|\mathcal{S}_{l-1}| - 1} \boldsymbol{\Upsilon}_{\mathcal{S}_{l-1}} \mathbf{1}_{|\mathcal{S}_{l-1}| \times 1}. \tag{4.22}$$

This additional step requires $(K - l + 1)(K - l)$ additions and $K - l + 1$ divisions per iteration since $|\mathcal{S}_{l-1}| = K - l + 1$. The total number of operations required by ICIBS is summarized in Table 4.2. Additionally, ICIBS performs one linear search in a $(K - l - 1)$-dimensional space in order to find the user with the highest ICI.

Compared to CBS, ICIBS performs additional arithmetic operations inside its loop, which increases the computational burden. However, ICIBS also performs fewer searches in order to find the user to be dropped from the transmission, which is an advantage compared to CBS. Besides that, ICIBS, like CBS, is a decremental user selection approach, which, differently from SOS and S-SOS, leads to reduced computational burden when the number of selected users $L$ is close to the actual number of users $K$.

### 4.8.5 Simplified Inter-channel Interference-based Selection

The complexity of the S-ICIBS is concentrated in the computation of (4.12), which requires $(K - l)$ additions, $(K - l)$ multiplications, and $(K - l)$ divisions. The total number of operations is summarized in Table 4.2. At first glance, the S-ICIBS does not seem to yield an improvement because it performs extra multiplications compared to ICIBS. However, the computational advantages of (4.12) become more evident as $K$ increases.

### 4.8.6 Fading-ratio Based Selection

The computational burden of FRBS is very similar to that of ICIBS, with the addition of one new step to compute the FR. At each iteration $l$, FRBS computes (4.11) and (4.19), which can be rewritten as a matrix equation given by

$$\boldsymbol{\delta}^{(l)} = \frac{1}{|\mathcal{S}_{l-1}| - 1} \mathsf{Diag}\left(\boldsymbol{\beta}_{\mathcal{S}_{l-1}}\right)^{-1/2} \boldsymbol{\Upsilon}_{\mathcal{S}_{l-1}} \mathbf{1}_{|\mathcal{S}_{l-1}| \times 1}. \tag{4.23}$$

This step requires $(K-l+1)(K-l)$ additions, $2(K-l+1)$ divisions, and $K-l+1$ square root computations per iteration since $|\mathcal{S}_{l-1}| = K-l+1$. Additionally, FRBS performs one linear search in a $(K - l - 1)$-dimensional space to find the user with the highest FR. The computational complexity of FRBS is summarized in Table 4.4.

Table 4.4: FRBS' Computational Complexity

| | **Number of Operations** |
|---|---|
| **Additions** | $4K^2M + K(K-1)(2K+5)/6 - L(L+1)(L-1)/3$ |
| **Multiplications** | $4K^2M + K^2 - K$ |
| **Division** | $K^2 + K(K+1) - L(L+1)$ |
| **Square Root** | $K(K-1) - L(L+1)/2$ |

## 4.9 Concluding Remarks

In this chapter a comprehensive review of the user selection algorithms for massive MIMO systems has been provided, including a thorough analysis of the computational complexity of the user selection algorithms. Moreover, it is shown that there are practical cases in which the LoS propagation model may lead to significant levels of interference among users within a cell and such cases are not satisfactorily addressed by the existing user selection algorithms. To this end, a new user selection algorithm based on ICI, called ICIBS, was proposed. Unlike other techniques, the ICIBS accounts for the ICI in a global manner, thus yielding better results than the other algorithms especially in cases where there are many users interfering with one another and similar results in scenarios having low-interference levels. Furthermore, another novel algorithm to perform user selection in massive MIMO systems based on the average interference among all users taking into account the small- and large-scale fading, called FRBS, was proposed. Additionally, although the thesis has focused on LoS propagation, all algorithms can also be applied to different channel models, such as the Rician fading model. From our experience, however, the benefits in SE due to the use of user selection algorithms are more prominent as the Rician fading model tends to the LoS model, whereas they become negligible for i.i.d. Rayleigh fading. In the next two chapters, simulation results regarding the performance of the ICIBS and FRBS will be presented and discussed.

# Chapter 5

# Performance Evaluation of the ICIBS Algorithm

## 5.1 Overview

In this chapter, the proposed ICIBS algorithm is compared to SOS [43] and CBS [9] algorithms. These algorithms were combined with MRT, ZF, and the MMSE [16] precoders. Equal power allocation was used since the aim is to evaluate the impact of user selection. The performance is assessed via numerical simulations by analyzing the effect of the number of selected users on the system's throughput and computational complexity.[1] All codes used in this work are available on GitHub through the following link: `https://github.com/rafaelschaves/user-selection-for-massive-mimo-under-los-propagation`. The user selection algorithms were evaluated under three different scenarios:

- ***Perfect CSI:*** to evaluate the improvement afforded by the user selection algorithms when complete and perfect knowledge of the channel is available.
- ***Imperfect CSI:*** to evaluate the performance of the user selection algorithms when only imperfect knowledge of the channel is available.
- ***Ultra Clustered-crowded environment:*** to evaluate the improvement provided by the user selection algorithms when all the users are clustered in a small section of the cell. This scenario is really challenging for user selection algorithms due to the proximity of the users, i.e., the AoAs corresponding to these users are very similar, thus increasing the inter-channel interference level.

[1] The throughput is given by

$$\mu = BR_{\text{sum}} \text{ [bps]}, \tag{5.1}$$

where $B \in \mathbb{R}_+$ is the bandwidth in Hz.

Table 5.1: Simulation Parameters for the ICIBS

| | **Parameters** |
|---|---|
| **Number of Antennas** | $M \in \{50, 100\}$ |
| **Number of Users** | $K \in \{10, 25, 50, 100, 150\}$ |
| **Cell Radius** | $R = 500$ m |
| **Bandwidth** | $B = 20$ MHz |
| **Large-scale Fading** | $\beta_k = -148 - 37.6 \log_{10}(d_k \times 10^{-3})$ dB |
| **BS Power** | 10 W |
| **BS Antenna Gain** | 0 dBi |
| **User Antenna Gain** | 0 dBi |
| **Monte-Carlo Ensemble** | $5,000$ |
| **Precoding Algorithms** | MRT, ZF, and MMSE |
| **User Selection Algorithms** | SOS, CBS, and ICIBS |

## 5.2 System Parameters

The simulation set-up was strongly inspired by that of [9]. For the simulations, a 500-m radius hexagonal single-cell massive MIMO system with $M \in \{50, 100\}$ and $K \in \{10, 50, 75, 100, 150\}$ was used. The UR-LoS channel with a ULA, carrier frequency of 2 GHz, and bandwidth $B = 20$ MHz were used in the simulations. The large-scale coefficient was known by the BS and is defined as [59]

$$\beta_k = -148 - 37.6 \log_{10} \left( \frac{d_k}{1 \text{ km}} \right) \text{ [dB]}, \tag{5.2}$$

where $d_k \in \mathbb{R}_+$ is the distance between the $k$th user and the BS. Further, we considered the worst possible scenario in the cell, where all users were at the cell edge, yielding $\beta = -137$ dB for each user. Although this assumption seems restrictive at first glance, it makes it possible to highlight the impact of small-scale fading on the system performance and how it can be compensated through user selection. The radiated power at the BS was 10 W, the BS and user antenna gain was 0 dBi, and the noise figure for the users was 9 dB. Hence, the DL SNR was 132 dB, yielding an effective SNR $\bar{\rho}$ of $-5$ dB. Moreover, the throughput was calculated using $2,000$ realizations of the UR-LoS fading channel. The simulations parameters are summarized in Table 5.1.

## 5.3 Perfect CSI

In this section, the throughput of massive MIMO systems was analyzed considering perfect CSI at the BS. This setup deliberately aimed to avoid the effect of errors in the precoders in order to highlight the improvement brought about by user selection to the throughput. For this case, two different scenarios were simulated: first one

with $M = 50$ and $K \in \{10, 50, 75\}$, and the second one with $M = 100$ and $K \in \{10, 100, 150\}$.

Fig. 5.1 illustrates the average throughput *versus* the number of users for $M \in \{50, 100\}$ and $K \in \{10, 25, 50, 75, 100, 150\}$ when the MRT, ZF, and MMSE precoders are used. As can be observed, the performance of ZF and MMSE precoders degrade with increasing number of users until to the point where they both stop working since $K > M$. This degraded throughput when the ZF and MMSE precoders are used is expected since for a fixed $M$, increasing $K$ results in higher probability of having close users, consequently leading to an ill-conditioned channel matrix. For the case where the MRT precoder is used, as can be observed, it is possible to serve much more users than the number of antennas. However, for the case of large $K$, increasing the number of users further does not yield a significant increase in the throughput. In fact, the throughput is limited by the number of antennas and the SNR [16]. In this case, the limitation of the maximum throughput means that individual users are penalized due to the addition of new users to the network. Once the network maximum throughput is achieved, in order to have a new user accessing the network, the remaining users will have their throughput decreased. Thus, even when the MRT precoder is used the number of users impact the performance of the massive MIMO system. The aforementioned problems can be solved by performing user selection at the BS.

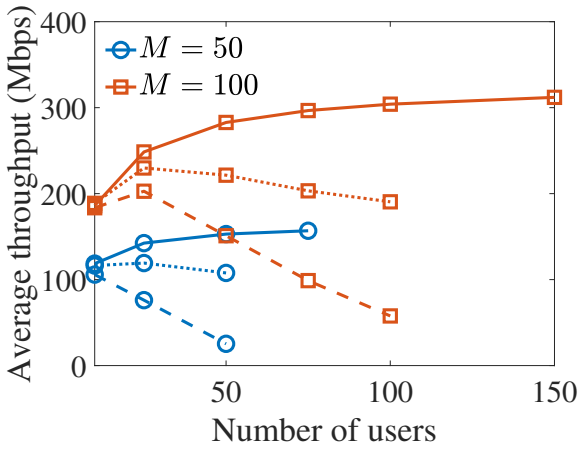


Figure 5.1: Average throughput *versus* the number of users for $M \in \{50, 100\}$. ($-$ MRT, $--$ ZF, and $\cdots$ MMSE)

Fig. 5.2 depicts the average throughput *versus* the number of selected users $L$ for $M \in \{50, 100\}$ and different number of users $K \in \{10, 50, 75, 100, 150\}$, wherein $L = K$ corresponds to keeping all users (i.e., *no user selection*). The figure shows that there was a number of selected users that maximizes the throughput and this number varied depending on the particular user selection algorithm. The concavity of the curves shows that the user selection benefited the system throughput, even

when $M \gg K$. In the worst case, which happened when the user selection algorithms were used with the ZF precoder, the user selection improved the throughput by at least 16.88% and 4.52% for $M = 50$ and $M = 100$, respectively, considering the maximum achieved throughput. Figs. 5.2a–5.2c illustrate user selection for $M = 50$ and $K \in \{10, 50, 75\}$. In this case, all the algorithms achieved a very close maximum performance. Indeed, in the best case, ICIBS was only 0.56% and 1.29% better than SOS and CBS, respectively. For $M = 100$, the achieved maximum throughput performances were still very similar with ICIBS being 0.47% and 1.23% better than SOS and CBS, as depicted in Figs. 5.2d–5.2f. It is worth highlighting that in Fig. 5.2c and 5.2f, the user selection enabled the use of ZF and MMSE precoders since they can only be used when $K \leq M$, which is already an advantage by itself.

Fig. 5.3 shows the *cumulative distribution function* (CDF) of the throughput for $M \in \{50, 100\}$, $L = \lceil K/2 \rceil$, and varying the number of users $K$. As can be observed in this figure, the performance of the user selection algorithms varied with $K$ and the precoder used. For $M = 50$, the ICIBS algorithm outperformed the others for all values of $K$, except for $K = 75$, as shown in Figs. 5.3a–5.3c. For $K = 75$, the SOS provided the best performance with ZF, ICIBS with MMSE, and CBS performing slightly better with MRT. Moreover, with this number of selected users, the precoding algorithms had a significant impact on the performance; the ZF and MMSE performing better with small $K$ and MRT yielding a better performance for large $K$. In Figs. 5.3d–5.3f, for $M = 100$, the same pattern of curves was observed as in Figs. 5.3a–5.3c, with the only difference being the achieved throughput, which was higher due to the higher multiplexing gain provided by the larger array.

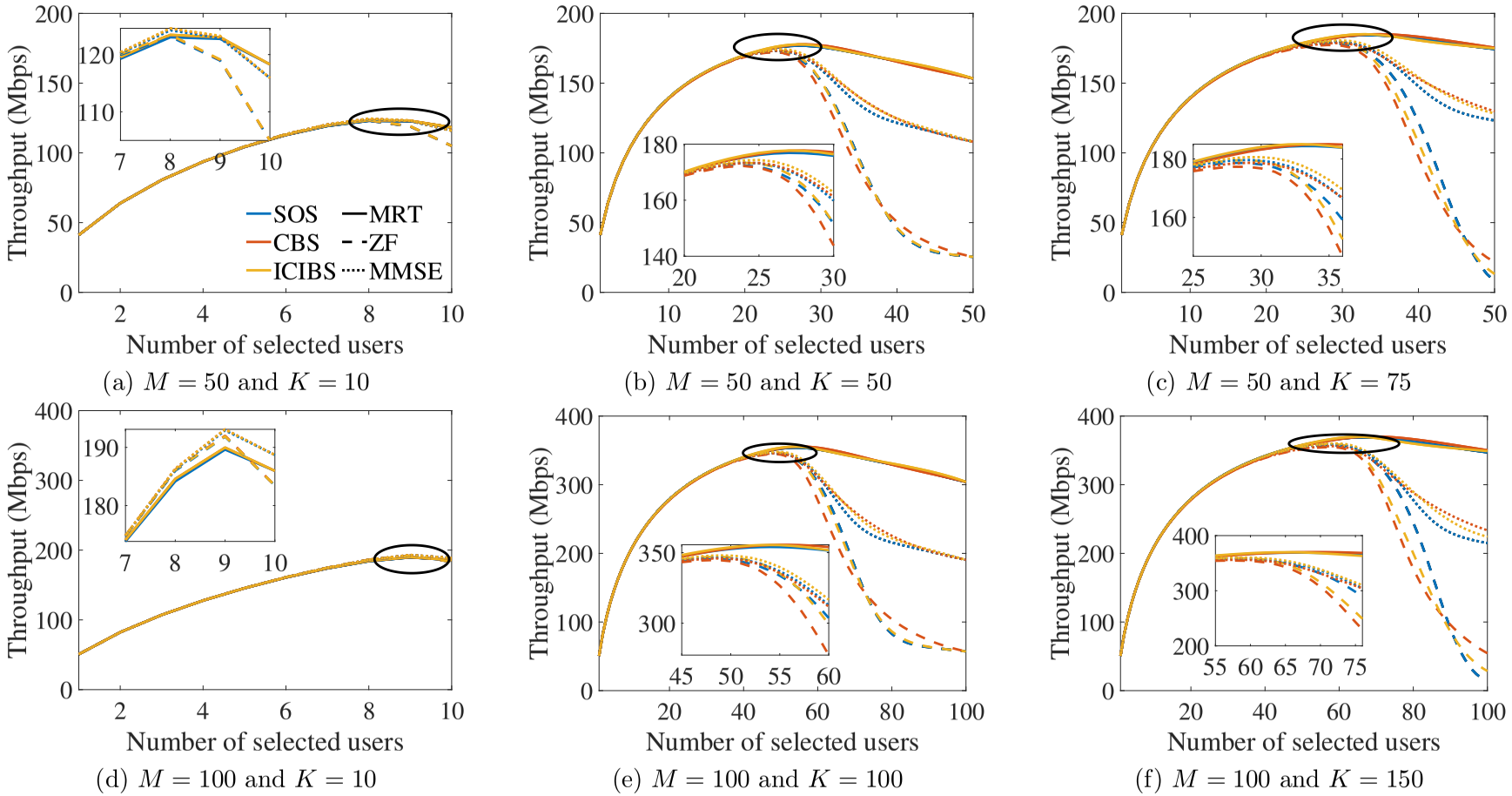


(a) $M = 50$ and $K = 10$ (b) $M = 50$ and $K = 50$ (c) $M = 50$ and $K = 75$

(d) $M = 100$ and $K = 10$ (e) $M = 100$ and $K = 100$ (f) $M = 100$ and $K = 150$

Figure 5.2: Average throughput *versus* the number of selected users $L$ for $M \in \{50, 100\}$, considering different number of users $K$. The line style (solid, dashed or dotted line) determines the precoder, whereas the colors specify the user selection algorithm. The yellow solid line, e.g., represents the results achieved by the ICIBS scheme considering an MRT precoder.

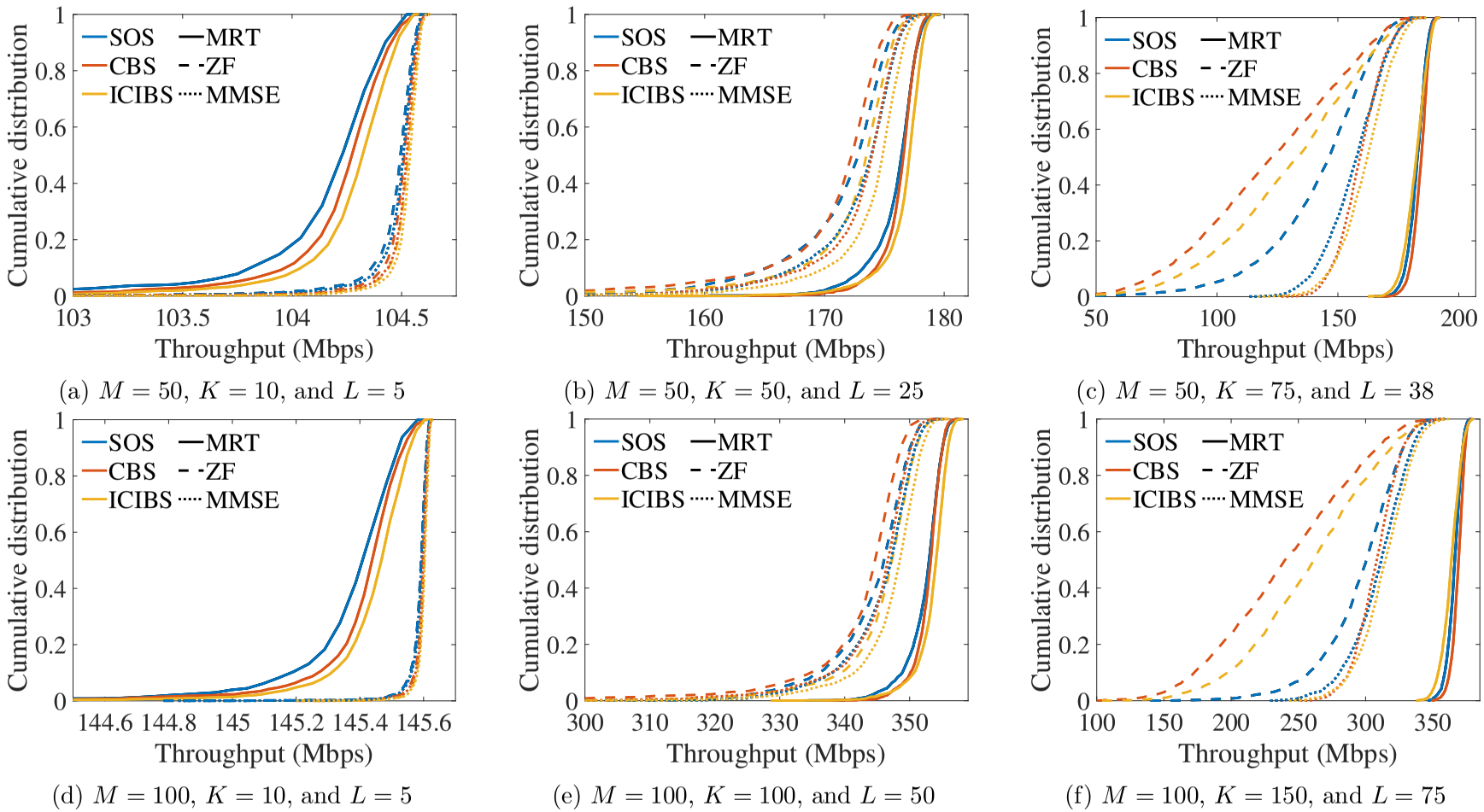


(a) $M = 50$, $K = 10$, and $L = 5$

(b) $M = 50$, $K = 50$, and $L = 25$

(c) $M = 50$, $K = 75$, and $L = 38$

(d) $M = 100$, $K = 10$, and $L = 5$

(e) $M = 100$, $K = 100$, and $L = 50$

(f) $M = 100$, $K = 150$, and $L = 75$

Figure 5.3: *Cumulative distribution function* of the throughput for $L = \lceil K/2 \rceil$ and $M \in \{50, 100\}$, considering different number of users $K$. The line style (solid, dashed or dotted line) determines the precoder, whereas the colors specify the user selection algorithm. The yellow solid line, e.g., represents the results achieved by the ICIBS scheme considering an MRT precoder.

## 5.4 Computational Complexity

This section analyzes the computational burden behavior of the user selection algorithms with the number of selected users $L$ and the number of antennas $M$. For this analysis, we used a scenario with $K = 100$ and $M \in \{50, 100\}$. The computational burden of the user selection algorithms was compared in terms of the *floating point operations* (flops) count. We consider that a division and a square root operation are equivalent to one flop, similar to that of an addition and a multiplication.

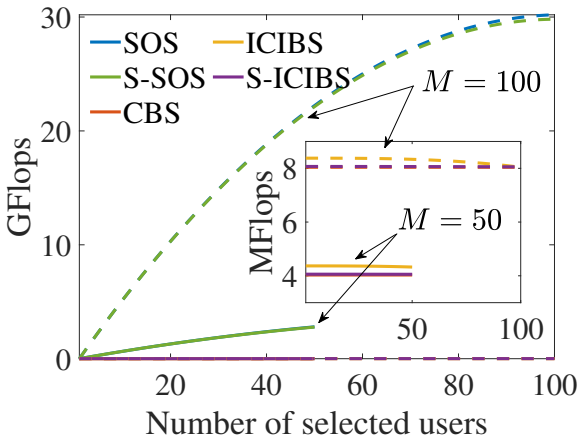


Figure 5.4: Giga flops count *versus* the number of selected users for $K = 100$ and $M \in \{50, 100\}$.

Fig. 5.4 depicts the flops count *versus* the number of selected users $L$. As can be observed in this figure, the computational burden of SOS and S-SOS grows rapidly with $L$ due to the incremental nature of this type of algorithm. Additionally, the simplified version does present a significant decrease of the computational burden in this case. Moreover, the computational burden of SOS and S-SOS is significantly higher than that of CBS, ICIBS, and ICIBS, requiring at least $10^9$ more operations. Furthermore, S-ICIBS reduces the computational burden compared to ICIBS, achieving a similar one to CBS without requiring expensive linear searches like CBS. In conclusion, SOS and S-SOS can be prohibitive for massive MIMO systems, depending on the system parameters. ICIBS is very appealing to massive MIMO networks due to its low complexity and very good performance.

## 5.5 Imperfect CSI

This section analyzes the robustness of the user selection algorithms to a possible error, which leads to the imperfect CSI scenario. This scenario is closer to what happens in practical massive MIMO systems, wherein channel estimation errors stem from several sources, such as inherent inaccuracies of the channel estimation algorithm, and/or from the pilot contamination from different cells in a multi-cell

scenario, as explained in Section 2.4. For this analysis, we considered the channel estimate as in (2.26) with $\sigma_\varepsilon^2 \in \{0, 10^{-3}, 10^{-2}, 10^{-1}, 10^{0}\}$.

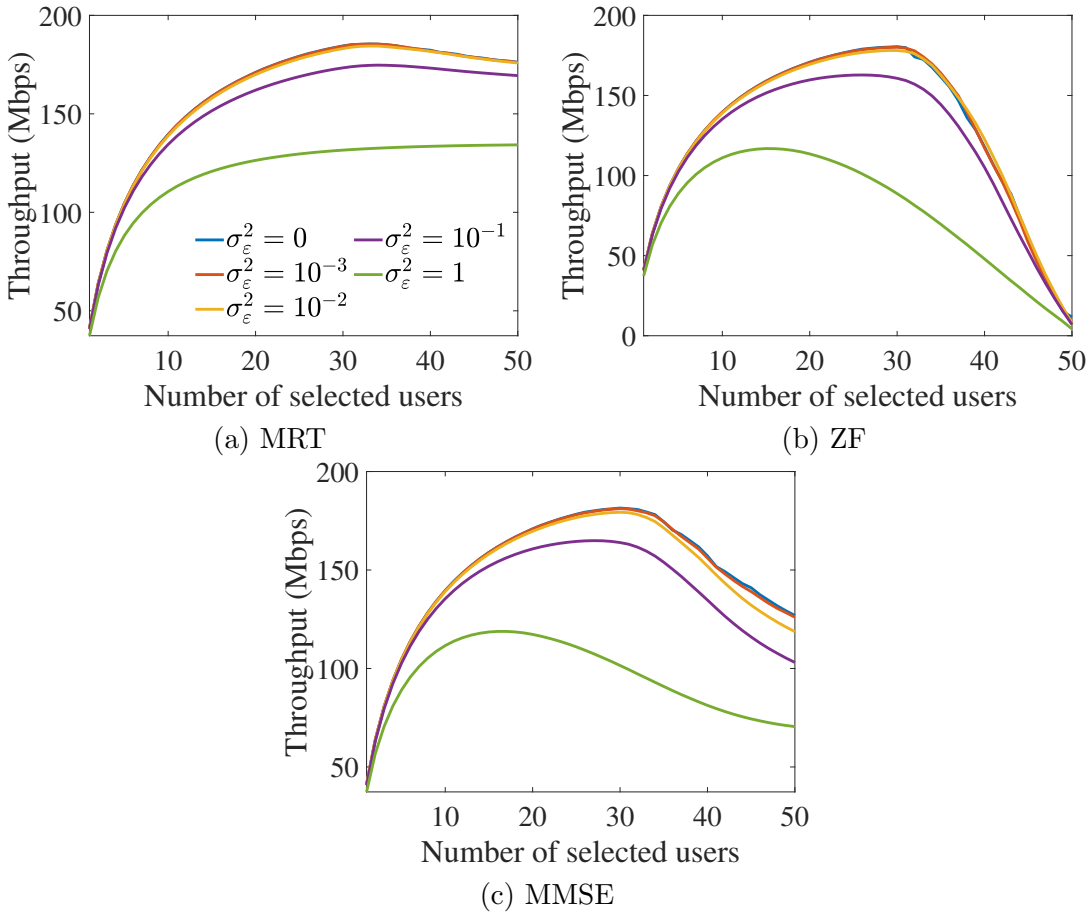


(a) MRT (b) ZF

(c) MMSE

Figure 5.5: Average throughput *versus* the number of selected users $L$ with imperfect CSI knowledge for the ICIBS algorithm, considering $M = 50$, $K = 75$, different precoding algorithms, and different $\sigma_\varepsilon^2$.

Fig. 5.5 shows the average throughput *versus* the number of selected users $L$ with imperfect CSI knowledge for the ICIBS algorithm, considering $M = 50$, $K = 75$, different precoding algorithms, and different $\sigma_\varepsilon^2$. For the sake of simplicity, we only show the results for the ICIBS algorithms since the other user selection algorithms have similar performances. As it can be observed from this figure, the performance of ICIBS has the same pattern as in Fig. 5.2 with variations in the throughput due to the errors in the channel estimation. For small $\sigma_\varepsilon^2$, the performance of ICIBS is close to the case when perfect CSI is available for all precoders. For large $\sigma_\varepsilon^2$, the ICIBS has a significant performance gap when compared to the case with perfect CSI knowledge. Furthermore, it is worth highlighting that, in the case with $\sigma_\varepsilon^2 = 1$, the throughput as a function of the number of selected users when the MRT precoder is used is monotonically increasing, unlike in the other cases. This phenomenon happens due to the fact that the channel estimate for this case with high channel estimation error is more like an i.i.d. Rayleigh than an LoS channel, which explains

the monotonic behavior.

Fig. 5.6 depicts the performance comparison between ICIBS and the other user selection algorithms in terms of the maximum achieved throughput and the optimum number of selected user $L^\star$, i.e., the number of selected users that leads to the maximum achieved throughput. As it can be observed in Figs. 5.6a–5.6c, the maximum achieved throughput is very similar for all of the user selection algorithms considering all precoding algorithms. On the other hand, the optimum number of selected users varies for different user selection algorithms operating under different levels of channel estimation error as can be observed in Figs. 5.6d–5.6f. It is desirable to serve as many users as possible. The major difference in the amount of users served by the algorithms happens when the MRT precoder is used in a scenario with $\sigma_\varepsilon^2 = 10^{-1}$. In this case, the CBS is able to serve two more users than SOS and ICIBS. In general, ICIBS and CBS serve more users than SOS in scenarios with low levels of channel estimation errors ($\sigma_\varepsilon^2 \leq 10^{-2}$), whereas for high levels of channel estimation error, the optimum number of selected users depends on the precoder besides the user selection algorithm.

## 5.6 Ultra Clustered-crowded Scenario

In this section, we analyze the performance of the user selection algorithms in an *ultra clustered-crowded scenario*, meaning that $K > M$ and all the users are clustered in the same section of the cell, as depicted in Fig. 5.7. For the simulations in this case, we considered $M = 50$, $K = 75$, $\theta_0 \in \{0°, 45°\}$, and $\Delta\theta \in \{1°, 1.5°, \cdots, 4.5°, 5°\}$.

Fig. 5.8 illustrates the average per-user throughput *versus* the size of the sector where the users are distributed. As can be observed in Fig. 5.8a, ICIBS performs better than SOS and CBS for some values of $\Delta\theta$, yielding slightly increased throughput. This improvement is more evident for MRT and MMSE precoders since the performance of all user selection algorithms can be considered equal for the ZF precoder. It is worth highlighting the drop in the ICIBS performance around $\Delta\theta = 3.6°$, which seems consistent for all precoding algorithms. This drop in the performance can be explained by the fact that for a ULA with $M = 50$ antennas, the directivity of the array is $\pi/M$, thus for $\Delta\theta$ around $\pi/M$, it is already possible to have small correlation between some users, which may be a problem for ICIBS since it takes advantage from situations where the correlation among the users is very high and its global usage of the interference among the users leverages the selection. In Fig. 5.8b, we can observe the same pattern of Fig. 5.8a, with the performance drop around $\Delta\theta = 5°$, which may be due to the fact that the array is steered to 45°.

Fig. 5.9 depicts the average throughput *versus* the number of selected users $L$ for $\Delta\theta = 1.5°$. Like in the case presented in Section 5.3, the user selection also improved

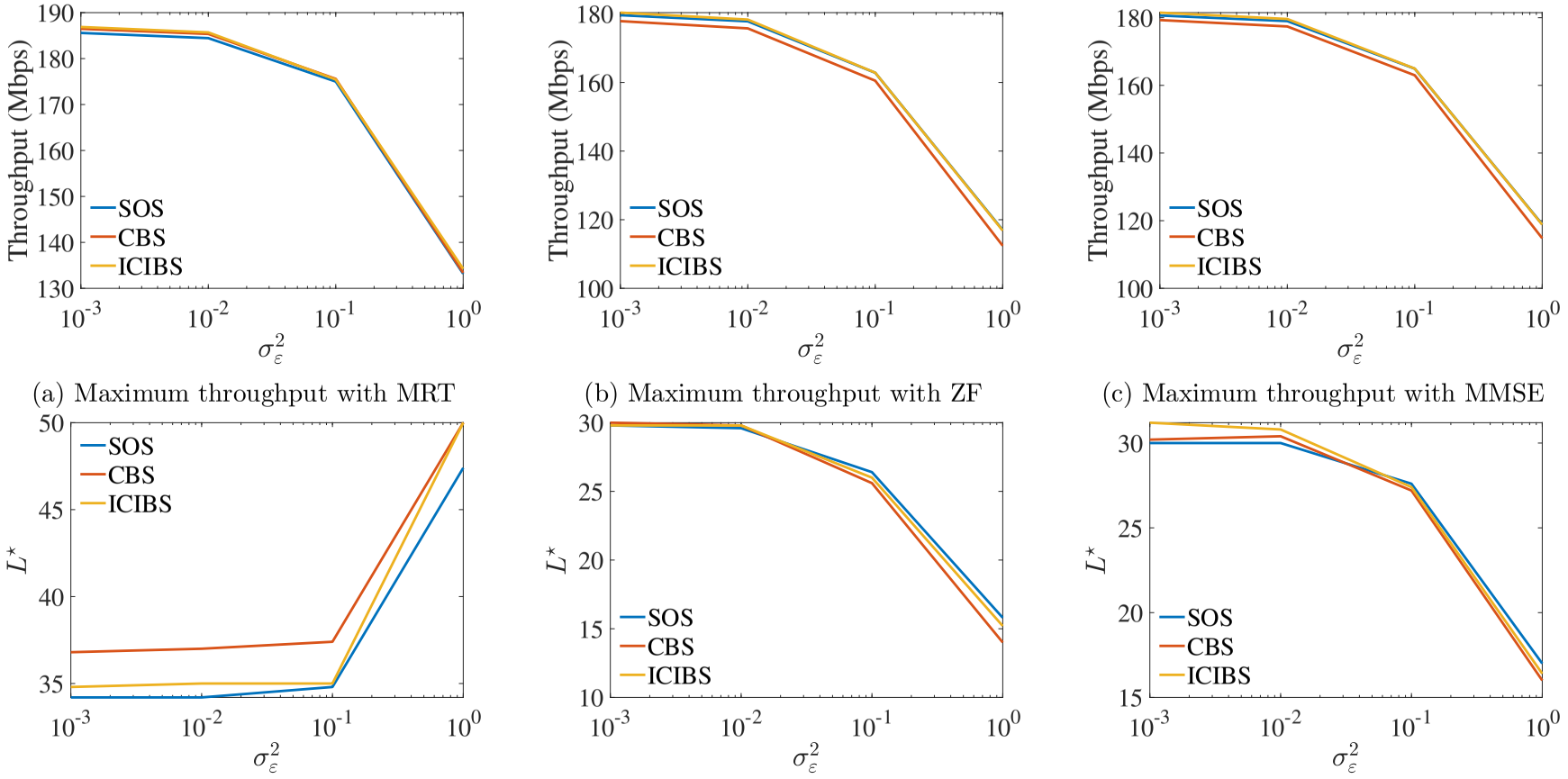


(a) Maximum throughput with MRT (b) Maximum throughput with ZF (c) Maximum throughput with MMSE

(d) $L^\star$ with MRT (e) $L^\star$ with ZF (f) $L^\star$ with MMSE

Figure 5.6: Maximum achieved throughput and optimum number of selected users $L^\star$ *versus* the variance of the channel estimation error $\sigma_\varepsilon^2$ for $M \in \{50, 100\}$, considering different user selection and precoding algorithms.

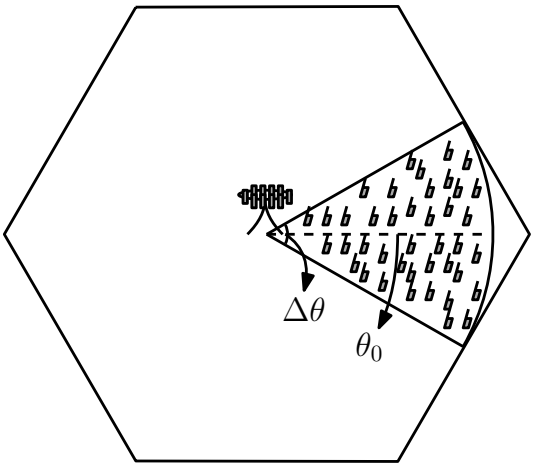


Figure 5.7: Example of an ultra clustered-crowded scenario used in the simulations, where $\theta_0$ is the direction of the sector of the cell and $\Delta\theta$ is the aperture angle.

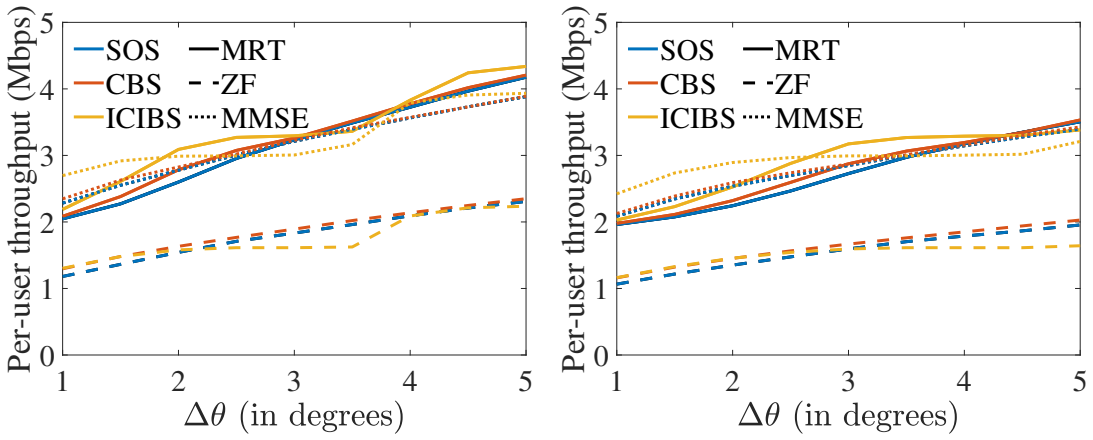


(a) $\theta_0 = 0°$ (b) $\theta_0 = 45°$

Figure 5.8: Average per-user throughput *versus* $\Delta\theta$ for $M = 50$ and $K = 75$. The line style (solid, dashed or dotted line) determines the precoder, whereas the colors specify the user selection algorithm. The yellow solid line, e.g., represents the results achieved by the ICIBS scheme considering an MRT precoder.

the system throughput, achieving maximum throughput for all algorithms when $L^\star = 2$ users are served with both ZF and MMSE, and $L^\star = 1$ user is served with MRT. In this case, both CBS and ICIBS achieved the same maximum performance, and, at their peaks, they were 19.98% and 23.03% better than SOS for ZF and MMSE, respectively. Moreover, the performance of SOS and CBS decreased faster with $L$ than that of ICIBS, which is an advantage if it is necessary to work with $L > L^\star$. For example, for $L = 38$, ICIBS achieved a throughput of 19.09 Mbps and 14.02 Mbps with MRT and MMSE, which were still 10.94% and 21.91% better than SOS and CBS with the same precoders. The performance of the user selection algorithms with ZF precoder was impaired in this scenario due to the proximity of the users, which lead to an ill-conditioned channel matrix, and even the user

selection could not help in this case.

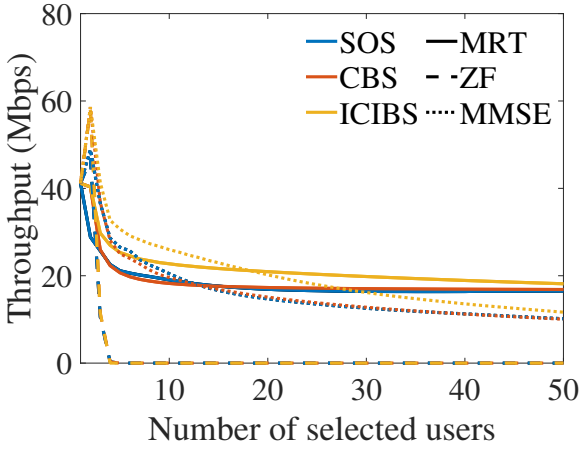


Figure 5.9: Average throughput *versus* the number of selected users $L$ for $M = 50$, $K = 75$, $\Delta\theta = 1.5°$, and $\theta_0 = 0°$. The line style (solid, dashed or dotted line) determines the precoder, whereas the colors specify the user selection algorithm. The yellow solid line, e.g., represents the results achieved by the ICIBS scheme considering an MRT precoder.

Fig. 5.10 shows the CDF of the throughput for $\Delta\theta = 1.5°$ and $L = 38$. The benefit that ICIBS provided in this type of scenario is clearly evident from this figure. For both MRT and MMSE precoders, ICIBS yielded a significant gain in the 95PT over the other user selection algorithms. ICIBS achieved a 95PT of 18.27 Mbps and 11.57 Mbps with MRT and MMSE precoders, resulting in improved performance of at least 7.66% over the other user selection algorithms. Although the ICIBS did not yield significant improvements in terms of system throughput in the results presented in Section 5.3, the results due to ICIBS presented in this section were significantly superior in comparison to the competing user selection algorithms. The fundamental difference between the scenario simulated in this section from the scenario in Section 5.3 lies in the inter-channel interference level. Indeed, in this section, since the users are concentrated in a small portion of the cell, there are more users interfering with each other simultaneously, thus the inter-channel interference is more severe. This is why the ICIBS outperformed other competing approaches.

## 5.7 Practical Guidelines

This subsection discusses the suitability of the user selection algorithms in practical scenarios, summarizing the main findings of massive MIMO systems under LoS propagation, and explaining how to use the obtained results for aiding the design of massive MIMO systems. Firstly, it is worth highlighting that the user selection would not imply an additional cost to the BS since all the user selection algorithms are implemented digitally and can share the BS's *digital signal processor* (DSP)

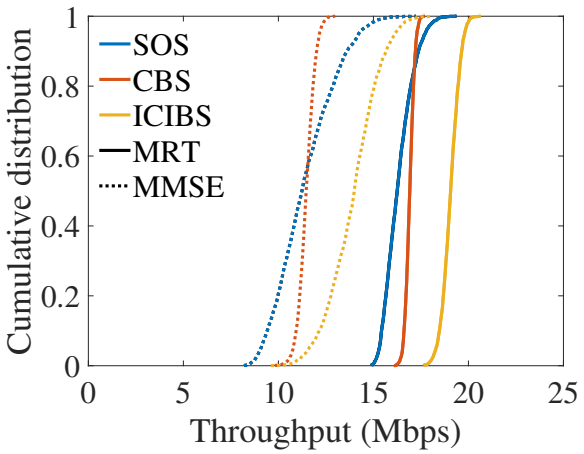


Figure 5.10: *Cumulative distribution function* of the throughput for $M = 50$, $K = 75$, $L = 38$, $\Delta\theta = 1.5°$, and $\theta_0 = 0°$. The line style (solid, dashed or dotted line) determines the precoder, whereas the colors specify the user selection algorithm. The yellow solid line, e.g., represents the results achieved by the ICIBS scheme considering an MRT precoder.

units. Therefore, user selection algorithms can be easily used in massive MIMO systems.

As it can be observed from the results presented throughout this section, the performance of all of the user selection algorithms are very sensitive to the parameters of the system. Thus, the most suitable algorithm depends on the application and the scenario. For example, if the aim is to maximize the achieved throughput without concerning with the number of served users, the most suitable algorithm is the ICIBS with ZF and MMSE precoders, followed by CBS with MRT precoder. However, if the system has a requirement to serve specific minimum number of users $L$, then the most suitable algorithm is the one that yields the highest throughput for that particular $L$. In general, for the case where $K \leq M$ and $L \leq \lceil K/2 \rceil$, the ICIBS outperforms the other user selection algorithms by a small amount for all precoder types. On the other hand, when $K \leq M$ and $L = \lceil K/2 \rceil$, CBS yields the highest throughput using the MRT precoder, SOS yields the highest throughput using the ZF precoder, and ICIBS yields the highest throughput using the MMSE precoder. Moreover, SOS generally tends to perform better than CBS and ICIBS when ZF is used for $K/2 < L \leq M$. However, the performance with ZF precoder is so degraded in LoS propagation for that range of $L$ such that it is advisable to use another precoder in this case.

Another important factor is the computational complexity, which can be a hindrance in practical applications. The computational burden of the SOS rapidly grows with the number of antennas $M$ and the number of selected users $L$, which is not desirable since massive MIMO systems use very large $M$. The SOS should be considered only in cases where one can have a significant gain in the throughput.

Therefore, the high computational burden of the SOS is an impediment for its use in massive MIMO systems.

The final point to consider in the design of massive MIMO systems with user selection is the cell usage. In the simulations, we considered two possible scenarios where the whole cell and only a section of the cell was used. The previous comments are based on the case when the whole cell was used. However, when only a small section of the cell is used, the ICIBS outperforms all of the other algorithms. Further, the ultra clustered-crowded scenario used in the performance analysis represents some real scenarios that are increasingly common nowadays, such as large scale social, cultural, and sporting events, where a dedicated and efficient communication system is necessary.

## 5.8 Concluding Remarks

In this chapter, simulation results regarding the performance of the ICIBS algorithm were presented and discussed. The performance of the ICIBS was evaluated when combined with different linear precoders for various system configurations considering perfect and imperfect CSI under the LoS propagation channel has been evaluated. It is worth highlighting the ultra clustered-crowded scenario, where all the users are clustered in a small section of the cell. In this scenario, the proposed algorithm significantly outperformed the competitors algorithms, showing the relevance of ICIBS in a scenario that is increasingly common nowadays.

# Chapter 6

# Performance Evaluation of the FRBS Algorithm

## 6.1 Simulation Parameters

The performance of the proposed FRBS algorithm is evaluated and compared with the *exhaustive search with equal power allocation* (ESEPA), *exhaustive search with max-min fairness power allocation* (ESMMFPA), LSFRS [4], SOS [43], CBS [9], and ICIBS approaches via numerical simulations, by analyzing the effect of the number of selected users on the average sum-throughput and the min-throughput. Moreover, EPA is used to evaluate the sum-throughput and MMFPA is used for evaluating the min-throughput. Furthermore, the MRT and ZF precoders are used in the simulations with a view to evaluate the performance for different precoders. All codes used for generating the results presented in this section are available in `https://github.com/rafaelschaves/user-selection-with-large-scale-fading`.

The simulation scenario considers a massive MIMO system with $M = 50$ antennas operating in 500-m radius hexagonal single-cell with a carrier frequency of 1.9 GHz, and bandwidth of 20 MHz. The large-scale fading is composed of the path loss and the shadow fading. The path loss is modeled by the COST 231 Hata propagation model [85], whereas the shadow fading is modeled by a log-normal distribution [1]. Moreover, the large-scale fading coefficients is assumed to be known by the BS, the shadow fading is log-normally distributed with zero mean and 8 dB standard deviation, the radiated power at the BS is 10 W, with BS and user antenna gains of 0 dBi, and the noise figure for the users is 9 dB, leading to a DL SNR of 132 dB, such as the scenario in [9]. The simulations parameters are summarized in Table 6.1.

Table 6.1: Simulation Parameters for the FRBS

| | **Parameters** |
|---|---|
| **Number of Antennas** | $M = 50$ |
| **Number of Users** | $K \in \{10, 25, 75\}$ |
| **Cell Radius** | $R = 500$ m |
| **Carrier Frequency** | $f_c = 1.9$ GHz |
| **Bandwidth** | $B = 20$ MHz |
| **Path Loss** | COST 231 Hata |
| **Shadow Fading** | Lognormal$(0, 8$ dB$)$ |
| **BS Power** | 10 W |
| **BS and User Antenna Gain** | 0 dBi |
| **Precoding Algorithms** | MRT and ZF |
| **User Selection Algorithms** | ESEPA, ESMMFPA, LSFRS, SOS, CBS, ICIBS, and FRBS |

## 6.2 Performance of the FRBS

In this section, we compare the performance of the FRBS algorithm with that of the ESEPA, ESMMFPA, and SOS algorithms. These algorithms are the only ones capable of making use of both the small- and large-scale fading. Additionally, in the simulations we consider $K \in \{10, 25\}$, and the throughput is calculated using 100 realizations of the UR-LoS fading channel. The number of realizations as well as $K$ are small to enable the use of ES solutions.

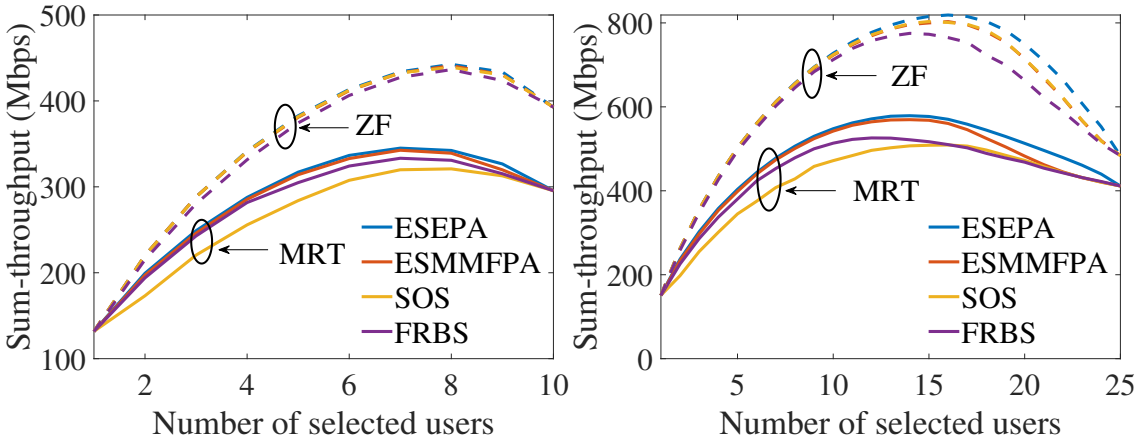


(a) $K = 10$ (b) $K = 25$

Figure 6.1: Average sum-throughput *versus* the number of selected users with EPA, considering different number of users.

Fig. 6.1 depicts the average sum-throughput *versus* the number of selected users $L$ with EPA, wherein $L = K$ corresponds to keeping all users, i.e., the user selection algorithms are turned off. The figure shows that there is a specific number of selected users $L^\star$ that maximizes the sum-throughput and this number varies depending on

Table 6.2: Optimum Values Achieved by the Algorithms for $K = 10$

| | **MRT** | | **ZF** | |
|---|---|---|---|---|
| | $L^\star$ | Sum-throughput (Mbs) | $L^\star$ | Sum-throughput (Mbps) |
| **ESEPA** | 7 | 345.04 | 8 | 442.59 |
| **ESMMFPA** | 7 | 342.58 | 8 | 441.00 |
| **SOS** | 8 | 320.92 | 8 | 439.12 |
| **FRBS** | 7 | 333.26 | 8 | 436.44 |

Table 6.3: Optimum Values Achieved by the Algorithms for $K = 25$

| | **MRT** | | **ZF** | |
|---|---|---|---|---|
| | $L^\star$ | Sum-throughput (Mbs) | $L^\star$ | Sum-throughput (Mbps) |
| **ESEPA** | 14 | 578.88 | 16 | 818.84 |
| **ESMMFPA** | 14 | 569.46 | 16 | 803.13 |
| **SOS** | 16 | 509.10 | 15 | 803.41 |
| **FRBS** | 12 | 525.91 | 14 | 775.13 |

the user selection algorithm used. The concavity of the curves shows that the user selection improved the system throughput, i.e., the throughput at $L^\star$ was higher than that at $L = K$. Considering Fig. 6.1a, the maximum performance of FRBS and SOS were close to that of ESEPA, which was taken as the benchmark. Indeed, in the worst case,[1] the ESEPA was only 6.99% and 1.39% better than SOS and FRBS, respectively. In this case, FRBS achieved a maximum sum-throughput of 333.26 Mbps with $L^\star = 7$ and 436.44 Mbps with $L^\star = 8$ when MRT and ZF were used, respectively. The optimum values obtained by all the algorithms for $K = 10$ are summarized in Table 6.2. Additionally, with increased number of users $K$, the maximum performance of FRBS and SOS were still close to that of ESEPA, albeit with a slight increase in the gap among their peaks, as illustrated in Fig. 6.1b. In the worst case, ESEPA was 12.05% and 5.34% better than SOS and FRBS, respectively, with FRBS achieving a maximum sum-throughput of 525.91 Mbps with $L^\star = 12$ and 775.13 Mbps with $L^\star = 14$ when MRT and ZF were used, respectively. The optimum values obtained by all the algorithms for $K = 25$ are summarized in Table 6.3. As can be observed from Tables 6.2 and 6.3, for $K = 10$ and $K = 25$, the optimum number of users obtained by the FRBS is very close to the optimum obtained by ESEPA, meaning that FRBS achieved the best tradeoff in terms of network throughput and user coverage.

Despite the fact that FRBS and SOS have similar performances, FRBS has a huge advantage in terms of computational burden measured in flops count as depicted in Fig. 6.2. The figure shows the computational burden *versus* the number

[1]By worst case, we mean the precoder whose performance yielded the largest gap between a given algorithm (SOS or FRBS) and the benchmark curve (ESEPA). In this case, the precoder that yielded the largest performance gaps was the MRT precoder.

of selected users $L$. As can be observed, the computational burden of FRBS is almost insensitive to $L$, whereas the computational burden of SOS increases rapidly with $L$. The SOS required in the order of $10^3$ more flops than FRBS, with these additional flops increasing with $K$. Hence, FRBS is more scalable with varying number of users $K$ and selected users $L$.

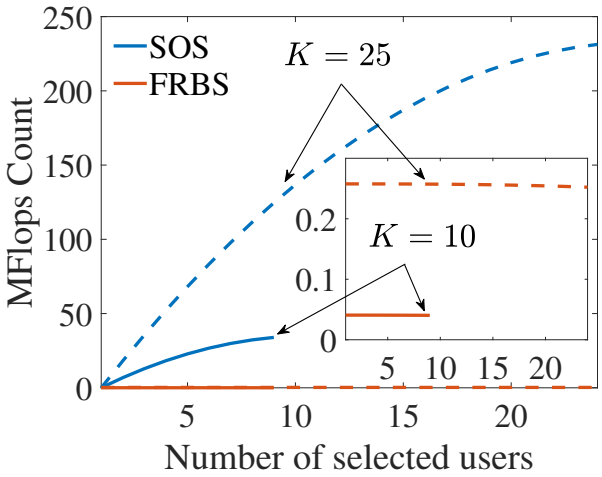


Figure 6.2: Computational burden *versus* the number of selected users measured in flops count for SOS and FRBS.

Fig. 6.3 illustrates the average min-throughput *versus* the number of selected users $L$ with MMFPA. As can be seen in Fig. 6.3a, FRBS outperformed SOS when MRT precoder was used, achieving results very close to that of ESMMFPA. On the other hand, in Fig. 6.3b, the gap between FRBS and ESMMFPA increased with the number of users $K$ when the MRT and ZF precoders were used. However, the FRBS min-throughput was higher than that of the SOS for $L \leq 15$, and similar to SOS for $15 \leq L \leq K$ when MRT was used. Additionally, when ZF was used, FRBS and SOS had similar min-throughputs for $L \leq 10$ and the gap between their min-throughputs started increasing for $10 \leq L \leq K$.

It is worth highlighting that the performance of FRBS and SOS are very dependent on the system parameters, such as the number of antennas $M$, number of users $K$, and the cell radius. However, from our practical experience with these algorithms the following general conclusions can be drawn:

- Increasing the number of users $K$ results in the same pattern of curves shown in Figs. 6.1 and 6.3, but with higher throughputs since there are more users.
- Increasing the number of antennas $M$ results in the same pattern of curves shown in Figs. 6.1 and 6.3, but with higher throughputs due to the multiplexing gain provided by the larger number of antennas.
- Increasing the cell radius results in lower average large-scale fading and consequently lower average SNR. When operating in a large cell, both FRBS and

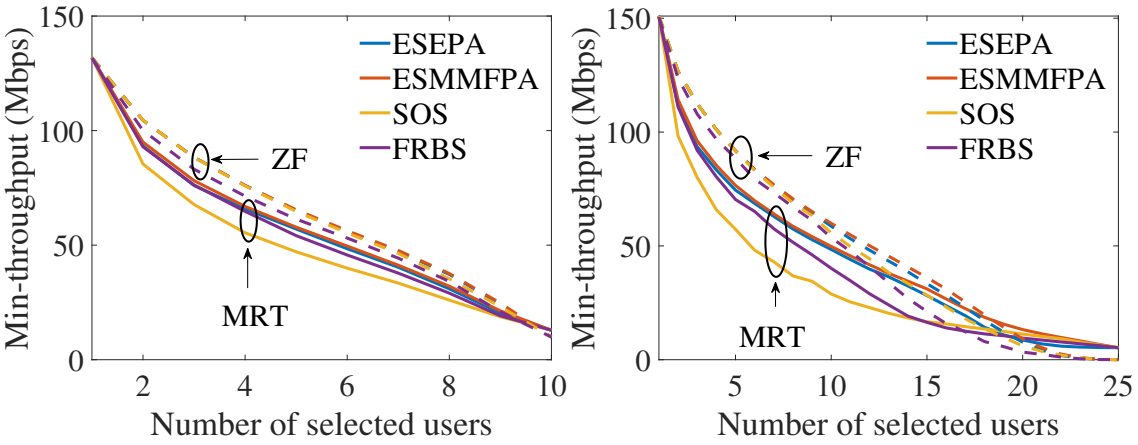


(a) $K = 10$ (b) $K = 25$

Figure 6.3: Average min-throughput *versus* the number of selected users with MMFPA, considering different number of users.

Table 6.4: Optimum Values Achieved by the SSFA Algorithms for $K = 75$

| | **MRT** | | **ZF** | |
|---|---|---|---|---|
| | $L^\star$ | Sum-throughput (Mbs) | $L^\star$ | Sum-throughput (Mbps) |
| **CBS** | 32 | 757.37 | 33 | 1,085.37 |
| **ICIBS** | 31 | 788.67 | 33 | 1,085.06 |
| **FRBS** | 24 | 777.45 | 22 | 1,370.62 |

SOS serve less users at their sum-throughput peaks, i.e., the peaks presented in Fig. 6.1 move to the left with increasing cell radius.

### 6.2.1 FRBS *vs.* SSFA Algorithms

In this subsection, we compare the performance of the FRBS with that of CBS and ICIBS algorithms. Our goal is to evaluate the performance when the large-scale fading is taken into account along with the small-scale fading and compare with the performance when only the small-scale fading is considered. This analysis aims to quantify the importance of the large-scale fading for user selection in massive MIMO systems under LoS propagation. In the simulations, the throughput is calculated using 1,000 realizations of the UR-LoS fading channel and we consider $K = 75$ that represents a crowded scenario. This type of scenario is of paramount importance for massive MIMO systems since there are more users than antennas, representing situations that are likely to happen in practical applications.

The results shown in Figs. 6.1 and 6.3 demonstrate the efficacy of the proposed FRBS algorithm with its very low computational burden when compared to other user selection algorithms. In terms of comparing FRBS with SSFA algorithms such as CBS and ICIBS, Fig. 6.4 depicts the throughput *versus* the number of selected users $L$ with EPA for CBS, ICIBS, and FRBS with $K = 75$. Different from the

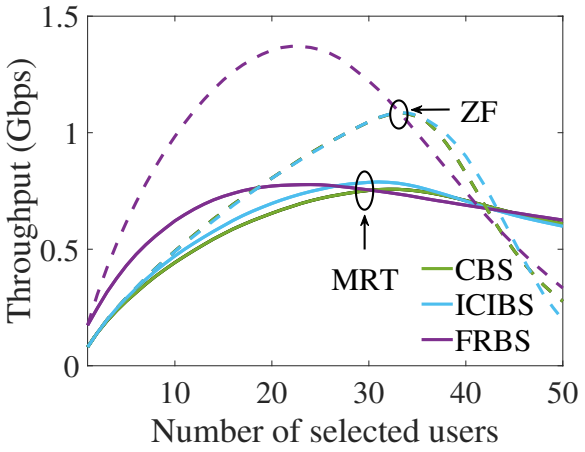


Figure 6.4: Average sum-throughput *versus* the number of selected users with EPA for CBS, ICIBS, and FRBS with $M = 50$ and $K = 75$.

scenario considered for Figs. 6.1 and 6.3, in this case we consider a crowded scenario ($K > M$) where the user selection is mandatory, at least when ZF precoder is used. As can be observed in Fig. 6.4, under such scenario FRBS achieved its maximum throughput serving fewer users than CBS and ICIBS. When MRT precoder is used, the maximum throughput achieved by the algorithms were very similar, as can be seen in Table 6.4. FRBS outperformed CBS and ICIBS for $L < 27$ and was slightly outperformed by them when $L > 27$. When ZF precoder is used, FRBS achieves a maximum throughput of $1,370.62$ Mbps, improving the maximum throughput obtained by CBS and ICIBS by 26.28%. Moreover, the throughput obtained by FRBS exhibited a significant advantage over that of CBS and ICIBS for any $L < 30$. For $L > 30$, CBS and ICIBS yielded a slightly improved throughput when compared to FRBS. These results indicate that the large-scale fading is more relevant to the throughput for small $L$, and ICI seems to be sufficient to achieve a reasonable throughput for high $L$. The choice of the best user selection algorithm depends on the choice of precoder to be used in the design of the network. If MRT is the chosen precoder, SSFA algorithms are the best choice as they achieve the same throughput levels as FRBS while serve more users, which is desirable from the network perspective. On the other hand, if the ZF precoder is chosen, the FRBS is the best possible algorithm since it achieves the best tradeoff in terms of network throughput and user coverage.

### 6.2.2 FRBS *versus* LSFA Algorithms

In this subsection, we compare the performance of the FRBS with that of the LS-FRS. Our goal is to evaluate the performance when the large-scale fading is taken into account along with the small-scale fading and compare with the performance

Table 6.5: Optimum Values Achieved by the LSFA Algorithms for $K = 75$

| | **MRT** | | **ZF** | |
|---|---|---|---|---|
| | $L^\star$ | Sum-throughput (Mbs) | $L^\star$ | Sum-throughput (Mbps) |
| **LSFRS** | 35 | 621.12 | 17 | 1,012.37 |
| **FRBS** | 24 | 777.45 | 22 | 1,370.62 |

when only the large-scale fading is considered. This analysis aims to quantify the importance of the small-scale fading for selecting users in massive MIMO systems under LoS propagation. This is one fundamental difference between massive MIMO systems under LoS propagation and NLoS propagation. For the NLoS case, the small-scale fading is averaged out and does not affect the SE of the system, which is not the case for LoS propagation. In the simulations, the throughput is calculated using 1,000 realizations of the UR-LoS fading channel and as before we consider $K = 75$.

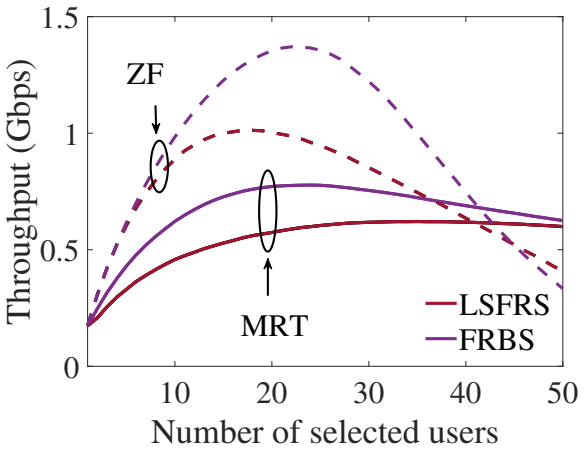


Figure 6.5: Average sum-throughput *versus* the number of selected users with EPA for LSFRS and FRBS with $M = 50$ and $K = 75$.

Fig. 6.5 shows the throughput *versus* the number of selected users $L$ with EPA for LSFRS and FRBS for $K = 75$. As can be observed in Fig. 6.5, for both MRT and ZF precoders, FRBS completely outperformed the LSFRS algorithm for almost every $L$. Both algorithms had similar performance for $L$ close to $M$. Considering the maximum obtained throughput, FRBS was 25.17% and 35.39% better than LSFRS when MRT and ZF precoders are used, respectively. These results indicate that the small-scale fading is of paramount importance to the performance of massive MIMO systems under LoS propagation and cannot be disregarded in the user selection process.

## 6.3 Concluding Remarks

In this chapter, simulation results regarding the performance of the FRBS algorithm was presented and discussed. The performance of the FRBS was evaluated via simulations when combined with different linear precoders and power allocation algorithms, and compared with other user selection algorithms. The results showed that FRBS provided the best cost-effective solution in terms of average sum-throughput, average min-throughput and the computational complexity when compared to the other user-selection schemes.

# Part II

# Cell-free Massive MIMO Systems

# Chapter 7

# Nonlinearities of Cell-Free Massive MIMO

## 7.1 Introduction

In this chapter, we evaluate the performance of an UL transmission of a semi-distributed CF massive MIMO network considering the impact of hardware impairments introduced by the *analog-to-digital* (AD) converters, e.g., quantization. To model the nonlinear distortion caused by quantization, we use the Bussgang decomposition [92], which allows us to decompose the output of a nonlinear function representing the quantization process as a linear function. Some works evaluated the impact of the quantization in the CPU, providing power allocation and UE assignment algorithms [67–71]. In [66], the authors studied the impact of general hardware impairments present in the APs and UEs on the performance of CF massive MIMO networks. The difference between the analysis presented in this chapter and the other works is that here we consider quantization effects in both the CPU and the APs. Hence, we show that quantization generates additional nonlinear interference effects to the signal processing performed in the CPU and the APs.

In addition to the quantization effects, we also consider that the CF massive MIMO network operates over a Rician fading channel, and derive the MMSE channel estimate taking into account the related quantization effects. We also provide the suboptimal scalable version of the MMSE estimate that limits the interference from other users. Moreover, we derive the UL SE for any given linear combiner used in the APs and any LSFD used in the CPU. Furthermore, we present the scalable version of the LP-MMSE combiner considering the quantization effects, and derive the optimal and scalable *nearly optimal* (n-opt) LSFD vectors used in the semi-distributed implementation of the network.

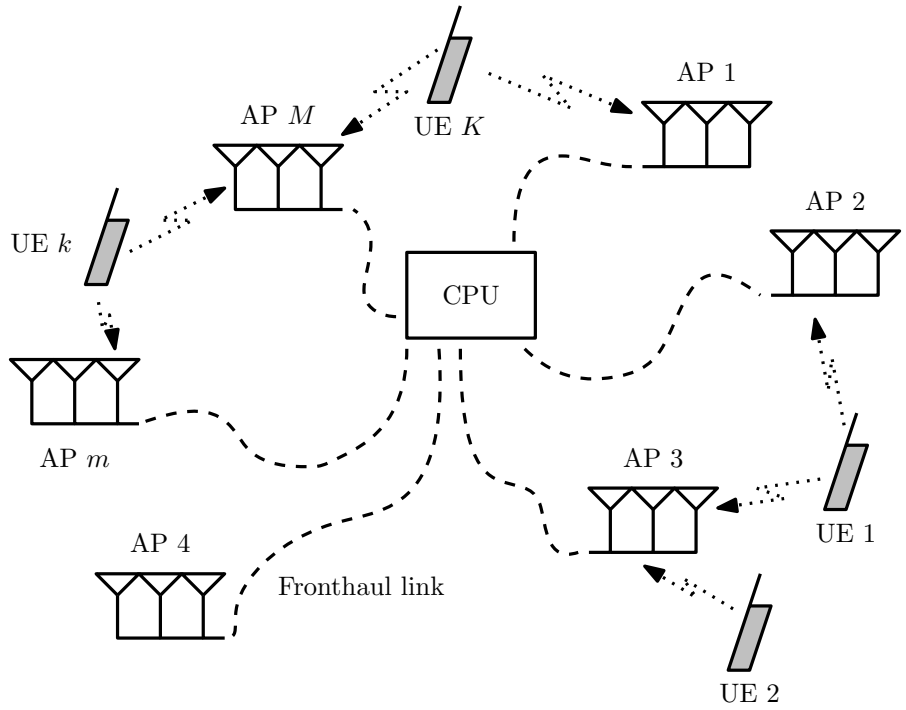


Figure 7.1: A CF massive MIMO network operating in uplink with $M$ APs equipped wit an $N$-antenna array distributed over a coverage area serving $K$ single-antenna UEs.

## 7.2 Cell-free Massive MIMO

Consider a CF massive MIMO network operating in UL, consisting of $M$ APs equipped with an $N$-antenna array distributed over a coverage area serving $K$ single-antenna UEs, as illustrated in Fig. 7.1. The CF massive MIMO network is deployed in a semi-distributed implementation, where the APs are responsible for the CSI acquisition and coarse detection of the signal, and the CPU is responsible for the UE assignment that happens during the initialization of the network and for the fine detection of the signal. Both the CPU and APs have nonlinearities associated with them caused by the AD converters in the antenna arrays and at the end of the fronthaul links, as shown in Fig. 7.2. The AD converters perform a uniform quantization with nonlinear function given by [67]

$$f(z) = \begin{cases} -\frac{2^b-1}{2}\Delta, & \text{for } z < -\left(2^{b-1}-1\right)\Delta \\ \left(l+\frac{1}{2}\right)\Delta, & \text{for } l\Delta \leq z < (l+1)\Delta,\ \forall l \in \mathcal{L}\,, \\ \frac{2^b-1}{2}\Delta, & \text{for } \left(2^{b-1}-1\right)\Delta \leq z \end{cases} \tag{7.1}$$

where $\Delta \in \mathbb{R}_+$ is the step size of the quantizer, $b \in \mathbb{N}$ is the number of quantization bits, and $\mathcal{L} = \{-2^{b-1}+1, \cdots, 2^{b-1}-2\}$.

In order to achieve the scalability of the CF massive MIMO system, the APs only transmit and decode signals from specific UEs, which are assigned in the initializa-

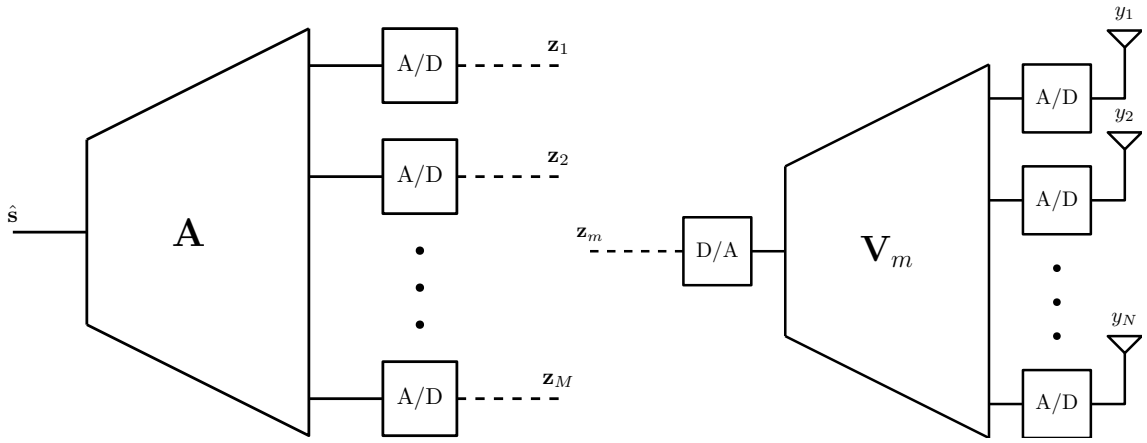


(a) CPU (b) AP

Figure 7.2: Block diagram of the CPU and APs for the CF massive MIMO network.

tion of the system or when new users enter the coverage area. We define a matrix $\mathbf{E} \in \mathbb{R}^{M \times K}$ specifying the connection between the APs and UEs, where $[\mathbf{E}]_{mk} = 1$ if the $m$th AP is allowed to communicate with the $k$th UE and $[\mathbf{E}]_{mk} = 0$ otherwise. For the sake of simplicity we define the sets

$$\mathcal{U}_m = \{k \in \mathcal{K} \mid [\mathbf{E}]_{mk} = 1\}, \tag{7.2}$$

$$\mathcal{A}_k = \{m \in \mathcal{M} \mid [\mathbf{E}]_{mk} = 1\}, \tag{7.3}$$

$$\mathcal{S}_k = \{k' \in \mathcal{K} \mid [\mathbf{E}]_{mk}[\mathbf{E}]_{mk'} \neq 0,\ \forall m \in \mathcal{M}\}, \tag{7.4}$$

where $\mathcal{K} = \{1, 2, \cdots, K\}$ is the set of all UE indices, $\mathcal{M} = \{1, 2, \cdots, M\}$ is the set of all AP indices, $\mathcal{U}_m$ is the index set of UEs served by the $m$th AP, $\mathcal{A}_k$ is the index set of APs serving the $k$th UE, and $\mathcal{S}_k$ is the index set of the UEs that are served partially by the same APs as the $k$th UE, including the $k$th UE.

The CF massive MIMO system operates in TDD mode, and the channel is estimated through a UL pilot transmission. The channel response of the system is constant in a coherence time-frequency block of length $\tau_c \in \mathbb{N}$ samples. In the UL, $\tau_p \in \mathbb{N}$ samples are reserved for the pilot transmission and $\tau_u = \tau_c - \tau_p$ samples for the data transmission. Let $\mathbf{h}_{mk} \in \mathbb{C}^{N \times 1}$ denote the channel between the $m$th AP and the $k$th UE, which is a random vector for every pair $(m, k) \in \mathcal{M} \times \mathcal{K}$. We consider a spatially correlated Rician fading channel given by [63, 93, 94]

$$\mathbf{h}_{mk} = \mathbf{h}_{mk}^{\mathrm{LoS}} \mathrm{e}^{\mathrm{j}\phi_{mk}} + \mathbf{h}_{mk}^{\mathrm{NLoS}}, \tag{7.5}$$

where $\mathbf{h}_{mk}^{\mathrm{LoS}} \in \mathbb{C}^{N \times 1}$ is the deterministic LoS component, $\phi_{mk} \sim \mathcal{U}(-\pi,\ \pi)$ is the phase shift due to UE mobility and phase noise associated with the array of the $m$th AP and the $k$th UE, and $\mathbf{h}_{mk}^{\mathrm{NLoS}} \sim \mathcal{CN}(\mathbf{0}, \mathbf{R}_{mk})$ is the stochastic NLoS component with spatial covariance matrix $\mathbf{R}_{mk} \in \mathbb{C}^{N \times N}$ and $\beta_{mk}^{\mathrm{NLoS}} = \mathsf{Tr}\left(\mathbf{R}_{mk}\right)/N$ is the large-

scale fading coefficient of the NLoS component. The LoS component of (7.5) is determined by the geometry of the APs' array and the large-scale fading. In this work, we consider that all the APs have the same ULA, and, therefore, the LoS component between the $m$th AP and the $k$th UE is given by

$$\mathbf{h}_{mk}^{\mathrm{LoS}} = \sqrt{\beta_{mk}^{\mathrm{LoS}}} \begin{bmatrix} 1 & \mathrm{e}^{-\mathrm{j}\pi \sin(\theta_{mk})} & \cdots & \mathrm{e}^{-\mathrm{j}(N-1)\pi \sin(\theta_{mk})} \end{bmatrix}^{\mathrm{T}}, \tag{7.6}$$

where $\beta_{mk}^{\mathrm{LoS}} \in \mathbb{R}_+$ is the large-scale fading coefficient of the LoS component, $\theta_{mk} \sim \mathcal{U}(-\pi,\ \pi)$ is the incidence angle of the $k$th UE, and the array of the $m$th AP.

## 7.3 The Bussgang Decomposition

Different from what is assumed in many theoretical developments, practical systems are nonlinear in nature due to several impairments, such as the nonlinearity of practical power amplifiers or the finite resolution of the quantizers. A popular tool used to analyze such systems is the so-called *Bussgang decomposition*, which is a straightforward consequence of the Bussgang theorem [92]. The Bussgang decomposition, as the name suggests, decomposes the output of a memoryless nonlinear function as

$$\mathbf{z} = \mathbf{f}(\mathbf{x}) = \mathbf{A}\mathbf{x} + \mathbf{q}, \tag{7.7}$$

where $\mathbf{x} \in \mathbb{C}^{M\times 1}$ is the input of the nonlinear function, $\mathbf{z} \in \mathbb{C}^{M\times 1}$ is the output of the nonlinear function, $\mathbf{f}(\cdot)$ denotes a memoryless nonlinear function, $\mathbf{A} \in \mathbb{C}^{M\times M}$ is the Bussgang gain, $\mathbf{q} \in \mathbb{C}^{M\times 1}$ is the distortion; this additive distortion is modeled as a zero-mean non-Gaussian random variable that is uncorrelated with input $\mathbf{x}$. The Bussgang gain is defined as

$$\mathbf{A} = \mathbf{C}_{\mathbf{zx}}\mathbf{C}_{\mathbf{x}}^{-1}, \tag{7.8}$$

where $\mathbf{C}_{\mathbf{zx}} = \mathsf{Cov}\{\mathbf{z}, \mathbf{x}\}$ and $\mathbf{C}_{\mathbf{x}} = \mathsf{Cov}\{\mathbf{x}\}$.

***Remark 7.1***. The Bussgang decomposition can be viewed as the linear MMSE estimate of $\mathbf{z}$ given $\mathbf{x}$, with estimation error $\mathbf{q}$ [95]. Therefore, if the input $\mathbf{x}$ is jointly Gaussian distributed with other random variables, the distortion $\mathbf{q}$ is also uncorrelated with such random variable, which does not hold in the case of non-Gaussian inputs.

The model in (7.7) has been widely used to analyze the performance of MIMO systems with nonlinearities. In MIMO systems, $\mathbf{x}$ is the input of the antennas and $\mathbf{q}$ is the distortion caused by the impairments, which is caused by the finite-resolution AD converters in our case. Additionally, it is assumed that there is no crosstalk among the branches of different antennas, as can be seen in Fig. 7.2. Thus, for

MIMO systems, equation (7.7) can be rewritten as

$$\mathbf{z} = \mathbf{f}(\mathbf{x}) = \begin{bmatrix} f_1(x_1) \\ f_2(x_2) \\ \vdots \\ f_M(x_M) \end{bmatrix} = \mathsf{Diag}\left(a_1, a_2, \cdots, a_M\right)\mathbf{x} + \mathbf{q}, \tag{7.9}$$

or

$$z_m = a_m x_m + q_m, \ \forall m \in \mathcal{M}. \tag{7.10}$$

With knowledge of the input $\mathbf{x}$ and the output $\mathbf{z}$, we can use the Price theorem [96] with (7.10) in order to independently compute the gains $a_1, a_2, \cdots, a_M$. However, one disadvantage of (7.10) is the dependence of the variance of the quantizer input in the computation of the Bussgang gain, which is a hindrance in the design of some quantizer parameters. For example, the optimal step size of a uniform quantizer as in (7.1) depends on the Bussgang gain alongside other parameters [67]. An alternative to (7.10) is normalizing the input signal by its variance and amplifying the output of the quantizer by the original input variance [67]. Hence, equation (7.10) can be rewritten as

$$\begin{aligned} f_m(x_m) &= \sigma_m f_m\left(\frac{x_m}{\sigma_m}\right) \\ &= \tilde{a}_m x_m + \sigma_m \tilde{q}_m, \end{aligned} \tag{7.11}$$

where $\sigma_m^2 = \mathsf{Var}\{x_m\}$ is the variance of the input $x_m$, $\tilde{a}_m \in \mathbb{C}$ is the Bussgang gain for a normalized input and $\tilde{q}_m$ is the distortion noise for a normalized input with variance $\sigma_{\tilde{q}_m}^2$. With this approach, we can use tabulated values for $\tilde{a}_m$ and $\sigma_{\tilde{q}_m}^2$, which do not depend on the input of the quantizer. In summary, by using (7.11), we can avoid the computation of $a_m$ and $\sigma_{q_m}^2$ every time the input changes, being the advantage of this strategy. The optimum step size of the quantizer and corresponding $\tilde{a}$ and $\sigma_{\tilde{q}_m}^2$ are summarized in Table 7.1 from [70].

It is worth highlighting that despite of $\mathbf{A}$ being a diagonal matrix in (7.9), it does not imply that the entries of the distortion $\mathbf{q}$ is uncorrelated. Since the distortion $\mathbf{q}$ is uncorrelated with $\mathbf{x}$, its covariance matrix $\mathbf{C_q} = \mathsf{Cov}\{\mathbf{q}\}$ can be written as

$$\mathbf{C_q} = \mathbf{C_z} - \mathbf{A}\mathbf{C_x}\mathbf{A}^{\mathrm{H}}. \tag{7.12}$$

Then, we can see that the distortion is only uncorrelated if the output and the input are both uncorrelated. In MIMO systems, the input of the quantizers are correlated since each antenna receives a different linear combination of the transmitted signals. The covariance matrix of the output signal and the Bussgang gain

Table 7.1: Bussang Parameters for the Quantizer in (7.1) with Normalized Input

| $b$ | $\tilde{a}$ | $\sigma_{\tilde{q}}^2$ | $\Delta^\star$ |
|---|---|---|---|
| 1 | 0.6366 | 0.2313 | 1.596 |
| 2 | 0.88115 | 0.10472 | 0.9957 |
| 3 | 0.96256 | 0.036037 | 0.586 |
| 4 | 0.98845 | 0.011409 | 0.3352 |
| 5 | 0.996505 | 0.003482 | 0.1881 |
| 6 | 0.99896 | 0.0010389 | 0.1041 |
| 7 | 0.99969 | 0.0003042 | 0.0558 |
| 8 | 0.999912 | 0.0000876 | 0.0307 |
| 9 | 0.999975 | 0.0000249 | 0.0165 |
| 10 | 0.999993 | $6.99696 \times 10^{-6}$ | 0.0088 |
| 11 | 0.999998 | $1.94441 \times 10^{-6}$ | 0.004649 |
| 12 | 0.999999 | $5.35536 \times 10^{-7}$ | 0.0024484 |
| 13 | 0.9999998 | $1.46369 \times 10^{-7}$ | 0.001283 |
| 14 | 0.99999997 | $3.97394 \times 10^{-8}$ | 0.001283 |
| 15 | 1 | $1.0727 \times 10^{-8}$ | 0.000349 |

can be obtained by using the Price theorem [96]. For a uniform quantizer as the one in [67], $\mathbf{C_z}$ and $\mathbf{A}$ depend on the number of quantization bits $b$ and the step-size of the quantizer $\Delta$. The exact value of $\mathbf{C_q}$ was derived in [71] for the case of a uniform quantizer along with conditions to the uncorrelated distortion assumption be sufficiently good. For a conventional massive MIMO system, results in [97] have shown that the distortion of one-bit AD converters can be considered uncorrelated in some scenarios such as under low SNR regime and elevated number of users. Moreover, even in different scenarios, the authors in [98] have shown that hardware distortion correlation has negligible impact on the UL SE of massive MIMO systems. On the other hand, results in [71] have shown that the off-diagonal elements of $\mathbf{C_q}$ are sensitive to parameters of the CF massive MIMO network, such as the number of APs, the number of antennas at the APs, and the number of UEs. For example, in scenarios with $M > K$, the off-diagonal elements of $\mathbf{C_q}$ can be neglected, being only relevant for cases when $M \leq K$, which are not desired on CF massive MIMO systems. Additionally, approximating $\mathbf{C_q}$ by a diagonal matrix does not have significant impact in the uplink performance of CF massive MIMO systems when $M \gg K$ [68, 71]. Furthermore, the distortion noise can also be approximately considered uncorrelated in low SNR regime [97, 99]. Therefore, in this thesis, we consider $\mathbf{C_q} = \mathsf{Diag}\left(\mathsf{Var}\left\{q_1\right\}, \mathsf{Var}\left\{q_2\right\}, \cdots, \mathsf{Var}\left\{q_M\right\}\right)$.

## 7.4 Uplink Channel Estimation

The channel is estimated through $\tau_{\mathrm{p}}$ mutually orthogonal pilot signals, which are assigned to every UE when it accesses the network. The pilot signal of the $k$th UE is denoted by $\boldsymbol{\varphi}_{t_k} \in \mathbb{C}^{\tau_{\mathrm{p}} \times 1}$, where $t_k \in \{1, \cdots, \tau_{\mathrm{p}}\}$ is the index of the pilot assigned to the $k$th UE. By definition, we assume that $|\boldsymbol{\varphi}_{t_k 1}| = |\boldsymbol{\varphi}_{t_k 2}| = \cdots = |\boldsymbol{\varphi}_{t_k \tau_{\mathrm{p}}}| = 1$, yielding $\left\|\boldsymbol{\varphi}_{t_k}\right\|_2^2 = \tau_{\mathrm{p}}$. In CF massive MIMO systems, several UEs share the same pilot due to the fact that $K > \tau_{\mathrm{p}}$, which is typical of massive access systems. We denote

$$\mathcal{P}_k = \{k' \in \mathcal{K} | t_{k'} = t_k\} \tag{7.13}$$

as the set of UEs that use the same pilot as the $k$th UE, including the $k$th UE itself. The received signal at the $m$th AP during the pilot transmission $\mathbf{Y}_m^{\mathrm{p}} \in \mathbb{C}^{N \times \tau_{\mathrm{p}}}$ is given by

$$\mathbf{Y}_m^{\mathrm{p}} = \sum_{k \in \mathcal{K}} \sqrt{\rho_{\mathrm{ul}} \eta_k} \mathbf{h}_{mk} \boldsymbol{\varphi}_{t_k}^{\mathrm{T}} + \mathbf{N}_m, \tag{7.14}$$

where $\eta_k \in \mathbb{R}_+$ is the pilot power allocation coefficient for the $k$th UE and $\mathbf{N}_m \in \mathbb{C}^{N \times \tau_{\mathrm{p}}}$ is the receiver thermal noise, whose elements are i.i.d. with distribution $\mathcal{CN}(0, 1)$. The signal in (7.14) is quantized by the AD converters at the APs, which, for the sake of simplicity, use the same number of bits. This operation yields

$$\mathbf{f}_{\mathrm{AP}}(\mathbf{Y}_m^{\mathrm{p}}) = \tilde{a}_{\mathrm{AP}} \mathbf{Y}_m^{\mathrm{p}} + \mathbf{Q}_m^{\mathrm{p}}, \tag{7.15}$$

where $\mathbf{Q}_m^{\mathrm{p}} \in \mathbb{C}^{N \times \tau_{\mathrm{p}}}$ is the distortion matrix, whose elements are zero-mean non-Gaussian random variables with variance given by

$$\mathsf{Var}\left\{[\mathbf{Q}_m^{\mathrm{p}}]_{nt}\right\} = \left(\sum_{k \in \mathcal{K}} \eta_k \mathsf{Var}\left\{h_{mkn}\right\} + 1\right) \sigma_{\tilde{q}}^2. \tag{7.16}$$

Due to the construction of the covariance matrix of NLoS component, $\mathbf{R}_{mk}$, we can say that $\mathsf{Var}\left\{h_{mkn}\right\} = \beta_{mk}^{\mathrm{NLoS}}\ \forall n \in \{1, \cdots, N\}$. Thus, equation (7.16) can be rewritten as

$$\mathsf{Var}\left\{[\mathbf{Q}_m^{\mathrm{p}}]_{nt}\right\} = \left(\sum_{k \in \mathcal{K}} \eta_k \beta_{mk}^{\mathrm{NLoS}} + 1\right) \sigma_{\tilde{q}}^2. \tag{7.17}$$

The quantized version of the received signal $\mathbf{Y}_m^{\mathrm{p}}$ is the observation used to estimate all the channels served by the $m$th AP. Note that the channel estimation can be either carried out directly at the $m$th AP or delegated to the CPU. However, the distributed fashion is preferred due to the fact that it is less sensitive to the limitations in the fronthaul link. It is worth highlighting that the $m$th AP only needs to estimate channels of UE that belong to $\mathcal{U}_m$. This process makes the CF massive MIMO system scalable. In order to estimate the channel of the $k$th UE,

the $m$th AP multiplies the received signal $\mathbf{Y}_m^{\mathrm{p}}$ with the normalized conjugate of the associated pilot $\boldsymbol{\varphi}_{t_k}$. The processed signal is given by

$$\begin{aligned}\mathbf{y}_{mt_k}^{\mathrm{p}} &= \frac{1}{\sqrt{\tau_{\mathrm{p}}}}\mathbf{f}(\mathbf{Y}_m^{\mathrm{p}})\boldsymbol{\varphi}_{t_k}^* \\ &= \sum_{k'\in\mathcal{K}} \tilde{a}_{\mathrm{AP}}\sqrt{\frac{\rho_{\mathrm{ul}}\eta_{k'}}{\tau_{\mathrm{p}}}}\mathbf{h}_{mk'}\boldsymbol{\varphi}_{t_{k'}}^{\mathrm{T}}\boldsymbol{\varphi}_{t_k}^* + \frac{\tilde{a}_{\mathrm{AP}}}{\sqrt{\tau_{\mathrm{p}}}}\mathbf{N}_m\boldsymbol{\varphi}_{t_k}^* + \frac{1}{\sqrt{\tau_{\mathrm{p}}}}\mathbf{Q}_m^{\mathrm{p}}\boldsymbol{\varphi}_{t_k}^* \\ &= \tilde{a}_{\mathrm{AP}}\sqrt{\rho_{\mathrm{ul}}\eta_k\tau_{\mathrm{p}}}\mathbf{h}_{mk} + \sum_{k'\in\mathcal{P}_k\setminus\{k\}} \tilde{a}_{\mathrm{AP}}\sqrt{\rho_{\mathrm{ul}}\eta_{k'}\tau_{\mathrm{p}}}\mathbf{h}_{mk'} + \tilde{a}_{\mathrm{AP}}\mathbf{n}_{mt_k} + \mathbf{q}_{mt_k}^{\mathrm{p}}, \end{aligned} \tag{7.18}$$

where the first term of the RHS is the desired channel, the second term is interference caused by the same pilot being used by other users, the third term is the thermal noise that is $\mathbf{n}_{mt_k} \sim \mathcal{CN}(\mathbf{0}, \mathbf{I}_N)$ since $\left\|\boldsymbol{\varphi}_{t_k}\right\|_2^2 = \tau_{\mathrm{p}}$, and the fourth term is the effective distortion produced by $\boldsymbol{\varphi}_{t_k}^*$.

### 7.4.1 Phase-aware MMSE Estimator

Let us assume that $\mathbf{h}_{mk}^{\mathrm{LoS}}$, $\phi_{mk}$, and $\mathbf{R}_{mk}$, $\forall k \in \mathcal{P}_k$, are available for the $m$th AP. Based on the processed received pilot in (7.18), the phase-aware MMSE estimate of $\mathbf{h}_{mk}$ is given by the following lemma.

**Lemma 7.1**
*The phase-aware MMSE estimate of the channel between the $m$th AP and the $k$th UE using the observation $\mathbf{y}_{mt_k}^{\mathrm{p}}$ is*

$$\hat{\mathbf{h}}_{mk} = \mathbf{h}_{mk}^{LoS}\mathrm{e}^{\mathrm{j}\phi_{mk}} + \tilde{a}_{\mathrm{AP}}^3\sqrt{\rho_{ul}\eta_k\tau_{\mathrm{p}}}\mathbf{R}_{mk}\boldsymbol{\Psi}_{mt_k}^{-1}(\mathbf{y}_{mt_k}^{\mathrm{p}} - \mathsf{E}\left\{\mathbf{y}_{mt_k}^{\mathrm{p}}\right\}), \tag{7.19}$$

*where*

$$\mathsf{E}\left\{\mathbf{y}_{mt_k}^{\mathrm{p}}\right\} = \tilde{a}_{\mathrm{AP}}\sum_{k'\in\mathcal{P}_k}\sqrt{\rho_{ul}\eta_{k'}\tau_{\mathrm{p}}}\mathbf{h}_{mk'}^{LoS}\mathrm{e}^{\mathrm{j}\phi_{mk'}}, \tag{7.20}$$

*and $\boldsymbol{\Psi}_{mt_k}$ is the covariance matrix of (7.18) given by*

$$\boldsymbol{\Psi}_{mt_k} = \sum_{k'\in\mathcal{P}_k}\rho_{ul}\eta_{k'}\tau_{\mathrm{p}}\mathbf{R}_{mk'} + \left(1 + \zeta_{\mathrm{AP}} + \zeta_{\mathrm{AP}}\sum_{k'\in\mathcal{K}}\eta_{k'}\beta_{mk'}^{NLoS}\right)\mathbf{I}_N, \tag{7.21}$$

*where $\zeta_{\mathrm{AP}} = \sigma_{\tilde{q}}^2/\tilde{a}_{\mathrm{AP}}^2$.*

*The estimate $\hat{\mathbf{h}}_{mk}$ and estimation error $\tilde{\mathbf{h}}_{mk} = \mathbf{h}_{mk} - \hat{\mathbf{h}}_{mk}$ are independent vectors given by*

$$\hat{\mathbf{h}}_{mk} = \mathbf{h}_{mk}^{LoS}\mathrm{e}^{\mathrm{j}\phi_{mk}} + \hat{\mathbf{h}}_{mk}^{NLoS}, \tag{7.22}$$

$$\tilde{\mathbf{h}}_{mk} \sim \mathcal{CN}(\mathbf{0}, \mathbf{C}_{mk}), \tag{7.23}$$

*where* $\hat{\mathbf{h}}_{mk}^{NLoS} \sim \mathcal{CN}(\mathbf{0}, \mathbf{B}_{mk})$, *and*

$$\mathbf{B}_{mk} = \mathsf{Cov}\left\{\hat{\mathbf{h}}_{mk}\right\} = \tilde{a}_{\mathrm{AP}}^{6}\tau_{\mathrm{p}}\eta_{k'}\mathbf{R}_{mk}\boldsymbol{\Psi}_{mt_k}^{-1}\mathbf{R}_{mk}, \tag{7.24}$$

$$\mathbf{C}_{mk} = \mathsf{Cov}\left\{\tilde{\mathbf{h}}_{mk}\right\} = \mathbf{R}_{mk} - \mathbf{B}_{mk}. \tag{7.25}$$

*Proof.* The MMSE estimate of Gaussian random vector such as $\mathbf{h}_{mk}$ is given by [59][1]

$$\begin{aligned}\hat{\mathbf{h}}_{mk} &= \mathsf{E}\left\{\mathbf{h}_{mk}|\mathbf{y}_{mt_k}^{\mathrm{p}}\right\} \\ &= \mathsf{E}\left\{\mathbf{h}_{mk}\right\} + \mathsf{Cov}\left\{\mathbf{h}_{mk}, \mathbf{y}_{mt_k}^{\mathrm{p}}\right\}\mathsf{Cov}\left\{\mathbf{y}_{mt_k}^{\mathrm{p}}\right\}^{-1}(\mathbf{y}_{mt_k}^{\mathrm{p}} - \mathsf{E}\left\{\mathbf{y}_{mt_k}^{\mathrm{p}}\right\}).\end{aligned} \tag{7.26}$$

Moreover, the covariance matrix $\mathsf{Cov}\left\{\hat{\mathbf{h}}_{mk}\right\}$ is given by

$$\begin{aligned}\mathsf{Cov}\left\{\hat{\mathbf{h}}_{mk}\right\} &= \mathsf{E}\left\{\left(\hat{\mathbf{h}}_{mk} - \mathsf{E}\left\{\hat{\mathbf{h}}_{mk}\right\}\right)\left(\hat{\mathbf{h}}_{mk} - \mathsf{E}\left\{\hat{\mathbf{h}}_{mk}\right\}\right)^{\mathrm{H}}\right\} \\ &= \mathsf{Cov}\left\{\mathbf{h}_{mk}, \mathbf{y}_{mt_k}^{\mathrm{p}}\right\}\mathsf{Cov}\left\{\mathbf{y}_{mt_k}^{\mathrm{p}}\right\}^{-1}\mathsf{Cov}\left\{\mathbf{y}_{mt_k}^{\mathrm{p}}\right\}\mathsf{Cov}\left\{\mathbf{y}_{mt_k}^{\mathrm{p}}\right\}^{-1}\mathsf{Cov}\left\{\mathbf{h}_{mk}, \mathbf{y}_{mt_k}^{\mathrm{p}}\right\} \\ &= \mathsf{Cov}\left\{\mathbf{h}_{mk}, \mathbf{y}_{mt_k}^{\mathrm{p}}\right\}\mathsf{Cov}\left\{\mathbf{y}_{mt_k}^{\mathrm{p}}\right\}^{-1}\mathsf{Cov}\left\{\mathbf{h}_{mk}, \mathbf{y}_{mt_k}^{\mathrm{p}}\right\}.\end{aligned} \tag{7.27}$$

From (7.5), we have that $\mathsf{E}\left\{\mathbf{h}_{mk}\right\} = \mathbf{h}_{mk}^{\mathrm{LoS}}\mathrm{e}^{\mathrm{j}\phi_{mk}}$, and since the thermal noise $\mathbf{n}_{mt_k}$ and the distortion $\mathbf{q}_{mt_k}^{\mathrm{p}}$ are zero-mean random variables, we have

$$\mathsf{E}\left\{\mathbf{y}_{mt_k}^{\mathrm{p}}\right\} = \tilde{a}_{\mathrm{AP}}\sum_{k'\in\mathcal{P}_k}\sqrt{\rho_{\mathrm{ul}}\eta_{k'}\tau_{\mathrm{p}}}\mathbf{h}_{mk'}^{\mathrm{LoS}}\mathrm{e}^{\mathrm{j}\phi_{mk'}}. \tag{7.28}$$

The cross-covariance matrix $\mathsf{Cov}\left\{\mathbf{h}_{mk}, \mathbf{y}_{mt_k}^{\mathrm{p}}\right\}$ is given by

$$\begin{aligned}\mathsf{Cov}\left\{\mathbf{h}_{mk}, \mathbf{y}_{mt_k}^{\mathrm{p}}\right\} = \tilde{a}_{\mathrm{AP}}\sum_{k'\in\mathcal{P}_k}\sqrt{\rho_{\mathrm{ul}}\eta_{k'}\tau_{\mathrm{p}}}\mathsf{E}\left\{\mathbf{h}_{mk}^{\mathrm{NLoS}}\left(\mathbf{h}_{mk'}^{\mathrm{NLoS}}\right)^{\mathrm{H}}\right\} + \tilde{a}_{\mathrm{AP}}\mathsf{E}\left\{\mathbf{h}_{mk}^{\mathrm{NLoS}}\mathbf{n}_{mt_k}^{\mathrm{H}}\right\} \\ + \mathsf{E}\left\{\mathbf{h}_{mk}^{\mathrm{NLoS}}(\mathbf{q}_{mt_k}^{\mathrm{p}})^{\mathrm{H}}\right\}.\end{aligned} \tag{7.29}$$

The NLoS component $\mathbf{h}_{mk}^{\mathrm{NLoS}}$ is uncorrelated with the NLoS from other UEs and with the thermal noise, and since it is part of the input of the quantizers, it is also uncorrelated with the processed distortion $\mathbf{q}_{mt_k}^{\mathrm{p}}$. Thus, (7.29) can be simplified to

$$\mathsf{Cov}\left\{\mathbf{h}_{mk}, \mathbf{y}_{mt_k}^{\mathrm{p}}\right\} = \tilde{a}_{\mathrm{AP}}\sqrt{\rho_{\mathrm{ul}}\eta_{k}\tau_{\mathrm{p}}}\mathbf{R}_{mk}. \tag{7.30}$$

By using similar arguments used to compute (7.30), the covariance matrix

[1]Note that $\mathbf{h}_{mk}$ is not a circularly symmetric Gaussian random vector, but it is still a Gaussian random variable.

$\mathsf{Cov}\left\{\mathbf{y}^{\mathrm{p}}_{mt_k}\right\}$ can be written as

$$\begin{aligned}\mathsf{Cov}\left\{\mathbf{y}^{\mathrm{p}}_{mt_k}\right\} &= \tilde{a}^2_{\mathrm{AP}} \sum_{k' \in \mathcal{P}_k} \rho_{\mathrm{ul}} \eta_{k'} \tau_{\mathrm{p}} \mathsf{E}\left\{\mathbf{h}^{\mathrm{NLoS}}_{mk'} \left(\mathbf{h}^{\mathrm{NLoS}}_{mk'}\right)^{\mathrm{H}}\right\} + \tilde{a}^2_{\mathrm{AP}} \mathsf{E}\left\{\mathbf{n}_{mt_k} \mathbf{n}^{\mathrm{H}}_{mt_k}\right\} + \mathsf{E}\left\{\mathbf{q}^{\mathrm{p}}_{mt_k} (\mathbf{q}^{\mathrm{p}}_{mt_k})^{\mathrm{H}}\right\} \\ &= \tilde{a}^2_{\mathrm{AP}} \sum_{k' \in \mathcal{P}_k} \rho_{\mathrm{ul}} \eta_{k'} \tau_{\mathrm{p}} \mathbf{R}_{mk'} + \left(\tilde{a}^2_{\mathrm{AP}} + \sigma^2_{\tilde{q}} + \sigma^2_{\tilde{q}} \sum_{k' \in \mathcal{K}} \eta_{k'} \beta^{\mathrm{NLoS}}_{mk'}\right) \mathbf{I}_N. \end{aligned} \tag{7.31}$$

Therefore, the MMSE estimate of $\mathbf{h}_{mk}$ is given by

$$\hat{\mathbf{h}}_{mk} = \mathbf{h}^{\mathrm{LoS}}_{mk} \mathrm{e}^{\mathrm{j}\phi_{mk}} + \tilde{a}^3_{\mathrm{AP}} \sqrt{\rho_{\mathrm{ul}} \eta_k \tau_{\mathrm{p}}} \mathbf{R}_{mk} \boldsymbol{\Psi}^{-1}_{mt_k} (\mathbf{y}^{\mathrm{p}}_{mt_k} - \mathsf{E}\left\{\mathbf{y}^{\mathrm{p}}_{mt_k}\right\}), \tag{7.32}$$

where $\boldsymbol{\Psi}_{mt_k}$ is given by (7.21). Furthermore, (7.22) and (7.23) resulted from the properties of the MMSE estimator. □

Note that (7.18) indicates that sharing pilot $\boldsymbol{\varphi}_{t_k}$ among the UEs in $\mathcal{P}_k$ generates mutual interference, and consequently degrades the system performance, which is the so-called *pilot contamination*. Moreover, due to the APs' AD converters, the MMSE estimate needs the large-scale fading coefficients from all the users. Technically, this would make the channel estimation unscalable, but this is a deterministic information that changes much slower than the small-scale information that would only be transmitted to the APs once in a while. Thus, it would not be a bottleneck to the channel estimation. However, a possible solution to make the estimation scalable is using a suboptimal estimation with $\bar{\boldsymbol{\Psi}}_{mt_k}$ given by

$$\bar{\boldsymbol{\Psi}}_{mt_k} = \sum_{k' \in \mathcal{P}_k} \rho_{\mathrm{ul}} \eta_{k'} \tau_{\mathrm{p}} \mathbf{R}_{mk'} + \left(1 + \zeta_{\mathrm{AP}} + \zeta_{\mathrm{AP}} \sum_{k' \in \mathcal{U}_m} \eta_{k'} \beta^{\mathrm{NLoS}}_{mk'}\right) \mathbf{I}_N. \tag{7.33}$$

## 7.5 Uplink Data Transmission

During the uplink data transmission, the $m$th AP receives the signal $\mathbf{y}_m \in \mathbb{C}^{N \times 1}$ from all users given by

$$\mathbf{y}_m = \sum_{k \in \mathcal{K}} \sqrt{\rho_{\mathrm{ul}} \eta_k}\, \mathbf{h}_{mk} s_k + \mathbf{n}_m, \tag{7.34}$$

where $\rho_{\mathrm{ul}} \in \mathbb{R}_+$ is the normalized uplink SNR, $\eta_k \in \mathbb{R}_+$ is the UL power allocation coefficient, $s_k \sim \mathcal{CN}(0,1)$ is the signal transmitted by the $k$th UE, and $\mathbf{n}_m \sim \mathcal{CN}(\mathbf{0}, \mathbf{I}_N)$ is the thermal noise at the $m$th AP. The signal in (7.34) is quantized by the AD converters at the APs, which, for the sake of simplicity, use the same

number of bits. This operation yields

$$\mathbf{f}_{\mathrm{AP}}(\mathbf{y}_m) = \sum_{k\in\mathcal{K}} \tilde{a}_{\mathrm{AP}}\sqrt{\rho_{\mathrm{ul}}\eta_k}\,\mathbf{h}_{mk}s_k + \tilde{a}_{\mathrm{AP}}\mathbf{n}_m + \mathbf{q}_m^{\mathrm{AP}}, \tag{7.35}$$

where $\mathbf{q}_m^{\mathrm{AP}} \in \mathbb{C}^{N\times 1}$ is the distortion matrix, whose elements are zero-mean non-Gaussian random variables with variance given by

$$\mathsf{Var}\left\{[\mathbf{q}_m^{\mathrm{AP}}]_n\right\} = \left(\sum_{k\in\mathcal{K}} \eta_k\beta_{mk}^{\mathrm{NLoS}} + 1\right)\sigma_{\tilde{q}^{\mathrm{AP}}}^2. \tag{7.36}$$

For the sake of simplicity, by using the arguments in Section 7.3 and (7.36), we rewrite (7.35) as

$$\mathbf{f}_{\mathrm{AP}}(\mathbf{y}_m) = \sum_{k\in\mathcal{K}} \tilde{a}_{\mathrm{AP}}\sqrt{\rho_{\mathrm{ul}}\eta_k}\,\mathbf{h}_{mk}s_k + \tilde{\mathbf{n}}_m, \tag{7.37}$$

where $\tilde{\mathbf{n}}_m = \tilde{a}_{\mathrm{AP}}\mathbf{n}_m + \mathbf{q}_m^{\mathrm{AP}}$ is the effective noise in the $m$th AP with

$$\sigma_{\tilde{\mathbf{n}}_m}^2 = \tilde{a}_{\mathrm{AP}}^2 + \left(\sum_{k\in\mathcal{K}} \eta_k\beta_{mk}^{\mathrm{NLoS}} + 1\right)\sigma_{\tilde{q}^{\mathrm{AP}}}^2, \tag{7.38}$$

whereas the scalable version of the variance is given by

$$\bar{\sigma}_{\tilde{\mathbf{n}}_m}^2 = \tilde{a}_{\mathrm{AP}}^2 + \left(\sum_{k\in\mathcal{U}_m} \eta_k\beta_{mk}^{\mathrm{NLoS}} + 1\right)\sigma_{\tilde{q}^{\mathrm{AP}}}^2. \tag{7.39}$$

For the CF massive MIMO deployment, as discussed before, in order to avoid overloading in the CPU and minimize the quantization effects, a semi-distributed implementation is adopted for the network. The APs are responsible for most of the computational tasks, whereas the CPU is responsible for a low cost final estimation. More specifically, besides the channel estimation, every AP preprocesses its signals by computing local estimates of the received data and, then, broadcasts them to the CPU for final decoding, which is the so-called LSFD. Although all APs can physically receive the signal from all UEs, to guarantee the scalability of the network, only the APs in the set $\mathcal{A}_k$ processes the signal sent by the $k$th UE due to the AP selection. We denote by $\mathbf{v}_{mk} \in \mathbb{C}^{N\times 1}$ the combination vector selected by the $m$th AP for the $k$th UE, $\forall k \in \mathcal{U}_m$. Thus, the local estimate of $s_k \in \mathbb{C}$ $\forall k \in \mathcal{U}_m$ is given by

$$\begin{aligned} z_{mk} &= \mathbf{v}_{mk}^{\mathrm{H}}\mathbf{D}_{mk}\mathbf{f}_{\mathrm{AP}}(\mathbf{y}_m), \\ &= \tilde{a}_{\mathrm{AP}}\sqrt{\rho_{\mathrm{ul}}\eta_k}\,\mathbf{v}_{mk}^{\mathrm{H}}\mathbf{D}_{mk}\mathbf{h}_{mk}s_k + \mathbf{v}_{mk}^{\mathrm{H}}\mathbf{D}_{mk}\sum_{k'\in\mathcal{K}\setminus\{k\}} \tilde{a}_{\mathrm{AP}}\sqrt{\rho_{\mathrm{ul}}\eta_{k'}}\,\mathbf{h}_{mk'}s_{k'} + \mathbf{v}_{mk}^{\mathrm{H}}\mathbf{D}_{mk}\tilde{\mathbf{n}}_m. \end{aligned} \tag{7.40}$$

Any combining vector can be adopted in the above expression. The most common ones are the *maximum ratio combiner* (MRC) [29] and the LP-MMSE combiner [65] given by

$$\mathbf{v}_{mk}^{\text{MRC}} = \hat{\mathbf{h}}_{mk}, \tag{7.41}$$

$$\mathbf{v}_{mk}^{\text{LP-MMSE}} = \rho_{\text{ul}}\eta_k \boldsymbol{\Omega}_m^{-1}\hat{\mathbf{h}}_{mk}, \tag{7.42}$$

where

$$\boldsymbol{\Omega}_m = \sum_{k' \in \mathcal{U}_m} \rho_{\text{ul}}\eta_{k'} \left( \hat{\mathbf{h}}_{mk'}\hat{\mathbf{h}}_{mk'}^{\text{H}} + \mathbf{C}_{mk'} + \zeta_{\text{AP}}\beta_{mk'}^{\text{NLoS}}\mathbf{I}_N \right) + (1 + \zeta_{\text{AP}})\,\mathbf{I}_N. \tag{7.43}$$

Note that (7.42) is scalable since it does not take into consideration the information from all the UEs, only the one served by the $m$th AP. Results in [60] show that the SE achieved by the LP-MMSE combiner in a distributed implementation is very close to the one of the MMSE in the same type of implementation. Then, the local estimates are quantized and sent to the CPU, where they are linearly combined by using the weights $\{\alpha_{mk}\}$ to obtain

$$\begin{aligned}
\hat{s}_k &= \sum_{m \in \mathcal{M}} \alpha_{mk}^* f_{\text{CPU}}(z_{mk}) = \sum_{m \in \mathcal{M}} \alpha_{mk}^* f_{\text{CPU}}(\mathbf{v}_{mk}^{\text{H}}\mathbf{D}_{mk}\mathbf{y}_m) \\
&= \sum_{m \in \mathcal{M}} \alpha_{mk}^* \tilde{a}_{\text{CPU}}\tilde{a}_{\text{AP}}\sqrt{\rho_{\text{ul}}\eta_k}\,\mathbf{v}_{mk}^{\text{H}}\mathbf{D}_{mk}\mathbf{h}_{mk}s_k \\
&\quad + \alpha_{mk}^*\tilde{a}_{\text{CPU}}\mathbf{v}_{mk}^{\text{H}}\mathbf{D}_{mk} \sum_{k' \in \mathcal{K}\setminus\{k\}} \tilde{a}_{\text{AP}}\sqrt{\rho_{\text{ul}}\eta_{k'}}\,\mathbf{h}_{mk'}s_{k'} + \alpha_{mk}^* n'_{mk},
\end{aligned} \tag{7.44}$$

where

$$n'_{mk} = \tilde{a}_{\text{CPU}}\mathbf{v}_{mk}^{\text{H}}\mathbf{D}_{mk}\tilde{\mathbf{n}}_m + q_{mk}^{\text{CPU}}, \tag{7.45}$$

$$\mathsf{Var}\left\{n'_{mk}\right\} = \tilde{a}_{\text{CPU}}^2 \mathsf{E}\left\{ \left\| \mathbf{v}_{mk}^{\text{H}}\mathbf{D}_{mk} \right\|_2^2 \right\} \sigma_{\tilde{\mathbf{n}}}^2 + \mathsf{Var}\left\{ q_{mk}^{\text{CPU}} \right\}, \tag{7.46}$$

$$\mathsf{Var}\left\{q_{mk}^{\text{CPU}}\right\} = \sum_{k' \in \mathcal{K}} \rho_{\text{ul}}\eta_{k'} \mathsf{E}\left\{ \left\| \mathbf{v}_{mk}^{\text{H}}\mathbf{D}_{mk}\mathbf{h}_{mk'} \right\|_2^2 \right\} \sigma_{\tilde{q}^{\text{CPU}}}^2 + \mathsf{E}\left\{ \left\| \mathbf{v}_{mk}^{\text{H}}\mathbf{D}_{mk} \right\|_2^2 \right\} \sigma_{\tilde{q}^{\text{CPU}}}^2. \tag{7.47}$$

Therefore, equation (7.44) is simplified by

$$\begin{aligned}\hat{s}_k &= \tilde{a}_{\mathrm{CPU}}\tilde{a}_{\mathrm{AP}}\sqrt{\rho_{\mathrm{ul}}\eta_k}\left(\sum_{m\in\mathcal{M}}\alpha_{mk}^{*}\mathbf{v}_{mk}^{\mathrm{H}}\mathbf{D}_{mk}\mathbf{h}_{mk}\right)s_k \\ &+\sum_{k'\in\mathcal{K}\setminus\{k\}}\tilde{a}_{\mathrm{CPU}}\tilde{a}_{\mathrm{AP}}\sqrt{\rho_{\mathrm{ul}}\eta_{k'}}\left(\sum_{m\in\mathcal{M}}\alpha_{mk}^{*}\mathbf{v}_{mk}^{\mathrm{H}}\mathbf{D}_{mk}\mathbf{h}_{mk'}\right)s_{k'}+\sum_{m\in\mathcal{M}}\alpha_{mk}^{*}n'_{mk} \\ &= \tilde{a}_{\mathrm{CPU}}\tilde{a}_{\mathrm{AP}}\sqrt{\rho_{\mathrm{ul}}\eta_k}\,\boldsymbol{\alpha}_k^{\mathrm{H}}\boldsymbol{\gamma}_{kk}s_k+\sum_{k'\in\mathcal{K}\setminus\{k\}}\tilde{a}_{\mathrm{CPU}}\tilde{a}_{\mathrm{AP}}\sqrt{\rho_{\mathrm{ul}}\eta_{k'}}\,\boldsymbol{\alpha}_k^{\mathrm{H}}\boldsymbol{\gamma}_{kk'}s_{k'}+\boldsymbol{\alpha}_k^{\mathrm{H}}\mathbf{n}'_k, \quad (7.48)\end{aligned}$$

where $\boldsymbol{\alpha}_k = [\alpha_{1k}\ \alpha_{2k}\ \cdots\ \alpha_{Mk}]^{\mathrm{T}}$ is the LSFD weight vector, $\boldsymbol{\gamma}_{kk'} \in \mathbb{C}^{M\times 1}$ is the effective CF massive MIMO channel given by

$$\boldsymbol{\gamma}_{kk'} = \left[\mathbf{v}_{1k}^{\mathrm{H}}\mathbf{D}_{1k}\mathbf{h}_{1k'}\quad \mathbf{v}_{2k}^{\mathrm{H}}\mathbf{D}_{2k}\mathbf{h}_{2k'}\quad \cdots\quad \mathbf{v}_{Mk}^{\mathrm{H}}\mathbf{D}_{Mk}\mathbf{h}_{Mk'}\right]^{\mathrm{T}}. \quad (7.49)$$

The achievable SE for the CF massive MIMO system is obtained in the following theorem.

**Theorem 7.2**

*An achievable SE of the kth UE in the semi distributed operation is*

$$\mathit{SE}_k^{ul} = \frac{\tau_{\mathrm{u}}}{\tau_{\mathrm{c}}}\log_2\left(1+\mathit{SINR}_k^{ul}\right) \quad [b/s/Hz], \quad (7.50)$$

*where the effective SINR is given by*

$$\mathit{SINR}_k^{ul} = \frac{\rho_{ul}\eta_k|\boldsymbol{\alpha}_k^{\mathrm{H}}\mathsf{E}\left\{\boldsymbol{\gamma}_{kk}\right\}|^2}{\boldsymbol{\alpha}_k^{\mathrm{H}}\boldsymbol{\Gamma}_k\boldsymbol{\alpha}_k}, \quad (7.51)$$

*and*

$$\boldsymbol{\Gamma}_k = \sum_{k'\in\mathcal{K}}\rho_{ul}\eta_{k'}(\mathsf{E}\left\{\boldsymbol{\gamma}_{kk'}\boldsymbol{\gamma}_{kk'}^{\mathrm{H}}\right\}+\mathbf{J}_{kk'})-\rho_{ul}\eta_k\mathsf{E}\left\{\boldsymbol{\gamma}_{kk}\right\}\mathsf{E}\left\{\boldsymbol{\gamma}_{kk}^{\mathrm{H}}\right\}+\mathbf{F}_k, \quad (7.52)$$

$$\mathbf{J}_{kk'} = \frac{\zeta_{\mathrm{CPU}}}{\tilde{a}_{\mathrm{AP}}^2}\mathsf{Diag}\left(\mathsf{E}\left\{[\boldsymbol{\gamma}_{kk'}\boldsymbol{\gamma}_{kk'}^{\mathrm{H}}]_{11}\right\},\mathsf{E}\left\{[\boldsymbol{\gamma}_{kk'}\boldsymbol{\gamma}_{kk'}^{\mathrm{H}}]_{22}\right\},\cdots,\mathsf{E}\left\{[\boldsymbol{\gamma}_{kk'}\boldsymbol{\gamma}_{kk'}^{\mathrm{H}}]_{MM}\right\}\right), \quad (7.53)$$

$$\mathbf{F}_k = \frac{(\sigma_{\tilde{\mathbf{n}}}^2+\zeta_{\mathrm{CPU}})}{\tilde{a}_{\mathrm{AP}}^2}\mathsf{Diag}\left(\mathsf{E}\left\{\left\|\mathbf{v}_{1k}^{\mathrm{H}}\mathbf{D}_{1k}\right\|_2^2\right\},\mathsf{E}\left\{\left\|\mathbf{v}_{2k}^{\mathrm{H}}\mathbf{D}_{2k}\right\|_2^2\right\},\cdots,\mathsf{E}\left\{\left\|\mathbf{v}_{Mk}^{\mathrm{H}}\mathbf{D}_{Mk}\right\|_2^2\right\}\right). \quad (7.54)$$

*Proof.* Since the CPU does not have knowledge of the channel estimates, it treats the average effective channel gain $\tilde{a}_{\mathrm{CPU}}\tilde{a}_{\mathrm{AP}}\sqrt{\rho_{\mathrm{ul}}\eta_k}\,\boldsymbol{\alpha}_k^{\mathrm{H}}\mathsf{E}\left\{\boldsymbol{\gamma}_{kk}\right\}$ as the true effective channel. This assumption leads to a discrete memoryless interference channel with

input $s_k$ and output $\hat{s}_k$ given by

$$\hat{s}_k = \mathsf{DS}_k + \underbrace{\mathsf{BU}_k + \mathsf{IUI}_k + \mathsf{TN}_k}_{v_k}, \tag{7.55}$$

where

$$\mathsf{DS}_k = \tilde{a}_{\mathrm{CPU}}\tilde{a}_{\mathrm{AP}}\sqrt{\rho_{\mathrm{ul}}\eta_k}\,\boldsymbol{\alpha}_k^{\mathrm{H}}\mathsf{E}\left\{\boldsymbol{\gamma}_{kk}\right\}s_k, \tag{7.56}$$

$$\mathsf{BU}_k = \tilde{a}_{\mathrm{CPU}}\tilde{a}_{\mathrm{AP}}\sqrt{\rho_{\mathrm{ul}}\eta_k}\,(\boldsymbol{\alpha}_k^{\mathrm{H}}\boldsymbol{\gamma}_{kk} - \boldsymbol{\alpha}_k^{\mathrm{H}}\mathsf{E}\left\{\boldsymbol{\gamma}_{kk}\right\})s_k, \tag{7.57}$$

$$\mathsf{IUI}_k = \sum_{k'\in\mathcal{K}\setminus\{k\}} \tilde{a}_{\mathrm{CPU}}\tilde{a}_{\mathrm{AP}}\sqrt{\rho_{\mathrm{ul}}\eta_{k'}}\,\boldsymbol{\alpha}_k^{\mathrm{H}}\boldsymbol{\gamma}_{kk'}s_{k'}, \tag{7.58}$$

$$\mathsf{TN}_k = \boldsymbol{\alpha}_k^{\mathrm{H}}\mathbf{n}'_k, \tag{7.59}$$

denotes, for the $k$th user, the desired signal, the beamforming uncertainty, the inter-user interference, and the total noise, respectively. Equation (7.55) is equivalent to signal transmitted through a deterministic channel with additive zero-mean interference plus noise term $v_k$. The term $v_k$ is uncorrelated with the signal term in (7.55) since the distortion noise is uncorrelated with the quantizer input, and signals from different UEs are independent as well as the received noise at different APs. Besides that, the terms that compose $v_k$ are mutually uncorrelated between themselves. Therefore, using the result in [60], the channel capacity is given by

$$C_k \geq \log_2\left(1 + \frac{\mathsf{E}\left\{|\mathsf{DS}_k|^2\right\}}{\mathsf{E}\left\{|\mathsf{BU}_k|^2\right\} + \mathsf{E}\left\{|\mathsf{IUI}_k|^2\right\} + \mathsf{E}\left\{|\mathsf{TN}_k|^2\right\}}\right), \tag{7.60}$$

where

$$\mathsf{E}\left\{|\mathsf{DS}_k|^2\right\} = \tilde{a}_{\mathrm{CPU}}^2\tilde{a}_{\mathrm{AP}}^2\rho_{\mathrm{ul}}\eta_k\,|\boldsymbol{\alpha}_k^{\mathrm{H}}\mathsf{E}\left\{\boldsymbol{\gamma}_{kk}\right\}|^2, \tag{7.61}$$

$$\mathsf{E}\left\{|\mathsf{BU}_k|^2\right\} = \tilde{a}_{\mathrm{CPU}}^2\tilde{a}_{\mathrm{AP}}^2\rho_{\mathrm{ul}}\eta_k(\rho_{\mathrm{ul}}\eta_k\mathsf{E}\left\{|\boldsymbol{\alpha}_k^{\mathrm{H}}\boldsymbol{\gamma}_{kk}|^2\right\} - |\boldsymbol{\alpha}_k^{\mathrm{H}}\mathsf{E}\left\{\boldsymbol{\gamma}_{kk}\right\}|^2), \tag{7.62}$$

$$\mathsf{E}\left\{|\mathsf{IUI}_k|^2\right\} = \sum_{k'\in\mathcal{K}\setminus\{k\}} \tilde{a}_{\mathrm{CPU}}^2\tilde{a}_{\mathrm{AP}}^2\rho_{\mathrm{ul}}\eta_{k'}\mathsf{E}\left\{|\boldsymbol{\alpha}_k^{\mathrm{H}}\boldsymbol{\gamma}_{kk'}|^2\right\}, \tag{7.63}$$

$$\mathsf{E}\left\{|\mathsf{TN}_k|^2\right\} = \tilde{a}_{\mathrm{CPU}}^2\tilde{a}_{\mathrm{AP}}^2\boldsymbol{\alpha}_k^{\mathrm{H}}(\mathbf{J}_{kk'} + \mathbf{F}_k)\boldsymbol{\alpha}_k, \tag{7.64}$$

where $\mathbf{J}_{kk'}$ and $\mathbf{F}_k$ are given by (7.53) and (7.54), respectively. Therefore, substituting (7.61)–(7.64) into (7.60) yields

$$\begin{aligned} C_k &\geq \log_2\left(1 + \frac{\rho_{\mathrm{ul}}\eta_k\,|\boldsymbol{\alpha}_k^{\mathrm{H}}\mathsf{E}\left\{\boldsymbol{\gamma}_{kk}\right\}|^2}{\sum\limits_{k'\in\mathcal{K}}\rho_{\mathrm{ul}}\eta_{k'}\mathsf{E}\left\{|\boldsymbol{\alpha}_k^{\mathrm{H}}\boldsymbol{\gamma}_{kk'}|^2\right\} - \rho_{\mathrm{ul}}\eta_k|\boldsymbol{\alpha}_k^{\mathrm{H}}\mathsf{E}\left\{\boldsymbol{\gamma}_{kk}\right\}|^2 + \boldsymbol{\alpha}_k^{\mathrm{H}}(\mathbf{J}_{kk'} + \mathbf{F}_k)\boldsymbol{\alpha}_k}\right) \\ &\geq \log_2\left(1 + \frac{\rho_{\mathrm{ul}}\eta_k\,|\boldsymbol{\alpha}_k^{\mathrm{H}}\mathsf{E}\left\{\boldsymbol{\gamma}_{kk}\right\}|^2}{\boldsymbol{\alpha}_k^{\mathrm{H}}\boldsymbol{\Gamma}_k\boldsymbol{\alpha}_k}\right), \end{aligned} \tag{7.65}$$

where $\mathbf{\Gamma}_k$ is given by (7.52).

The equality in (7.65) is an achievable SE for the $k$th user. As a last step, only the fraction $\tau_{\mathrm{u}}/\tau_{\mathrm{c}}$ of the samples is used for UL data transmission, which results in the achievable SE stated in the theorem and measured in bit/s/Hz. □

The achievable SE in (7.50) holds for any vector $\boldsymbol{\alpha}_k$. However, the one that maximizes the SE is the LSFD. Note that the effective SINR in (7.51) is a generalized Rayleigh quotient with respect to $\boldsymbol{\alpha}_k$. Thus the optimal LSFD vector is obtained in the following corollary.

**Corollary *7.1***
*The effective SINR in* (7.51) *for the $k$th UE is maximized by*

$$\boldsymbol{\alpha}_k^{\star} = \rho_{ul}\eta_k \mathbf{\Gamma}_k^{-1} \mathsf{E}\left\{\boldsymbol{\gamma}_{kk}\right\}. \tag{7.66}$$

*This leads to the maximum value*

$$\mathit{SINR}_k^{\star ul} = \rho_{ul}\eta_k \mathsf{E}\left\{\boldsymbol{\gamma}_{kk^{\mathrm{H}}}\right\} \mathbf{\Gamma}_k^{-1} \mathsf{E}\left\{\boldsymbol{\gamma}_{kk}\right\}. \tag{7.67}$$

*Proof.* The matrix square root $\mathbf{\Gamma}_k^{1/2}$ of $\mathbf{\Gamma}_k$ exists since $\mathbf{\Gamma}_k$ is a positive definite matrix, thus we can define the new variable $\bar{\boldsymbol{\alpha}}_k = \mathbf{\Gamma}_k^{1/2}\boldsymbol{\alpha}_k$ and establish that

$$\mathsf{SINR}_k^{\mathrm{ul}} = \frac{|\bar{\boldsymbol{\alpha}}_k{}^{\mathrm{H}} \mathbf{\Gamma}_k^{-1/2} \sqrt{\rho_{\mathrm{ul}}\eta_k} \mathsf{E}\left\{\boldsymbol{\gamma}_{kk}\right\}|^2}{\bar{\boldsymbol{\alpha}}_k^{\mathrm{H}} \bar{\boldsymbol{\alpha}}_k}. \tag{7.68}$$

Equation (7.68) is a Rayleigh quotient, which is maximized by $\bar{\boldsymbol{\alpha}} = \rho_{\mathrm{ul}}\eta_k \mathbf{\Gamma}_k^{-1/2} \mathsf{E}\left\{\boldsymbol{\gamma}_{kk}\right\}$. Therefore,

$$\boldsymbol{\alpha}_k^{\star} = \sqrt{\rho_{\mathrm{ul}}\eta_k} \mathbf{\Gamma}_k^{-1} \mathsf{E}\left\{\gamma_{kk}\right\}, \tag{7.69}$$

and

$$\mathsf{SINR}_k^{\star \mathrm{ul}} = \rho_{\mathrm{ul}}\eta_k \mathsf{E}\left\{\boldsymbol{\gamma}_{kk^{\mathrm{H}}}\right\} \mathbf{\Gamma}_k^{-1} \mathsf{E}\left\{\boldsymbol{\gamma}_{kk}\right\}. \tag{7.70}$$

□

The optimum LSFD vector $\boldsymbol{\alpha}_k^{\star}$ is not scalable since the matrix $\mathbf{\Gamma}_k$ depends on the statistical matrix $\mathsf{E}\left\{\boldsymbol{\gamma}_{kk'}\boldsymbol{\gamma}_{kk'}^{\mathrm{H}}\right\}$ for all UEs in the network. In fact, this is expected because all UEs in the network produce interference at all APs, thereby the optimum LSFD vector must take all interference into consideration in order to make the best estimation. A possible scalable version of the LSFD is found by limiting how many interfering UEs are considered in the computation of $\mathbf{\Gamma}_k$. The common approach is taking only the UEs that are served partially by the same APs as the $k$th UE into consideration. Then, the optimal LSFD vector in (7.66) can be approximated by

the n-opt LSFD given by [60]

$$\boldsymbol{\alpha}_k^{\text{n-opt}} = \rho_{\text{ul}} \eta_k \bar{\boldsymbol{\Gamma}}_k^{-1} \mathsf{E}\left\{\boldsymbol{\gamma}_{kk}\right\}, \tag{7.71}$$

where

$$\bar{\boldsymbol{\Gamma}}_k = \sum_{k' \in \mathcal{S}_k} \rho_{\text{ul}} \eta_{k'} (\mathsf{E}\left\{\boldsymbol{\gamma}_{kk'} \boldsymbol{\gamma}_{kk'}^{\text{H}}\right\} + \mathbf{J}_{kk'}) - \rho_{\text{ul}} \eta_k \mathsf{E}\left\{\boldsymbol{\gamma}_{kk}\right\} \mathsf{E}\left\{\boldsymbol{\gamma}_{kk}^{\text{H}}\right\} + \mathbf{F}_k. \tag{7.72}$$

In the next section, we compare the performance of the MRC and the LP-MMSE combiner through simulations, considering semi-distributed and distributed implementations, and the effect of the quantization.

## 7.6 Simulation Results

### 7.6.1 Simulation Parameters

For the simulations, a CF massive MIMO network with $M = 100$ APs and $K = 40$ UEs was used, where each AP was equipped with an $N = 4$ antenna ULA. The CF massive MIMO network covered an area of 1 km $\times$ 1 km. A wrap-around topology is used to mimic a large network deployment without edges, where all APs and UEs are receiving interference from all directions. We assume that the APs and the UEs are deployed uniformly at random in the coverage area.

The large-scale fading coefficient is modeled as [60]

$$\beta_{km} = -30.5 - 36.7 \log_{10}(d_{km}) + F_{km}, \tag{7.73}$$

where $d_{km} \in \mathbb{R}_+$ is the three-dimensional distance between the $m$th AP and the $k$th UE in meters. The APs are deployed 10 m above the plane where the UEs are located, which acts as the minimum distance. This model matches with the 3GPP urban microcell model [85]. The shadow fading is $F_{km} \sim \mathcal{N}(0, \sigma_{\text{sf}}^2)$ and the terms from an AP to different UEs are correlated as [60]

$$\mathsf{E}\left\{F_{km} F_{ij}\right\} = \begin{cases} \sigma_{\text{sf}}^2 2^{-\frac{\delta_{ki}}{9 \text{ m}}}, & m = j \\ 0, & \text{otherwise} \end{cases}, \tag{7.74}$$

where $\delta_{ki} \in \mathbb{R}_+$ is the distance between the $k$th UE and the $i$th UE in meters. The large-scale fading coefficient model in (7.73) corresponds to a median channel gain of $-140.6$ dB at 1 km, where the median is achieved by $F_{km} = 0$ dB. Moreover, the large-scale fading coefficient model in (7.73) has a pathloss exponent $\alpha = 3.67$. The

Rician $\kappa$-factor is modeled as [31, 63]

$$\kappa_{mk} = 10^{1.3-0.003d_{mk}}, \tag{7.75}$$

and the large-scale fading coefficients for LoS and NLoS components are

$$\beta_{mk}^{\text{LoS}} = \frac{\kappa_{mk}}{\kappa_{mk}+1}\beta_{mk}, \tag{7.76}$$

$$\beta_{mk}^{\text{NLoS}} = \frac{1}{\kappa_{mk}+1}\beta_{mk}. \tag{7.77}$$

The $(i,j)$th element of the spatial correlation matrix $\mathbf{R}_{mk}$ are generated using the local scattering model given by [59, 60]

$$[\mathbf{R}_{mk}]_{ij} = \beta_{mk}^{\text{NLoS}} \int\int \mathrm{e}^{\mathrm{j}\pi(i-j)\sin(\bar{\varphi})\cos(\bar{\theta})} f(\bar{\varphi},\bar{\theta})\mathrm{d}\bar{\varphi}\mathrm{d}\bar{\theta}, \tag{7.78}$$

where

$$f(\bar{\varphi},\bar{\theta}) = \frac{1}{2\pi\sigma_{\boldsymbol{\varphi}}\sigma_{\theta}} \mathrm{e}^{-\frac{(\bar{\varphi}-\boldsymbol{\varphi})^2}{2\sigma_{\boldsymbol{\varphi}}^2}} \mathrm{e}^{-\frac{(\bar{\theta}-\theta)^2}{2\sigma_{\theta}^2}}, \tag{7.79}$$

and $\varphi$ and $\theta$ are the nominal azimuth and elevations angles, computed by drawing a straight line between AP and UE. The standard deviations $\sigma_{\boldsymbol{\varphi}} = 15^{\circ}$ and $\sigma_{\theta} = 15^{\circ}$ are called the *angular standard deviation* (ASD). In this model, the multipath components are Gaussian distributed around the nominal azimuth and elevation angles.

The communication takes place over a 20-MHz bandwidth with a total receiver noise power of $-94$ dBm, consisting of thermal noise and noise figure of 7 dB at the receiver, at both the APs and UEs. The maximum uplink transmit power of each UE is 100 mW. Each coherence block consists of $\tau_{\text{c}} = 200$ samples. This value matches well with a 2-ms coherence time and a 100-kHz coherence bandwidth, which correspond to high mobility and large channel dispersion in sub-6-GHz bands. The training time for each coherence block is $\tau_{\text{p}} = 10$ samples. Each UE transmits the pilot signal with full power $\eta_k = 100$ mW. In order to assign the pilots and generate the *dynamic cooperation clustering* (DCC), we apply the access and the joint pilot assignment and AP selection algorithm in [60, 65]. The simulation parameters are summarized in Table 7.2.

### 7.6.2 Performance with Semi-distributed Implementation

In this section, we compared the performance of the LP-MMSE and MRC in a semi-distributed implementation with their performance in a distributed implementation. In this simulation, the APs and the CPU are both considered perfect hardware, i.e., there is no quantization effect. Therefore, the performance of the CF massive MIMO

Table 7.2: Simulation Parameters for the CF massive MIMO Network

| | **Parameters** |
|---|---|
| **Network Area** | 1 km × 1 km |
| **Network Layout** | Random deployment with wrap-around |
| **Number of APs** | $M = 100$ |
| **Number of Antennas per AP** | $N = 4$ |
| **Number of UEs** | $K = 40$ |
| **Bandwidth** | 20 MHz |
| **Receiver Noise Power** | $-94$ dBm |
| **UL Transmit Power** | 100 mW |
| **Coherence Block** | $\tau_c = 200$ |
| **Channel Gain (1 km)** | $-104.6$ dB |
| **Pathloss Exponent** | $\alpha = 3.67$ |
| **APs' Height** | 10 m |
| **Std. Dev. of Shadow Fading** | $\sigma_{sf} = 4$ |
| **Azimuth ASD** | $\sigma_{\varphi} = 15^{\circ}$ |
| **Elevation ASD** | $\sigma_{\theta} = 15^{\circ}$ |

system is only evaluated over the spatial correlated Rician fading channel.

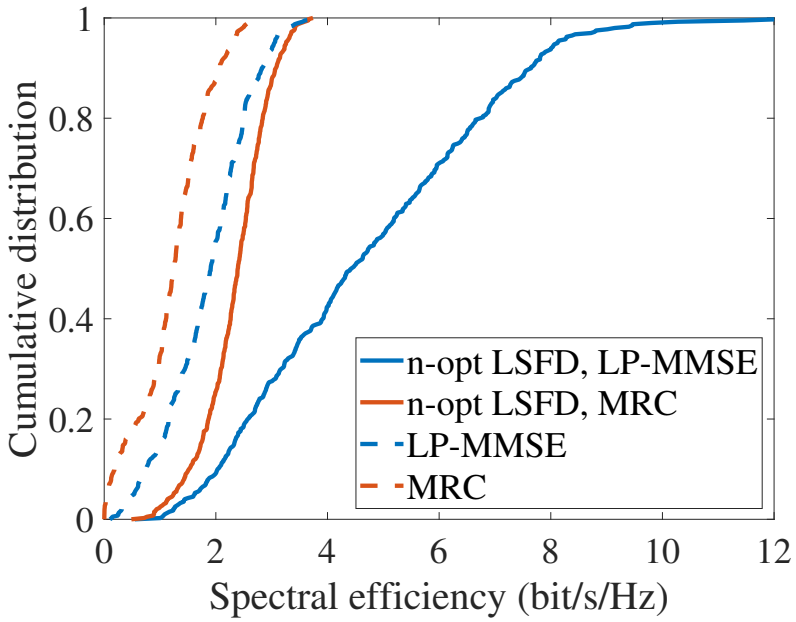


Figure 7.3: Spectral efficiency of the CF massive MIMO system over spatial correlated Rician fading channel with semi-distributed and distributed implementations.

Fig. 7.3 depicts the CDF of the SE of the CF massive MIMO system with different combiners. As can be observed in this figure, the semi-distributed implementation can significantly improve the performance of the CF massive MIMO system when compared with a distributed implementation. Moreover, the LP-MMSE combiner with LSFD outperformed the MRC with LSFD, improving the 95PT by 39.61%.

### 7.6.3 Effects of the Quantization

In this section, we evaluate the impact of the quantization on the performance of a CF massive MIMO system with semi-distributed and distributed implementations. In this scenario, both the CPU and the APs have non-ideal AD converts. Therefore, the performance of the CF massive MIMO system is evaluated over the spatial correlated Rician fading channel combined with the quantization distortion.

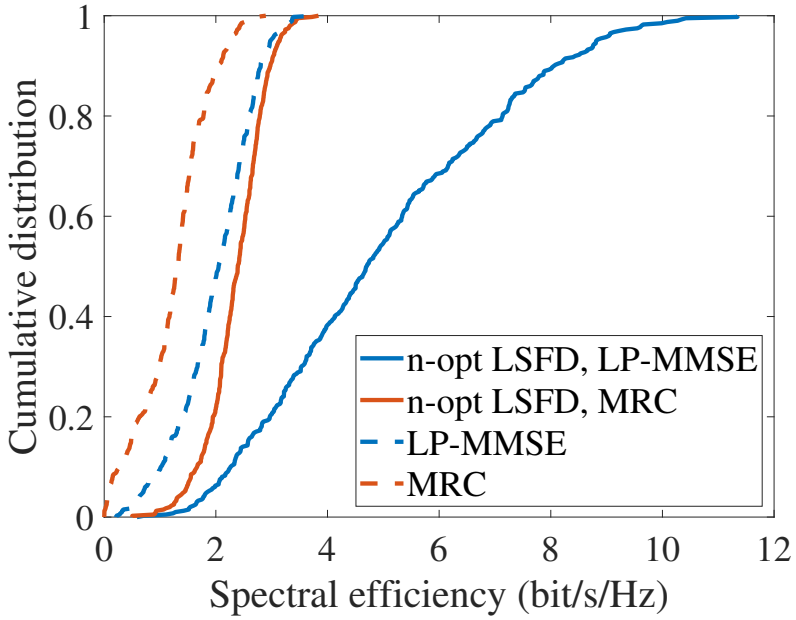


Figure 7.4: Spectral efficiency of the CF massive MIMO system over spatial correlated Rician fading channel with semi-distributed and distributed implementations, and 5-bit AD converters.

Fig. 7.3 depicts the CDF of the spectral efficiency of the CF massive MIMO system with different combiners and 5-bit AD converters in both CPU and APs. The figure shows that the semi-distributed implementation can significantly improve the performance of the CF massive MIMO system when compared with a distributed implementation. The LP-MMSE combiner with LSFD still outperformed the MRC with LSFD. However, for the case with $b = 5$ bits, the gap between the 95PT decreased due to the quantization effects, being 28.93% as opposed to 39.61% earlier on right without considering AD converters.

## 7.7 Concluding Remarks

In this chapter, we derived the MMSE channel estimate for a Rician fading channel and provided its scalable version taking into account the effects of quantization in the APs. Moreover, we presented the scalable LP-MMSE as well as the optimum

LSFD vector and its scalable version. It is worth highlighting that when quantization is considered in the analysis, it not only results in scaling of the signals by the Bussgang gain and the variance of the quantization noise, but it also increases the level of interference by adding the large-scale fading coefficient of all users in the network. The impact of this additional level of interference on the system performance has not been considered in theoretical analyses reported in the literature, being a contribution of this work.

# Part III

# Conclusion and Future Work

# Chapter 8

# Conclusion

## 8.1 Closing Thoughts

In this thesis, we presented new contributions to the massive MIMO field, covering conventional cellular and CF massive MIMO systems. More specifically, we explored power allocation algorithm aspects and user selection for the cellular massive MIMO systems and the impact of hardware nonlinearities on the performance of CF massive MIMO systems. Solutions for the aforementioned issues have a practical appeal since they are of real concern to the deployment of practical massive MIMO systems.

In the first part of the thesis, we presented a comprehensive review for massive MIMO systems under LoS propagation, showing important results and highlighting the main difference in the results when compared to massive MIMO systems under NLoS propagation, which are represented by the i.i.d. Rayleigh fading channels. Findings highlight the fact that unlike the well-studied case of i.i.d. Rayleigh fading channel, for LoS channels both the favorable propagation and asymptotically favorable propagation conditions can be violated irrespective of the number of users and antennas in the massive MIMO system, degrading the system performance. Additionally, we presented one of the main power allocation philosophy used in massive MIMO networks and addressed an issue associated with the initialization of a popular algorithm. We used the Perron-Frobenius theory to explain this issue and to derive a new search interval in order to guarantee the convergence of the algorithm. We also used the Gershgorin circle theorem to create a bound test that guarantees convergence and reduces the computational load of the algorithm.

In the first part of the thesis, we also presented a comprehensive review of the user selection algorithms for massive MIMO systems, and evaluated their performance when combined with different linear precoders for various system configurations considering perfect and imperfect CSI under the LoS propagation channel. In addition, we provided a thorough analysis of the computational complexity of the user se-

lection algorithms. Further, we showed that practical cases exist in which the LoS propagation model may lead to significant levels of interference among users within a cell and such cases are not satisfactorily addressed by the existing user selection algorithms. To this end, we proposed a new user selection algorithm based on ICI, called ICIBS and evaluated its performance. We have further extended the ICIBS algorithm, generalizing it to take into account both the small- and large-scale fading, which we referred to as FRBS algorithm. Unlike other techniques, the ICIBS and FRBS accounts for the ICI in a global manner, thus yielding better results than the other algorithms especially in cases where there are many users interfering with one another and similar results in scenarios having low-interference levels. Although the work mainly considered LoS propagation, all algorithms can also be applied to different channel models, such as the Rician fading model. From our experience, however, the benefits in SE due to the use of user selection algorithms are more prominent as the Rician fading model tends to the LoS model, whereas they become negligible and do not offer any visible benefits for i.i.d. Rayleigh fading.

In the second part of the thesis, we delved into the concept of CF massive MIMO and analyzed the performance of CF massive MIMO networks corrupted by the impairments caused by the AD converters. In order to evaluate the performance of the CF networks, we first derived the MMSE channel estimate for a Rician fading channel taking into consideration the effects caused by the quantization. We also derived the suboptimal scalable version of the MMSE estimates since the quantization makes it unscalable. In addition, we presented the scalable LP-MMSE considering the quantization effects. Moreover, we also derived the UL SINR expression for a generic linear combiner as well as the optimum LSFD vector. These contributions are important in analyzing the performance of practical CF massive MIMO networks.

## 8.2 Future Research Directions

Possible future research directions include:

- **The creation of automatic user selection algorithms:** All the algorithms presented in this thesis need the knowledge of the number of users to be selected. However this information is not always available and it is desired to select users based on some type of QoS. The difficulty here is to find the right constraint for the criteria used for the most common user selection algorithms. The algorithms presented in this thesis use heuristic criteria that are indirectly related with the ultimate performance of the massive MIMO systems. For example, the constraint on the ICI or the FR may not have a linear relation

with the constraint on the throughput.

- **The creation of a user selection algorithm for Rician fading channels:** In this thesis, we explained that LSFA user selection algorithms are suitable for NLoS propagation and for the LoS propagation, however, we need algorithms that are capable of dealing with both types of fading information. However, since the Rician fading is a mix of the LoS and NLoS propagation, an adaptive user selection algorithm can be used depending on the current propagation. For example, if the NLoS components are stronger than the LoS components, LSFA may be good enough to perform a proper selection. The challenge here is to define an adaptive strategy to choose the algorithm to perform the selection depending on the state of the channel. It is expected that this adaptive strategy would depend on the Rician $\kappa$-factor, but further research needs to be conducted.

# Bibliography


[1] MARZETTA, T. L., "Noncooperative Cellular Wireless with Unlimited Numbers of Base Station Antennas", *IEEE Transactions on Wireless Communications*, v. 9, n. 11, pp. 3590–3600, November 2010.

[2] LARSSON, E. G., EDFORS, O., TUFVESSON, F., *et al.*, "Massive MIMO for Next Generation Wireless Systems", *IEEE Communications Magazine*, v. 52, n. 2, pp. 186–195, February 2014.

[3] HOCHWALD, B. M., MARZETTA, T. L., TAROKH, V., "Multiple-Antenna Channel Hardening and Its Implications for Rate Feedback and Scheduling", *IEEE Transactions on Information Theory*, v. 50, n. 9, pp. 1893–1909, September 2004.

[4] MARZETTA, T. L., LARSSON, E. G., YANG, H., *et al.*, *Fundamentals of Massive MIMO*. 1 ed. Cambridge, Cambridge University Press, 2016.

[5] RUSEK, F., PERSSON, D., LAU, B. K., *et al.*, "Scaling Up MIMO: Opportunities and Challenges with Very Large Arrays", *IEEE Signal Processing Magazine*, v. 30, n. 1, pp. 40–60, January 2013.

[6] BJÖRNSON, E., LARSSON, E. G., MARZETTA, T. L., "Massive MIMO: Ten Myths and One Critical Question", *IEEE Communications Magazine*, v. 54, n. 2, pp. 114–123, February 2016.

[7] CHIEN, T. V., BJÖRNSON, E., "Massive MIMO Communications". In: *5G Mobile Communications*, Springer International Publishing, pp. 77–116, 2017.

[8] NGO, H. Q., LARSSON, E. G., MARZETTA, T. L., "Aspects of Favorable Propagation in Massive MIMO". In: *22nd European Signal Processing Conference*, pp. 76–80, Lisbon, September 2014.

[9] YANG, H., MARZETTA, T. L., "Massive MIMO with Max-Min Power Control in Line-of-Sight Propagation Environment", *IEEE Transactions on Communications*, v. 65, n. 11, pp. 4685–4693, November 2017.

[10] YANG, H., "User Scheduling in Massive MIMO". In: *IEEE 19th International Workshop on Signal Processing Advances in Wireless Communications*, pp. 1–5, Kalamata, June 2018.

[11] YANG, H., NGO, H. Q., LARSSON, E. G., "Multi-Cell Massive MIMO in LoS". In: *2018 IEEE Global Communications Conference*, pp. 1–6, December 2018.

[12] ROH, W., SEOL, J.-Y., PARK, J., *et al.*, "Millimeter-Wave Beamforming as an Enabling Technology for 5G Cellular Communications: Theoretical Feasibility and Prototype Results", *IEEE Communications Magazine*, v. 52, n. 2, pp. 106–113, February 2014.

[13] ALKHATEEB, A., El Ayach, O., LEUS, G., *et al.*, "Channel Estimation and Hybrid Precoding for Millimeter Wave Cellular Systems", *IEEE Journal of Selected Topics in Signal Processing*, v. 8, n. 5, pp. 831–846, October 2014.

[14] ZHOU, Z., FANG, J., YANG, L., *et al.*, "Channel Estimation for Millimeter-Wave Multiuser MIMO Systems via PARAFAC Decomposition", *IEEE Transactions on Wireless Communications*, v. 15, n. 11, pp. 7501–7516, August 2016.

[15] LARSSON, E. G., MARZETTA, T. L., NGO, H. Q., *et al.*, "Antenna Count for Massive MIMO: 1.9 GHz vs. 60 GHz", *IEEE Communications Magazine*, v. 56, n. 9, pp. 132–137, September 2018.

[16] TSE, D., VISWANATH, P., *Capacity of Wireless Channels*. Cambridge, Cambridge University Press, 2005.

[17] GAO, X., EDFORS, O., RUSEK, F., *et al.*, "Massive MIMO Performance Evaluation Based on Measured Propagation Data", *IEEE Transactions on Wireless Communications*, v. 14, n. 7, pp. 3899–3911, July 2015.

[18] OSSEIRAN, A., BOCCARDI, F., BRAUN, V., *et al.*, "Scenarios for 5G mobile and wireless communications: the vision of the METIS project", *IEEE Communications Magazine*, v. 52, n. 5, pp. 26–35, May 2014.

[19] CHALLITA, F., MARTINEZ-INGLES, M.-T., LIENARD, M., *et al.*, "Line-of-Sight Massive MIMO Channel Characteristics in an Indoor Scenario at 94 GHz", *IEEE Access*, v. 6, pp. 62361–62370, 2018.

[20] FLORDELIS, J., RUSEK, F., GAO, X., *et al.*, "Spatial Separation of Closely-Located Users in Measured Massive MIMO Channels", *IEEE Access*, v. 6, pp. 40253–40266, 2018.

[21] IJAZ, A., ZHANG, L., GRAU, M., *et al.*, "Enabling Massive IoT in 5G and Beyond Systems: PHY Radio Frame Design Considerations", *IEEE Access*, v. 4, pp. 3322–3339, June 2016.

[22] ANDREWS, J. G., ZHANG, X., DURGIN, G. D., *et al.*, "Are We Approaching the Fundamental Limits of Wireless Network Densification?", *IEEE Communications Magazine*, v. 54, n. 10, pp. 184–190, October 2016.

[23] INTERDONATO, G., BJÖRNSON, E., Quoc Ngo, H., *et al.*, "Ubiquitous Cell-Free Massive MIMO Communications", *EURASIP Journal on Wireless Communications and Networking*, v. 2019, n. 1, pp. 197, December 2019.

[24] ZHANG, J., CHEN, S., LIN, Y., *et al.*, "Cell-Free Massive MIMO: A New Next-Generation Paradigm", *IEEE Access*, v. 7, pp. 99878–99888, July 2019.

[25] VENKATESAN, S., LOZANO, A., VALENZUELA, R., "Network MIMO: Overcoming Intercell Interference in Indoor Wireless Systems". In: *Conference Record of the Forty-First Asilomar Conference on Signals, Systems and Computers*, pp. 83–87, Pacific Grove, November 2007.

[26] IRMER, R., DROSTE, H., MARSCH, P., *et al.*, "Coordinated Multipoint: Concepts, Performance, and Field Trial Results", *IEEE Communications Magazine*, v. 49, n. 2, pp. 102–111, February 2011.

[27] YOU, X.-H., WANG, D.-M., SHENG, B., *et al.*, "Cooperative Distributed Antenna Systems for Mobile Communications [Coordinated and Distributed MIMO", *IEEE Wireless Communications*, v. 17, n. 3, pp. 35–43, June 2010.

[28] HOSSEINI, K., YU, W., ADVE, R. S., "Large-Scale MIMO Versus Network MIMO for Multicell Interference Mitigation", *IEEE Journal of Selected Topics in Signal Processing*, v. 8, n. 5, pp. 930–941, October 2014.

[29] NGO, H. Q., ASHIKHMIN, A., YANG, H., *et al.*, "Cell-Free Massive MIMO Versus Small Cells", *IEEE Transactions on Wireless Communications*, v. 16, n. 3, pp. 1834–1850, March 2017.

[30] RAO, S., ASHIKHMIN, A., YANG, H., "Internet of Things Based on Cell-Free Massive MIMO". In: *53rd Asilomar Conference on Signals, Systems, and Computers*, pp. 1946–1950, Pacific Grove, November 2019.

[31] WANG, X., ASHIKHMIN, A., WANG, X., "Wirelessly Powered Cell-Free IoT: Analysis and Optimization", *IEEE Internet of Things Journal*, v. 7, n. 9, pp. 8384–8396, September 2020.

[32] I, C.-L., ROWELL, C., HAN, S., *et al.*, "Toward Green and Soft: A 5G Perspective", *IEEE Communications Magazine*, v. 52, n. 2, pp. 66–73, February 2014.

[33] YANG, H., MARZETTA, T. L., "Energy Efficiency of Massive MIMO: Cell-Free vs. Cellular". In: *2018 IEEE 87th Vehicular Technology Conference (VTC Spring)*, pp. 1–5, Porto, June 2018.

[34] NGO, H. Q., TRAN, L.-N., DUONG, T. Q., *et al.*, "On the Total Energy Efficiency of Cell-Free Massive MIMO", *IEEE Transactions on Green Communications and Networking*, v. 2, n. 1, pp. 25–39, March 2018.

[35] BJÖRNSON, E., SANGUINETTI, L., "Scalable Cell-Free Massive MIMO Systems", *IEEE Transactions on Communications*, v. 68, n. 7, pp. 4247–4261, July 2020.

[36] 3GPP TR 21.915, *Digital cellular telecommunications system (Phase 2+) (GSM); Universal Mobile Telecommunications System (UMTS); LTE; 5G; Release description; Release 15*, Report, 2019.

[37] ETSI, *Anual Report*, Report, 2018.

[38] NGO, H. Q., MATTHAIOU, M., LARSSON, E. G., "Massive MIMO with Optimal Power and Training Duration Allocation", *IEEE Wireless Communications Letters*, v. 4, n. 6, pp. 605–608, April 2014.

[39] WANG, X., WANG, Y., NI, W., *et al.*, "Sum Rate Analysis and Power Allocation for Massive MIMO Systems with Mismatch Channel", *IEEE Access*, v. 6, pp. 16997–17009, 2018.

[40] TAN, C. W., "Wireless Network Optimization by Perron-Frobenius Theory". In: *48th Annual Conf. Info. Sci. Sys.*, pp. 1–6, Princeton, March 2014.

[41] CHIEN, T. V., BJÖRNSON, E., LARSSON, E. G., "Joint Power Allocation and User Association Optimization for Massive MIMO Systems", *IEEE Transactions on Wireless Communications*, v. 15, n. 9, pp. 6384–6399, September 2016.

[42] CHIEN, T. V., BJORNSON, E., LARSSON, E. G., "Joint Pilot Design and Uplink Power Allocation in Multi-Cell Massive MIMO Systems", *IEEE Transactions on Wireless Communications*, v. 17, n. 3, pp. 2000–2015, March 2018.

[43] YOO, T., GOLDSMITH, A., "On the Optimality of Multiantenna Broadcast Scheduling Using Zero-Forcing Beamforming", *IEEE Journal on Selected Areas in Communications*, v. 24, n. 3, pp. 528–541, March 2006.

[44] FARSAEI, A., ALVARADO, A., WILLEMS, F. M. J., *et al.*, "An Improved Dropping Algorithm for Line-of-Sight Massive MIMO With Max-Min Power Control", *IEEE Communications Letters*, v. 23, n. 6, pp. 1109–1112, June 2019.

[45] DIMIć, G., SIDIROPOULOS, N. D., "On Downlink Beamforming with Greedy User Selection: Performance Analysis and a Simple New Algorithm", *IEEE Transactions on Signal Processing*, v. 53, n. 10, pp. 3857–3868, October 2005.

[46] JIANG, J., BUEHRER, R. M., TRANTER, W. H., "Greedy Scheduling Performance for a Zero-Forcing Dirty-Paper Coded System", *IEEE Transactions on Communications*, v. 54, n. 5, pp. 789–793, May 2006.

[47] COSTA, M., "Writing on Dirty Paper", *IEEE Transactions on Information Theory*, v. 29, n. 3, pp. 439–441, May 1983.

[48] WEINGARTEN, H., STEINBERG, Y., SHAMAI, S. S., "The Capacity Region of the Gaussian Multiple-Input Multiple-Output Broadcast Channel", *IEEE Transactions on Information Theory*, v. 52, n. 9, pp. 3936–3964, September 2006.

[49] BENMIMOUNE, M., DRIOUCH, E., AJIB, W., *et al.*, "Joint Transmit Antenna Selection and User Scheduling for Massive MIMO Systems". In: *IEEE Wireless Communications and Networking Conference*, pp. 381–386, New Orleans, March 2015.

[50] DIERKS, S., JUENGER, N., "Scheduling for Massive MIMO with Few Excess Antennas". In: *20th International ITG Workshop on Smart Antennas*, pp. 40–44, Munich, March 2016.

[51] KUERBIS, M., BALASUBRAMANYA, N. M., LAMPE, L., *et al.*, "User Scheduling in Massive MIMO Systems with a Large Number of Devices". In: *IEEE 28th Annual International Symposium on Personal, Indoor, and Mobile Radio Communications*, pp. 1–6, Montreal, October 2017.

[52] LIU, H., GAO, H., YANG, S., *et al.*, "Low-Complexity Downlink User Selection for Massive MIMO Systems", *IEEE Systems Journal*, v. 11, n. 2, pp. 1072–1083, June 2017.

[53] SHEIKH, T. A., BORA, J., HUSSAIN, M. A., "Sum-Rate Performance of Massive MIMO Systems in Highly Scattering Channel with Semi-Orthogonal and Random User Selection", *Radioelectronics and Communications Systems*, v. 61, n. 12, pp. 547–555, December 2018.

[54] HUANG, S., YIN, H., LI, H., *et al.*, "Decremental User Selection for Large-Scale Multi-User MIMO Downlink with Zero-Forcing Beamforming", *IEEE Wireless Communications Letters*, v. 1, n. 5, pp. 480–483, October 2012.

[55] FARSAEI, A., ALVARADO, A., WILLEMS, F. M. J., *et al.*, "An Improved Dropping Algorithm for Line-of-Sight Massive MIMO With Tomlinson–Harashima Precoding", *IEEE Communications Letters*, v. 23, n. 11, pp. 2099–2103, November 2019.

[56] NAM, J., ADHIKARY, A., AHN, J.-Y., *et al.*, "Joint Spatial Division and Multiplexing: Opportunistic Beamforming, User Grouping and Simplified Downlink Scheduling", *IEEE Journal of Selected Topics in Signal Processing*, v. 8, n. 5, pp. 876–890, October 2014.

[57] LEE, G., SUNG, Y., "A New Approach to User Scheduling in Massive Multi-User MIMO Broadcast Channels", *IEEE Transactions on Communications*, v. 66, n. 4, pp. 1481–1495, April 2018.

[58] FARSAEI, A., SHEIKH, A., GUSTAVSSON, U., *et al.*, "DropNet: An Improved Dropping Algorithm Based on Neural Networks for Line-of-Sight Massive MIMO", *IEEE Access*, v. 9, pp. 29441–29448, 2021.

[59] BJÖRNSON, E., HOYDIS, J., SANGUINETTI, L., "Massive MIMO Networks: Spectral, Energy, and Hardware Efficiency", *Foundations and Trends® in Signal Processing*, v. 11, n. 3-4, pp. 154–655, 2017.

[60] DEMIR, Ö. T., BJÖRNSON, E., SANGUINETTI, L., "Foundations of User-Centric Cell-Free Massive MIMO", *Foundations and Trends in Signal Processing*, v. 14, n. 3-4, pp. 162–472, 2021.

[61] NAYEBI, E., ASHIKHMIN, A., MARZETTA, T. L., *et al.*, "Precoding and Power Optimization in Cell-Free Massive MIMO Systems", *IEEE Transactions on Wireless Communications*, v. 16, n. 7, pp. 4445–4459, July 2017.

[62] NGUYEN, L. D., DUONG, T. Q., NGO, H. Q., *et al.*, "Energy Efficiency in Cell-Free Massive MIMO with Zero-Forcing Precoding Design", *IEEE Communications Letters*, v. 21, n. 8, pp. 1871–1874, August 2017.

[63] OZDOGAN, O., BJÖRNSON, E., LARSSON, E. G., "Massive MIMO With Spatially Correlated Rician Fading Channels", *IEEE Transactions on Communications*, v. 67, n. 5, pp. 3234–3250, May 2019.

[64] INTERDONATO, G., NGO, H. Q., FRENGER, P., *et al.*, "Downlink Training in Cell-Free Massive MIMO: A Blessing in Disguise", *IEEE Transactions on Wireless Communications*, v. 18, n. 11, pp. 5153–5169, November 2019.

[65] CHEN, S., ZHANG, J., BJÖRNSON, E., *et al.*, "Structured Massive Access for Scalable Cell-Free Massive MIMO Systems", *IEEE Journal on Selected Areas in Communications*, v. 39, n. 4, pp. 1086–1100, April 2021.

[66] ZHANG, J., WEI, Y., BJÖRNSON, E., *et al.*, "Performance Analysis and Power Control of Cell-Free Massive MIMO Systems with Hardware Impairments", *IEEE Access*, v. 6, pp. 55302–55314, 2018.

[67] BASHAR, M., CUMANAN, K., BURR, A. G., *et al.*, "Max–Min Rate of Cell-Free Massive MIMO Uplink With Optimal Uniform Quantization", *IEEE Transactions on Communications*, v. 67, n. 10, pp. 6796–6815, October 2019.

[68] BASHAR, M., CUMANAN, K., BURR, A. G., *et al.*, "Energy Efficiency of the Cell-Free Massive MIMO Uplink With Optimal Uniform Quantization", *IEEE Transactions on Green Communications and Networking*, v. 3, n. 4, pp. 971–987, December 2019.

[69] BASHAR, M., AKBARI, A., CUMANAN, K., *et al.*, "Exploiting Deep Learning in Limited-Fronthaul Cell-Free Massive MIMO Uplink", *IEEE Journal on Selected Areas in Communications*, v. 38, n. 8, pp. 1678–1697, August 2020.

[70] BASHAR, M., NGO, H. Q., CUMANAN, K., *et al.*, "Uplink Spectral and Energy Efficiency of Cell-Free Massive MIMO With Optimal Uniform Quantization", *IEEE Transactions on Communications*, v. 69, n. 1, pp. 223–245, January 2021.

[71] BASHAR, M., XIAO, P., TAFAZOLLI, R., *et al.*, "Limited-Fronthaul Cell-Free Massive MIMO With Local MMSE Receiver Under Rician Fading and Phase Shifts", *IEEE Wireless Communications Letters*, v. 10, n. 9, pp. 1934–1938, September 2021.

[72] SENETA, E., *Non-negative Matrices and Markov Chains*, Springer Series in Statistics. New York, Springer, 1981.

[73] ANDREWS, J. G., BUZZI, S., CHOI, W., *et al.*, "What Will 5G Be?", *IEEE Journal on Selected Areas in Communications*, v. 32, n. 6, pp. 1065–1082, June 2014.

[74] BOCCARDI, F., HEATH, R. W., LOZANO, A., *et al.*, "Five Disruptive Technology Directions for 5G", *IEEE Communications Magazine*, v. 52, n. 2, pp. 74–80, February 2014.

[75] JIANG, C., ZHANG, H., REN, Y., *et al.*, "Machine Learning Paradigms for Next-Generation Wireless Networks", *IEEE Wireless Communications*, v. 24, n. 2, pp. 98–105, April 2017.

[76] VAN TREES, H. L., *Optimum Array Processing*. 1 ed. New York, John Wiley & Sons, Inc., 2002.

[77] GAO, X., EDFORS, O., LIU, J., *et al.*, "Antenna Selection in Measured Massive MIMO Channels Using Convex Optimization". In: *IEEE Globecom Workshops*, pp. 129–134, Atlanta, December 2013.

[78] GAO, X., EDFORS, O., TUFVESSON, F., *et al.*, "Multi-Switch for Antenna Selection in Massive MIMO". In: *IEEE Global Communications Conference*, pp. 1–6, San Diego, December 2014.

[79] GAO, X., EDFORS, O., TUFVESSON, F., *et al.*, "Massive MIMO in Real Propagation Environments: Do All Antennas Contribute Equally?", *IEEE Transactions on Communications*, v. 63, n. 11, pp. 3917–3928, November 2015.

[80] WU, X., BEAULIEU, N. C., LIU, D., "On Favorable Propagation in Massive MIMO Systems and Different Antenna Configurations", *IEEE Access*, v. 3, pp. 5578 – 5593, April 2017.

[81] LU, L., LI, G. Y., SWINDLEHURST, A. L., *et al.*, "An Overview of Massive MIMO: Benefits and Challenges", *IEEE Journal of Selected Topics in Signal Processing*, v. 8, n. 5, pp. 742–758, October 2014.

[82] COVER, T. M., THOMAS, J. A., *Elements of Information Theory*. 2 ed. New Jersey, John Wiley & Sons, Inc., 2006.

[83] YANG, H., MARZETTA, T. L., "Max-Min SINR Dependence on Channel Correlation in Line-of-Sight Massive MIMO". In: *IEEE Global Communications Conference*, pp. 1–6, Singapore, December 2017.

[84] KNUTH, D. E., "Big Omicron and big Omega and big Theta", *ACM SIGACT News*, v. 8, n. 2, pp. 18–24, April 1976.

[85] ETSI 3GPP, *Digital Cellular Telecommunications System (Phase 2+); Radio Network Planning Aspects*, Report, ETSI, 2010.

[86] LI, X., JIN, S., SURAWEERA, H. A., *et al.*, "Statistical 3-D Beamforming for Large-Scale MIMO Downlink Systems Over Rician Fading Channels", *IEEE Transactions on Communications*, v. 64, n. 4, pp. 1529–1543, April 2016.

[87] MAO, J., GAO, J., LIU, Y., *et al.*, "Simplified Semi-Orthogonal User Selection for MU-MIMO Systems with ZFBF", *IEEE Wireless Communications Letters*, v. 1, n. 1, pp. 42–45, February 2012.

[88] LIU, J., SHE, X., CHEN, L., "A Low Complexity Capacity-Greedy User Selection Scheme for Zero-Forcing Beamforming". In: *IEEE 69th Vehicular Technology Conference*, pp. 1–5, Barcelona, April 2009.

[89] TRÈVES, F., *Topological Vector Spaces, Distributions and Kernels*. 1 ed. San Diego, Academic Press, 1967.

[90] SANGUINETTI, L., BJORNSON, E., HOYDIS, J., "Toward Massive MIMO 2.0: Understanding Spatial Correlation, Interference Suppression, and Pilot Contamination", *IEEE Transactions on Communications*, v. 68, n. 1, pp. 232–257, January 2020.

[91] BJÖRNSON, E., HOYDIS, J., KOUNTOURIS, M., *et al.*, "Massive MIMO Systems With Non-Ideal Hardware: Energy Efficiency, Estimation, and Capacity Limits", *IEEE Transactions on Information Theory*, v. 60, n. 11, pp. 7112–7139, November 2014.

[92] BUSSGANG, J. J., *Crosscorrelation Functions of Amplitude-Distorted Gaussian Signals*, Report, Research Laboratory of Electronics, Massachusetts Institute of Technology, Cambridge, 1952.

[93] OZDOGAN, O., BJÖRNSON, E., ZHANG, J., "Performance of Cell-Free Massive MIMO With Rician Fading and Phase Shifts", *IEEE Transactions on Wireless Communications*, v. 18, n. 11, pp. 5299–5315, November 2019.

[94] WANG, Z., ZHANG, J., BJÖRNSON, E., *et al.*, "Uplink Performance of Cell-Free Massive MIMO Over Spatially Correlated Rician Fading Channels", *IEEE Communications Letters*, v. 25, n. 4, pp. 1348–1352, April 2021.

[95] DEMIR, O. T., BJÖRNSON, E., "The Bussgang Decomposition of Nonlinear Systems: Basic Theory and MIMO Extensions [Lecture Notes]", *IEEE Signal Processing Magazine*, v. 38, n. 1, pp. 131–136, January 2021.

[96] PRICE, R., "A Useful Theorem for Nonlinear Devices Having Gaussian Inputs", *IEEE Transactions on Information Theory*, v. 4, n. 2, pp. 69–72, June 1958.

[97] LI, Y., TAO, C., SECO-GRANADOS, G., *et al.*, "Channel Estimation and Performance Analysis of One-Bit Massive MIMO Systems", *IEEE Transactions on Signal Processing*, v. 65, n. 15, pp. 4075–4089, August 2017.

[98] BJÖRNSON, E., SANGUINETTI, L., HOYDIS, J., "Hardware Distortion Correlation Has Negligible Impact on UL Massive MIMO Spectral Efficiency", *IEEE Transactions on Communications*, v. 67, n. 2, pp. 1085–1098, February 2019.

[99] KAKKAVAS, A., MUNIR, J., MEZGHANI, A., *et al.*, "Weighted Sum Rate Maximization for Multi-User MISO Systems with Low Resolution Digital to Analog Converters". In: *20th International ITG Workshop on Smart Antennas*, pp. 516–523, Munich, March 2016.